Dislocation Core Effects on Mobility

Wei Cai[1]*, Vasily V. Bulatov[1]†, Jinpeng Chang[2], Ju Li[2]‡ and Sidney Yip[2]§

[1] Lawrence Livermore National Laboratory,
University of California, Livermore, CA 94551

[2] Department of Nuclear Engineering,
Massachusetts Institute of Technology, Cambridge, MA 02139

November 18, 2002

To appear as a chapter in *Dislocations in Solids*,
F.R.N. Nabarro and J.P. Hirth, ed.

---

*Mailing Address: LLNL L-353, 7000 East Ave, Livermore, CA 94551 Phone: (925)424-5443 Fax: (925)423-7040 Email: caiwei@llnl.gov

†Phone: (925)-423-0124 Email: bulatov1@llnl.gov

‡Present address: Department of Materials Science and Engineering, Ohio State University, Columbus, OH 43210.

§To whom correspondence should be addressed. Mailing address: M.I.T. Room 24-208, 77 Mass Ave, Cambridge, MA 02139. Phone: (617)253-3809 Fax: (617) 258-8863 Email: syip@mit.edu

Contents

1 Introduction

The purpose of this chapter is to discuss the atomic structure and interactions in the dislocation core and their effects on dislocation mobility from the standpoint of theoretical concepts, physical models and simulation studies, with due consideration of relevant experimental results. Several previous chapters in this series provide the necessary background and more extensive exposition into several topics to be discussed here: Bullough and Tewary, "Lattice Theories of Dislocations" (vol. 2, 1979), Weertman and Weertman, "Moving Dislocations" (vol. 3, 1980), Schoeck, "Thermodynamics and Thermal Activation of Dislocations" (vol. 3, 1980), and M. Duesbery, "The Dislocation Core and Plasticity" (vol. 8, 1989). Rather than being comprehensive, our intent in this new chapter is to highlight some of the recent developments in understanding dislocation core structure and mobility. These include the driving forces and activation barriers for dislocation motion, the models which relate mobility to core properties, and the results of atomistic simulations at the levels of first-principles calculations and empirical and semi-empirical interatomic potentials. In our discussions, the major emphasis is placed on physical ideas and observations. In fact, technical details of modeling and experiments are only briefly mentioned and only where required for clarification of physics issues or for interpretation of results.

In this introductory section we provide general background and introduce several basic concepts in order to frame the discussion given in three subsequent sections dealing with particular crystal structures and material types: FCC metals, diamond-cubic semiconductors, and BCC metals. The reason for treating FCC materials first is that historically the understanding of core effects on dislocation mobility developed mostly in conjunction with this crystallography class. FCC systems give us a good chance to discuss some of the better established views and approaches and set the stage for contrasting these with more recent observations of core effects in other materials. Dislocation cores in FCC materials tend to be planar and spread out in extent; they dissociate into partials that interact with each other and move by gliding on a slip plane. Dislocation response to stress in these systems generally obeys the Schmid law established for macroscopic crystal plasticity. A well-known model, due to Peierls and Nabarro, provides a simple framework that captures dislocation core and mobility behavior in FCC metals reasonably well. In contrast, dislocation cores and dislocation mobility in semiconductors are affected by strong directional bonding that is responsible for the

appearance of a rich family of secondary core defects. The existence of glide and shuffle sets of dislocation positions in diamond cubic semiconductors introduces still more complexity with regard to the role of core mechanisms in dislocation motion. Plasticity behavior of BCC metals is controlled, to a large extent, by the motion of screw dislocations. The core of screw dislocations is relatively compact but in some BCC metals exhibits a tendency to three-way non-planar dissociation or polarization. Dislocation mobility exhibits large deviation from the canonical Schmid behavior as a function of stress. The connection between details of core structure and mobility of screw dislocations in BCC metals has been a topic of intense research but remains somewhat controversial. Of all known material systems, the most pronounced and intricate core effects arguably are observed in ordered intermetallic alloys, such as nickel-based superalloys or TiAl composites. These however are discussed in great detail in a recent volume (vol. 10) of this series and will not be considered here.

Since the most recent chapter by M.S. Duesbery (vol. 8) that was dedicated to dislocation core and crystal plasticity, several important developments have come to fore that brought about significant progress towards quantitative analysis of the dislocation core structure and its effects on mobility. A major factor in these recent developments is the emergence of new capabilities for accurate first-principles electronic structure calculations of dislocation core structure, energy and mobility. Over the same period, the models based on the empirical potentials have been used to explore realistic complexity of fully three-dimensional dynamics of individual dislocations and dislocation groups. These recent simulations revealed a rich sub-structure of secondary core defects and multiple mechanisms of dislocation motion in 3D. Yet another principal development of the past decade is the emergence of the fully three-dimensional mesoscale simulation methodology of Dislocation Dynamics (DD) that can be used, in principle, for computational prediction of overall crystal plasticity behavior from the underlying physics of dislocation motion. For this impressive development to deliver on its ultimate promise, understanding of the core mechanisms of dislocation mobility is crucial. Fidelity of DD simulations places high demands on the accuracy of dislocation mobility functions that can be derived and parameterized from direct atomistic simulations, dislocation theory and experimental observations. On the experimental side, new capabilities for HREM allow for direct observations of the secondary structure of dislocations and approach the limits of resolution required to resolve the relevant details of the dislocation core structure [1].

However, reading through this chapter one is likely to observe that the progress towards understanding dislocation core effects has not been always steady. A few seemingly well established ideas and concepts now appear to be in conflict with the more recent data, while other previous inconsistencies no longer exist in light of the new results. Even if it is disturbing that a number of key issues in dislocation mobility remain controversial, we consider this as an indication to critically revisit, given the new capabilities, some of the existing concepts in dislocation physics. We believe the situation presents an opportunity to develop new knowledge of dislocation mobility that is more coherent and quantitative than previously existed.

Basic concepts

Plastic strain produced in response to shear stress is a cumulative result of multiple displacements along the crystallographic slip planes in quanta of the Burgers vector. Conservative dislocation motion or glide involves local atomic displacements that proceed through switching one or few interatomic bonds at a time. In comparison, homogeneous shear along the crystallographic slip plane requires switching all interatomic bonds across the plane at once and, as such, must be prohibitively expensive energetically unless the stress reaches rather high values near the theoretical shear strength (typically of the order of $\mu/10$, with μ the shear modulus of the material). Experimentally observed values of the yield stress are typically much lower than this ideal shear resistance, with notable exceptions of deformation response of whiskers [2] and single crystals under nano-indentation [3, 4].

Exactly how a dislocation moves is defined by the energetics of bond-switching rearrangements required for its translation by a unit atomic distance in the glide plane. Somewhat loosely, one can define the core as a region of crystal lattice around the dislocation line in which the relative displacements of the neighboring atoms exceed the elastic limit (say 2% in terms of the local shear strain). Given the highly non-linear character of interatomic interactions in the core, it is clearly the relative motion of the core atoms that contributes most to the energetics of dislocation translation. Conversely, the relative displacements of the atoms outside the core will not contribute as much to the energy of dislocation translation. The latter is a sensitive function of the core structure, including the details of the atomic arrangement in the core, and of the atomic pathways by which this structure changes when the dislocation moves. Core structure under zero stress has

received much attention over the years given its real or presumed connection to the mechanisms of dislocation motion. In the subsequent sections we will discuss various approaches to modeling and observing dislocation core structure developed for various materials. We will also give examples of insights one can obtain by considering the core structure of dislocation both under zero and non-zero stress.

The core could exist in several metastable structures that differ from each other by virtue of some in-core rearrangements. Here, the nonlinear interatomic forces between the individual atoms including the local bonding topology come into play. The difference between one core structure and another manifests itself in a difference in the core free energy. Experiments are unable to provide precise information on the core energies, such data can be obtained only from atomistic calculations. Although the total (elastic + core) energy of the dislocation is a physical quantity, its partitioning into core and elastic energies is, to a large extent, arbitrary and depends on the choice of the core cutoff parameter - core reference radius. The latter should not be identified with a physical extent of the non-linear region of the core, although these two parameters are often confused. The core free energy is the factor that determines the stability of a particular atomistic structure. In comparing core energies of various metastable core structures, one must use the same core cutoff parameter which, otherwise, can be arbitrary. For the same reason, one must report a particular value of the core cutoff radius selected for partitioning the dislocation energy.

Another fundamental property is the minimum stress required for the dislocation to move, i.e. the Peierls stress. Given the defining role dislocations play in crystal plasticity, the Peierls stress is related, although not necessarily directly, to the macroscopic yield stress above which the crystal deforms plastically. In reality, dislocation motion can be assisted by thermal fluctuations. Thus the minimal stress to move a dislocation is a function of temperature and the time over which dislocation motion is observed, both in simulations or and in laboratory experiments. In contrast, Peierls stress is an idealized concept, defined as the minimal stress to move a dislocation at zero temperature. Experimentally, this is related to the yield stress measured at vanishingly low temperatures. In computational models, the zero temperature condition corresponds to quasi-static relaxations, where the system stay close to its ground state. In such cases, quantum effects of the nuclei, such as zero-point vibrations, are usually ignored, even though the interaction forces between atoms can be solved by quantum mechanical treatment of the

electrons. When the conditions are met where both thermal fluctuation and quantum tunnelling effects can be ignored, Peierls stress becomes a well defined measure of intrinsic lattice resistance to dislocation motion, and serves as a connection between experiments and simulations. We will encounter it frequently in the discussions throughout the chapter.

Closely related to the Peierls stress is another measure of the lattice resistance to dislocation motion - the Peierls barrier. It is defined as the energy barrier that a straight dislocation must surmount in order to move to a neighboring lattice position - Peierls valley. The Peierls barrier is of course defined per unit length of the dislocation line. At a low but non-zero temperature this barrier can be overcome locally, by spontaneous formation of a kink pair which throws a small part of the dislocation into the neighboring Peierls valley. The kinks can then propagate along the line and either recombine or run away from each other, completing translation of the whole line. Under zero stress the barriers for forward and backward motion are exactly equal. However, under non-zero stress one of these barriers is reduced while the other one becomes higher so that directional dislocation motion (glide) begins. If the stress rises still further, at some point the smaller of the two barriers vanishes altogether - this condition corresponds to reaching the Peierls stress. Also, at high enough temperatures the Peierls barrier can become totally washed out: in such conditions kink mechanisms play no or little role while the overall mobility of an unpinned dislocation is controlled by viscous friction due to the interaction between moving dislocations and phonons and electrons. All these and other, less apparent, regimes of dislocation motion are discussed in the following three sections in conjunction with FCC, diamond cubic and BCC material systems.

2 FCC Metals

At room temperature, noble metals (Cu, Ag, Au), platinum group metals (Rh,Pd,Pt,Ir), some alkaline metals (Ca, Sr) and Al, Ni and Pb assume the face-centred cubic (FCC) close packed structure. FCC metals and alloys are technologically important both as structural materials (especially Al alloys and stainless steel) and as special application materials, e.g. interconnects in the electronic circuitry. Most FCC materials can combine stiffness with formability and remain ductile down to low temperatures. Because their mechanical properties can be significantly affected and improved by alloying, FCC metals are ideal base materials for alloy design. Many of the useful properties of these materials are direct results of the underlying dislocation behavior. As such, dislocations in FCC and other close-packed metals have been the focus of much attention in the past, making these materials the most widely studied group from this point of view.

2.1 Core Structure

Much of the dislocation behavior observed in FCC metals and alloys results from the Shockley dissociation, by which perfect $\frac{1}{2}\langle 110\rangle$ dislocations split into two partial dislocations, bounding an area of stacking fault (SF). Expressed in Miller index notation such a reaction reads

$$\frac{1}{2}[110] = \frac{1}{6}[21\bar{1}] + \text{SF} + \frac{1}{6}[121] \ . \tag{1}$$

While the reduction of elastic energy achieved by this dissociation is considerable, this reaction can occur only if a stable low-energy stacking fault exists. In FCC materials stable stacking faults are found only in the {111} planes. The dissociated dislocations glide in the planes containing the stacking faults which simply move along with the partial dislocations. We emphasize that it is the availability of stable stacking faults in the {111} planes that defines the well-known predisposition for dislocations to glide on these planes, rather than the fact that these planes are the most widely spaced. In other material systems where stable stacking faults do not exist, the preference to gliding on any particular system of slip planes is less distinct (see for example the BCC section). Even in FCC aluminum which has a relatively high SF energy on the {111} plane, slip activity on {001} planes is sometimes observed [5](p. 272).
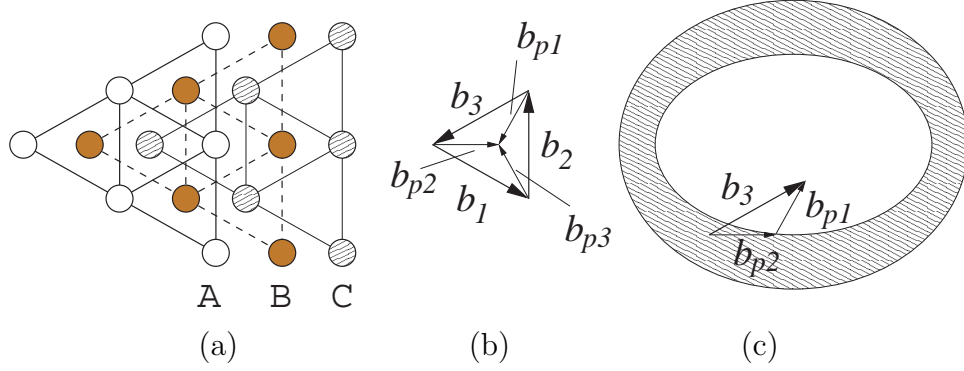
Figure 1: (a) Plane-on view of the {111} plane of FCC lattice. (b) Perfect Burgers vectors $\vec{b}_{1,2,3}$ and partial Burgers vectors $\vec{b}_{p1,p2,p3}$ on the {111} plane. (c) A perfect dislocation loop with Burgers vector $\vec{b}_3$, formed by first shifting the lattice by $\vec{b}_{p2}$ in the outer loop, and then shifting the lattice by $\vec{b}_{p1}$ in the inner loop, eliminating the stacking fault.

The existence of low-energy SF on the {111} planes is a consequence of the particular packing sequence of {111} atomic layers, a universal characteristic of all FCC metals. This packing is illustrated in a plane-on view through {111} planes (see Fig. 1(a)) in which three types of atomic layers with different in-plane positions are marked as A, B and C. Notice that the three layers are shifted by $1/3\langle 111 \rangle$ along the plane normal, forming a repeat pattern with periodicity $\langle 111 \rangle$. Each layer presents a regular triangular arrangement of atoms, the layers being stacked in such a way that atoms in layer B are lined up over the centres of the triangles formed by the atoms in layer A. Likewise, atoms in C are at the corresponding centres of the triangles in B or, equivalently, in the centres of the alternate triangles in A. Atoms in the next layer A are exactly aligned with the atoms in the layer A at the bottom, thus completing the stacking period.

An intrinsic stacking fault (ISF) is formed when atoms of one layer, say C, are shifted into the "wrong" triangles of the underlying B layer, and all the layers above C are shifted by the same amount leaving the relative stacking of all other layers unchanged. At this point, atoms in the shifted layer C are aligned with the atoms in the bottom layer A. Therefore the stacking sequence changes from $\cdots ABCAB \cdots$ to $\cdots AB|ABC \cdots$, where | indicates the location of the stacking fault. By shifting every second {111}

9

layer, the FCC stacking can be entirely transformed into a HCP structure, $\cdots ABABAB \cdots$. Given that this shift does not affect the relative positions of first and second nearest neighbors (18 atoms altogether), the energy difference between the two structures is expectedly small. With few notable exceptions, the energy of an isolated ISF is indeed quite low for most FCC metals, typically in the range from 10 to $200\,\mathrm{mJ/m^2}$ [5](p. 839). Shifting successively two layers in the same sense creates the so-called extrinsic stacking fault ($\cdots AB|A|CABC \cdots$). Finally, shifting every layer above a pre-selected $\{111\}$ plane in the same sense creates a perfect twin ($\cdots CBACBA \cdots$).

A partial dislocation loop can be viewed as the boundary separating an area of ISF from the rest of the plane. This partial shift can occur in any of the three equivalent directions $\vec{b}_{p1}, \vec{b}_{p2}, \vec{b}_{p3}$, shown by the arrows in Fig. 1(b). To make a complete (perfect) dislocation, two atomic layers bounding the ISF inside the first partial loop have to be shifted again along another partial shift direction. However, to avoid the atoms moving on top of each other, the second shift should be chosen from a different set of three partial shift directions, Fig. 1(c). Clearly, for every perfect dislocation with Burgers vector $\vec{b}$, only one combination of partial shifts $\vec{b}_{p1}$ and $\vec{b}_{p2}$ exists that avoids atomic run-ons and then only if introduced in a certain order. This simple observation lies behind the well-known leading-trailing partial rule usually formulated using the Thompson tetrahedron notation, see Fig. 3 (Axiom 10-1 in [5]).

The separation distance between two partials is defined mainly by the balance of two forces, the elastic repulsion between the partials and the attractive "glue" force due to the ISF. For the dissociation reaction of Eq. (1), continuum elasticity predicts that the equilibrium spacing X_0 between two straight parallel partial dislocations under zero stress is

$$X_0 = \frac{K'b^2}{\gamma_{ISF}} \; , \tag{2}$$

where K' is a certain combination of elastic constants that depends on the dislocation character angle, and γ_{ISF} is the stacking fault energy. In obtaining this formula, one considers the two partials as separate dislocations connected by an ISF. Alternatively, the whole assembly of two partials and the ISF can be viewed as an extended core of the perfect dislocation. This particular core structure of $\frac{1}{2}\langle 110 \rangle$ dislocations determines their mobility and, through that, the overall plasticity behavior of FCC metals and alloys.

Similar, albeit more complicated, dissociation reactions occur in $L1_2$ and $L1_0$ alloys. However, in contrast to FCC metals, dislocations in these ordered alloys can dissociate in rather complex ways due to the availability of stable stacking faults and anti-phase boundaries in various crystallographic planes. As a consequence, the ordered inter-metallic alloys exhibit perhaps the most interesting core effects in dislocation mobility. These have been reviewed extensively in volume 10 of this series.

2.2 Mobility

The common characteristic of highly mobile dislocations in FCC metals and alloys is a clear reflection of the common core structure of these dislocations. Atomistic calculations show that in FCC metals the Peierls stress is of the order of 100 MPa or lower for dislocations of all characters [6]. Correspondingly the value of the Peierls barrier is of the order of $\sim 0.005\text{eV/b}$. Therefore, even modest thermal agitation at low temperatures should be sufficient to surmount such a small barrier. For this reason the kink mechanisms that are so important in materials with high lattice resistance to dislocation motion (see the following sections) are not expected to play a major role in FCC metals. Molecular Dynamics (MD) simulations also reveal that at room temperature dislocations do not move in a fashion consistent with kink mechanisms; they continuously undergo small oscillations in response to thermal fluctuations. The resulting mobility is so high that in laboratory measurements it would be difficult to extract the intrinsic lattice resistance to dislocation motion where various extrinsic effects, such as dislocation-impurity interactions, are generally present. Indeed, experiments on very pure single crystals of Cu show that the yield stress essentially vanishes with increasing sample purity [7].

The reason for the low intrinsic resistance is generally the extended and planar nature of the dislocation core combined with the reduced Burgers vector of the partial dislocations. In addition to extension by dissociation, the core of partial dislocations is also planar and rather wide. It is exactly for this situation that the well-known model of Peierls and Nabarro (PN) was initially developed. This model relates resistance to dislocation motion to variations of dislocation energy as a function of the dislocation character reflecting periodicity of the host lattice. The energy is assumed to consist of two parts, an elastic strain energy stored in the two half-crystals, and a non-linear misfit energy γ due to bond distortions across the plane in which the
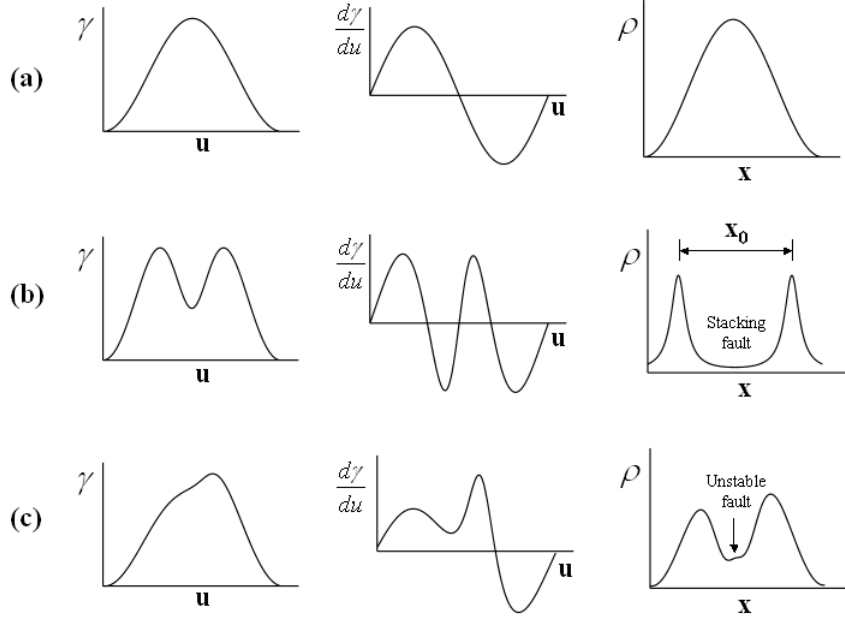
Figure 2: The generalized stacking fault energy $\gamma(u)$, its derivative $f(u) = d\gamma(u)/du$ and the distribution of Burgers vectors $\rho(x)$, whose relationship is given in Eq. (3). (a) A single peak in $\gamma(u)$ corresponds to a perfect (non-dissociated) dislocation. (b) A local minimum in $\gamma(u)$ corresponds to the stacking fault region of a dissociated dislocation. (c) Fractional dislocations bounding an unstable stacking fault.

core spreads. Suppose we consider the dislocation to be spread out in the x-z plane with the dislocation line running along the z-axis, and the displacement **u** oriented parallel to the Burgers vector **b**. The dislocation is represented by a continuous distribution of inter-planar misfit across the special plane given by the density of a continuous dislocation distribution $\rho(x) = du/dx$, normalized to the magnitude of the Burgers vector,

$$\int_{-\infty}^{\infty} \rho(x)dx = b \ . \tag{3}$$

The solution appears from a balance between the stress induced by $\rho(x)$ and

the restoring force $f(u) = -d\gamma/du$,

$$A \int_{-\infty}^{\infty} \frac{\rho(x')}{x - x'} dx' = -d\gamma/du = f(u) \quad (4)$$

where A is an appropriate constant and γ is assumed to be a periodic function of u. The function $\gamma(u)$ is usually referred to as the generalized stacking fault energy, or γ-surface. Mathematically the model can be viewed as a Hilbert transform between $\rho(x)$ and $f(u)$; given $\gamma(u)$ one can find $\rho(x)$ and vice versa. Fig. 2 shows three possibilities[1], a perfect dislocation (a) expressed by a single peak in $\gamma(u)$, a dislocation split into two partials with a stacking fault in between (b) showing a local minimum in $\gamma(u)$, and a dissociated dislocation with an unstable stacking fault (c) with some structure in $\gamma(u)$ but no local minimum. In case (c), one has two fractional dislocations with no well-defined stacking fault in between.

Based on the Peierls-Nabarro (PN)model, estimates of the Peierls stress τ_{PN} have been given for various materials [8, 9, 10, 11, 12, 13]. According to this model [9, 10], a wide core combined with a reduced Burgers vector should result in a reduced Peierls barrier. A similar relationship seems to hold for dislocation kinks: one extreme illustration was given in [13] where kinks on dissociated dislocations in Cu were examined. The kinks were found to have widths of the order of 50b. Fittingly, the barrier for kink migration was so small that a value could not be determined. The reported upper bound estimate of the migration barrier was only 10^{-6} eV showing that the description of dislocation mobility in terms of kink mechanisms is hardly appropriate in FCC metals.

It was noticed earlier that the interaction between partials can lead to further reduction of the lattice resistance to dislocation motion. Benoit et al [14] observed that, depending on the balance between inter-partial repulsion and SF attraction, the distance between the partials may become incommensurate with the periodicity of the Peierls potential. Under such conditions, dislocation mobility can be further reduced by the partials overcoming the Peierls barrier in an anti-phase manner. That is, while the leading partial is scaling up the barrier the trailing partial is already on the descending slope and vice versa. On the other hand, when the equilibrium distance is commensurate with the Peierls potential, the partials have to climb up the barrier

---

[1]Based on a lecture by V. Vitek at the Tri-Lab Short Course, "Dislocations in Materials", June 8-10, 1998, Lawrence Livermore National Laboratory, Livermore, CA.

13

simultaneously. This idea was further explored and quantified by Schoek [15] and Nabarro [12]. Specifically, when the separation between the partials are incommensurate with the Peierls potential, the effective Peierls stress becomes much smaller than that in the commensurate case, and acquires an exponential dependence similar to the original P-N formula. Nabarro [12] thus explains the above mentioned controversy by arguing that it is the dislocations with partial separations at a half-integral multiple of the Peierls valley spacing that controls the flow stress and Harper-Dorn creep experiments. This is due to the fluctuation of the internal stresses which cause the fluctuation of the partial separation, and the fact that the least strongly pinned dislocations control the experiment. On the other hand, the Bordoni peak experiments probe all the segments of the dislocation network, and the signal is not affected much by the internal stresses. Thus, the measurements agree better with Huntington's expression.

We note in passing that, in most FCC metals, such a coupling between the partials is expected to have a minor effect on dislocation mobility given that the lattice resistance to dislocation motion is very small in the first place. Such dynamic couplings are more likely to play a role in materials with high Peierls stress, such as silicon, as will be discussed in Section 3.

At temperatures that are not too low, dislocation mobility is controlled by various modes of dislocation-phonon interaction commonly referred to as phonon drag [16, 17]. MD simulations of dislocation motion in FCC metals are relatively straightforward and allow direct calculations of the drag coefficient [18, 19], which is the ratio between applied stress and dislocation velocity. In addition to high mobility, dislocation motion was observed to involve "breathing modes" in which the separation between two partials varies in time in a quasi-periodic fashion [20]. No noticeable anisotropy of dislocation mobility between edge and screw dislocations has been observed. At temperatures about 30K and below, interaction with electrons becomes important; this aspect of the problem is beyond the reach of MD simulations.

Because the intrinsic lattice resistance to the primary $\frac{1}{2}\langle 110 \rangle \{111\}$ slip is low in FCC metals, it is mainly the interaction between dislocations with other defects that gives rise to mechanical strength of the material. For example, the formation of LC junctions by two dislocations zipping together gives rise to work hardening. At the same time, interaction between dislocations and point defects, especially impurities, is an issue of considerable practical importance, given that solution hardening is a major means for altering mechanical properties of alloys. Below we discuss the effects of dis-
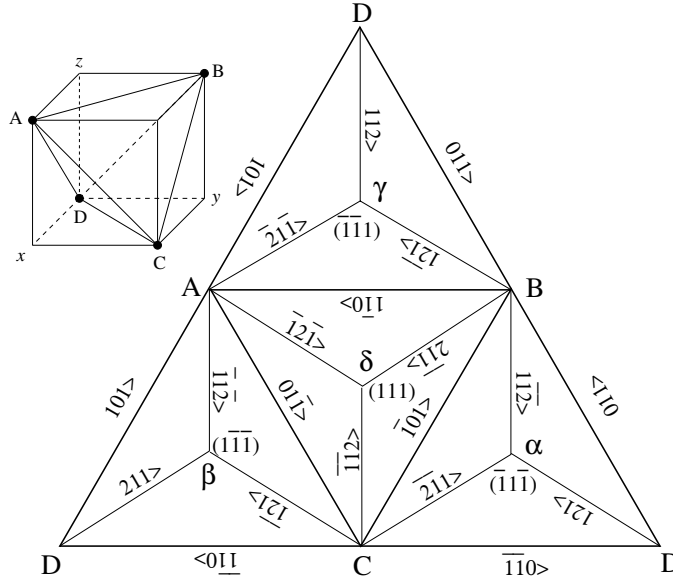
Figure 3: Thompson tetrahedron notation for FCC slip systems.

location interactions with other defects on its mobility in FCC metals and alloys.

2.3 Junctions

Interactions between dislocations result in the formation of junctions. The constraining effect of dislocation junctions on dislocation motion becomes increasingly more important with increasing strain. In FCC systems, junctions are formed in the collisions of two dislocations gliding on different {111} planes. For the description of dislocation reactions in FCC metals, the Thompson tetrahedron, shown in Fig. 3 [5], is helpful. Pairs of Roman letters represent perfect Burgers vectors, such as $AB = \frac{1}{2}[\bar{1}10]$, and Greek-Roman pairs represent partial Burgers vectors, such as $A\delta = \frac{1}{6}[\bar{1}2\bar{1}]$.

A Lomer-Cottrell (LC) junction is formed when two glissile dislocations BC on plane $d = (111)$ and CD on plane $b = (1\bar{1}\bar{1})$ collide and zip along direction AC. The reaction, expressed in Burgers vectors, is

$$BC(d) + CD(b) \quad \rightarrow \quad BD \tag{5}$$

$$\frac{1}{2}[10\bar{1}] + \frac{1}{2}[\bar{1}\bar{1}0] \quad \rightarrow \quad \frac{1}{2}[0\bar{1}\bar{1}] \tag{6}$$
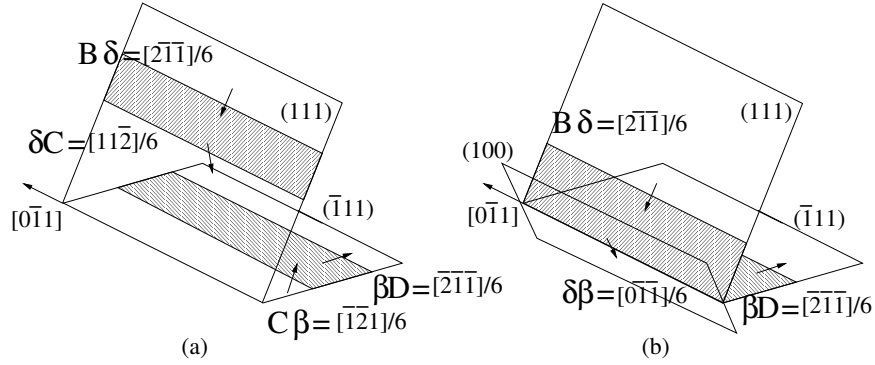
15

Figure 4: Formation of Lomer-Cottrell lock junction dislocation by reaction of two glissile dissociated dislocations.

The resulting dislocation has the same type of Burgers vector ($BD = \frac{1}{2}[0\overline{1}\overline{1}]$) as the incoming dislocations. But, because it is aligned along direction $AC = [01\overline{1}]$, its glide plane is (100). To appreciate the core structure of the LC junction dislocation, we note that both incoming dislocations are dissociated,

$$BC = B\delta + \delta C \tag{7}$$
$$CD = C\beta + \beta D \tag{8}$$

As shown in Fig. 4, the leading partials of the incoming dislocations react, thus forming a stair-rod dislocation through the reaction,

$$\delta C + C\beta \rightarrow \delta\beta \tag{9}$$
$$\frac{1}{6}[11\overline{2}] + \frac{1}{6}[\overline{1}21] \rightarrow \frac{1}{6}[0\overline{1}\overline{1}] \tag{10}$$

The resulting stair-rod dislocation has a Burgers vector exactly 1/3 of that of the LC junction dislocation and lies on the same (100) glide plane. From Fig. 4(b) it is easy to see that the LC dislocation is difficult to move because it is dissociated into two {111} planes that are inclined with respect to its own glide plane (100). This is supported by direct atomistic calculations that predict that the Peierls stress of extended junction locks in Ni is of the order of 10GPa [21, 22]. The core structure of the LC junction is shown in Fig. 5.

Recently, several large-scale atomistic simulations on dislocation junction in FCC metals [21, 23, 24] have shown that the junction energetics computed
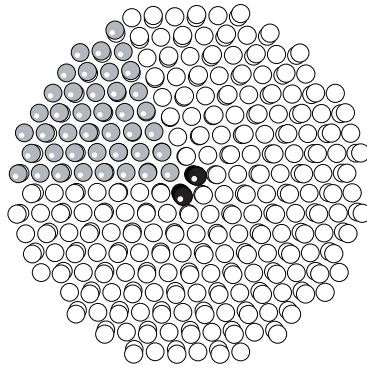
16

Figure 5: Core structure of LC junction dislocation [21] viewed along $[10\bar{1}]$ junction line. The junction (black atoms) appears at the intersection of two stacking faults resulting from two intersecting partial dislocations, each of a mixed, 30° character with respect to the junction line direction. In terms of atomic displacement, the combination of the two partials is equivalent to carving out a triangular wedge (grey atoms) and displacing the wedge matter away from the junction by $1/6[\bar{1}0\bar{1}]$ and along the junction line by $1/4[10\bar{1}]$.
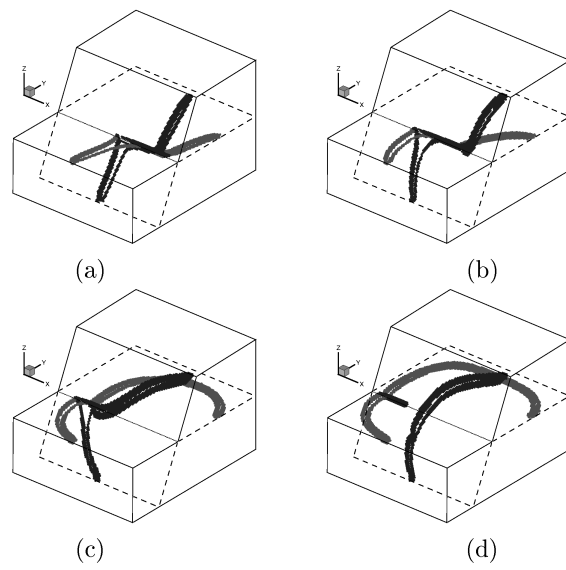
Figure 6: Unzipping of LC lock under increasing stress [23]. Stress is (a) 0.0μ, (b) 0.011μ, (c) 0.018μ, just before the junction breaks, and (d) 0.018μ at the end of the simulation.

from atomistic simulations [23] can also be accurately reproduced using a continuum model of dislocations, such as in dislocation dynamics (DD) [24]. Remarkably, two separate simulations [23, 24] agreed not only in the general appearance and strength of the Lomer-Cottrel (LC) junctions in Al but also in the fine details of junction configurations. The conclusion reached in this study was that the core does not contribute appreciably to the energetics of junction formation and destruction as long as these processes proceed through the zipping-unzipping mechanisms. The same conclusion was earlier made by Friedel [25] and confirmed in [21]. However, here we note that the sessile nature of the LC junction is another very strong effect of the core structure on dislocation mobility. In the above studies, the junction dislocation never moves in its nominal (100) glide plane; the only motion that is taking place is the translation of the triple nodes along the intersection line (Fig. 6). The junction strength against unzipping is defined as the stress at which the length of the junction dislocation reduces to zero, i.e. when the junction fully unzips. Assuming that the LC junction is completely sessile in the first place (a strong core effect), the critical stress to unzip the junction can be described quite accurately by continuum models (i.e. without any core contribution). If, on the other hand, the LC junction could move in its glide plane in response to, possibly large, stress, the dislocation core would have a large effect on the lattice resistance to the junction motion. This possibility will be discussed shortly.

An interesting consequence of junction zipping and unzipping was uncovered in [21]. This is the mechanism of "junction replacement" involving three dislocations. Initially, a pair of dislocations was observed to form a LC junction that unzips at a later stage in favor of a new, stronger junction, formed in a collision of one of the first two dislocations with a third dislocation. This observation suggested an interesting unit mechanism of "survival of the fittest" by which the distribution of junction strength is gradually shifted, in the course of strain hardening, towards stronger and stronger junctions. This is also a mechanism by which dislocation fluxes can effectively propagate through various elements of the hardening microstructure, e.g. dislocation bundles or cell walls, so that dislocations incorporated in a bundle or wall are released by incoming dislocations with the same Burgers vectors.

Let us now examine in more detail the core structure and its possible effect on the mobility of LC junctions. Consider the core shown in Fig. 4(b). It has been predicted that the equilibrium configuration of this complex core should be asymmetric, with one of the two stacking faults more extended

19

than the other [26]. Indeed, such an asymmetric configuration was observed in silicon by HREM [27]. Because the symmetry can break in two ways, the ground state core structure becomes doubly degenerate. This, as always, brings about a possibility of special point defects that can form at the boundary between two alternative core variants. In the following we will often refer to such zero-dimensional objects as reconstruction defects (RD). This fine structure of the core can affect the lock strength in the sense that lock dislocations may be able to move under stress, contrary to the commonly accepted notion of their sessile nature. This is because the extent of non-planar dissociation at the RD is significantly reduced compared to the rest of the LC dislocation: this local constriction creates a soft spot for possible mobility initiation on the {100} plane. Another possible way for "sessile" locks to move is nodal mechanisms. We note that one of the triple nodes on the LC junction can become fully or partially constricted. If so, the lock dislocations can respond to stress by moving this triple node in the plane containing the lock's Burgers vector. That the locks can be removed was actually reported based on a series of TEM observations [28]. This three-dimensional nature of dislocation junctions and locks is an interesting venue for further study.

2.4   Cross-slip

Cross-slip and climb are two mechanisms enabling dislocations to leave their glide planes. However, at low and moderate temperatures where climb is not operational, cross-slip of screw dislocations is the only means by which dislocation motion can spread to adjacent glide planes. In FCC systems, because of the planar dissociation into the Shockley partials, dislocations are confined to {111} planes in which they dissociate. Even if a dislocation is locally in a screw orientation, the planar dissociation confines it to move in the dissociation plane. Only rarely does some special event (cross-slip) takes place so that a dissociated screw dislocation changes its dissociation plane from the original glide plane to the cross-slip plane. In fact, in pure Al, where the SF energy is high and dissociation is largely suppressed, the confining effect of the {111} planes is greatly diminished and slip in planes other than {111} is observed [5](p. 272). Consequently, cross slip in Al is expected to occur much more frequently than in other FCC metals with lower SF energy, such as Cu or Ag.

Two mechanisms, namely Friedel-Escaig (FE) and Fleischer (FL), have been proposed so far for dislocation cross slip in FCC metals, and are illus-
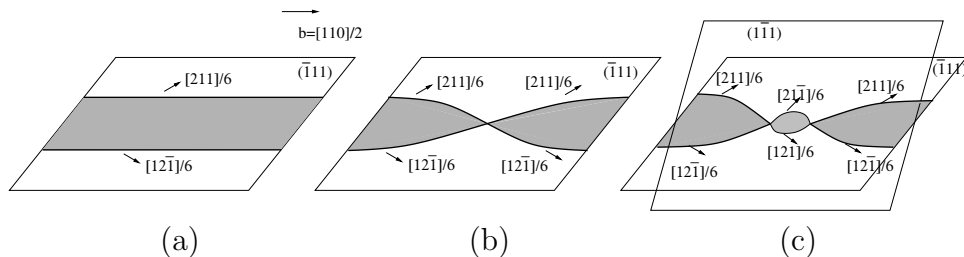
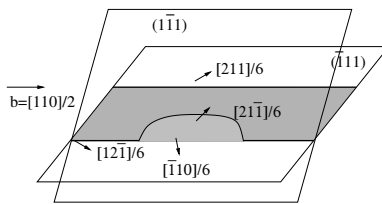Figure 7: Friedel-Escaig mechanism of dislocation cross-slip in FCC metals.

Figure 8: Fleischer mechanism of dislocation cross-slip in FCC metals.

trated in Fig. 7 and 8, respectively. The FE mechanism, which has received wide attention, involves constriction of two partials in the initial glide plane followed by re-dissociation into the cross-slip plane. In Fig. 7(a), a screw dislocation with total Burgers vector $\frac{1}{2}[110]$ is initially dissociated in $(\bar{1}11)$ plane, with the Burgers vectors for leading and trailing partials being $\frac{1}{6}[211]$ and $\frac{1}{6}[12\bar{1}]$, respectively. In Fig. 7(b), the two partials are shown to constrict to a point, assisted by thermal fluctuation and, possibly, local stress. Finally, in Fig. 7(c) the dislocation re-dissociates in $(1\bar{1}1)$ plane at the constriction point into two different partials, $\frac{1}{6}[21\bar{1}]$ and $\frac{1}{6}[121]$ respectively.

Although the FE mechanism has become widely accepted, until recently there has been no conclusive data to support its validity, except some indirect experimental evidence [29]. Recently, the mechanism of cross-slip in FCC Cu was examined in full atomistic details [30, 31, 32]. The FE cross-slip mechanism was shown to have a reasonably low activation barrier, especially if cross-slip is initiated at a pre-existing jog. Although the activation energy for the FE mechanism is seemingly in agreement with experimental estimates, some uncertainty still exist since the Fleischer (FL) mechanism of cross-slip may be a viable alternative to FE.

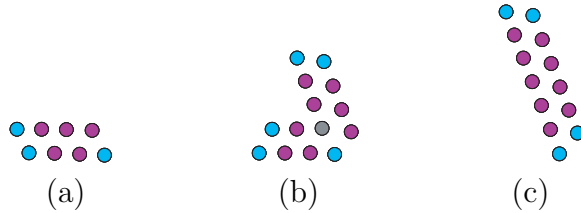In the FL mechanism, dislocation constriction is not required. As shown

Figure 9: Fleisher mechanism of dislocation cross slip in FCC Al observed in atomistic simulations. Atoms are shaded according to the so called centro-symmetry deviation (CSD) parameter. Only atoms with CSD significantly different from zero, i.e. local packing different from perfect FCC are shown.

in Fig. 8, a small segment on the trailing partial emits a small area of stacking fault in the cross-slip plane. In the cross-slip plane, this stacking fault is bounded by the leading $\frac{1}{6}[21\bar{1}]$ partial on one side and a $\frac{1}{6}[\bar{1}10]$ stair rod on the other. As the stacking fault in the cross-slip plane expands, the stacking fault on the original plane contracts around the stair rod dislocation. The leading $\frac{1}{6}[211]$ partial in the original plane eventually combines with the stair rod dislocation and forms the trailing $\frac{1}{6}[121]$ partial which is now ready to glide on the cross-slip plane. The end result is exactly the same as that shown in Fig. 7(c) but the atomic pathway is very different from the FE mechanism.

The FL mechanism was observed [33] in atomistic simulations of stress driven cross-slip in FCC Al, using the Ercolessi-Adams potential [34]. Fig. 9 shows the dislocation core structure before, during and after the cross-slip event. Only atoms with local packing significantly different from that of FCC are shown, indicating the position of stacking faults and partials. The simulation is quasi 2-dimensional in that the simulation cell is periodic along the dislocation line. In this case, the entire dislocation line undergoes cross-slip simultaneously, which is not exactly the same as the FL mechanism as shown in Fig. 8. Nonetheless, the cross-slip pathway clearly does not involve constriction and the non-planar core structure observed during the transition is in agreement with the FL mechanism. The core structure of the dislocation undergoing cross-slip via the FL mechanism resembles that of the Lomer-Cottrell dislocation junction, where the dislocation core dissociates into two {111} planes, bounding a stair-rod dislocation.

The above simulation was performed at zero temperature under shear stress τ applied in the plane perpendicular to the original glide plane. Cross-

slip occurs when τ reaches 1.4GPa. This is suggestive that the FL mechanism may become more favorable under high stress. On the other hand, the FE mechanism is usually considered to operate under low stress conditions. Further atomistic simulations in three dimensions can help establish the relative role of FE and FL mechanisms, but care should be taken to allow dislocations to explore a variety of cross-slip paths. In that regard, it should be noted that the simulations [32] that revealed the FE mechanism relied on the so called Nudged Elastic Band (NEB) method for finding a low energy pathway. Principally, the latter method is unable to sample transition paths that deviate significantly from the initial trial (or guess) path, which is usually taken as a straight line (in multi-dimensions) connecting the initial and final states. In [30, 31, 32] the initial and final states chosen for the NEB method favor the FE mechanism by symmetry.

2.5   Interaction with point defects

In this subsection we discuss a few recent results revealing the mechanisms of dislocation interaction with point defects and clusters in FCC metals. The classical theory predicts dislocation mobility to be highly sensitive to the nature of impurities, their concentration and mobilities. A variety of interaction mechanisms have been discussed in the context of Cottrell, Suzuki and Snoeck atmospheres [5](p. 639). Although generic aspects of interaction between substitutional impurities and dislocations are well understood, computational capabilities for predictive modeling are still lacking.

The problem of dislocation - point defect interaction is complex. The simplest case is probably the interaction with a substitutional atom at a large distance away from the dislocation. In this case, electronic structure calculations can be used to compute the size and stiffness misfit associated with the alloying impurity atoms [35]. This information can then be used in an elastic model to obtain the hardening effect of the impurity due to its long range interactions with dislocations.

When point defects are mobile, or they happen to lie on the path of a moving dislocation, it becomes important to account for their short-range (core) interactions. In this case, it is necessary to study systems with a large number of atoms, which are beyond the reach of accurate electronic structure methods. Direct MD simulations of the type presented in [36] in the context of pipe diffusion can be employed for the purpose. As we are forced to use molecular dynamics methods with empirical potentials, the major difficulty
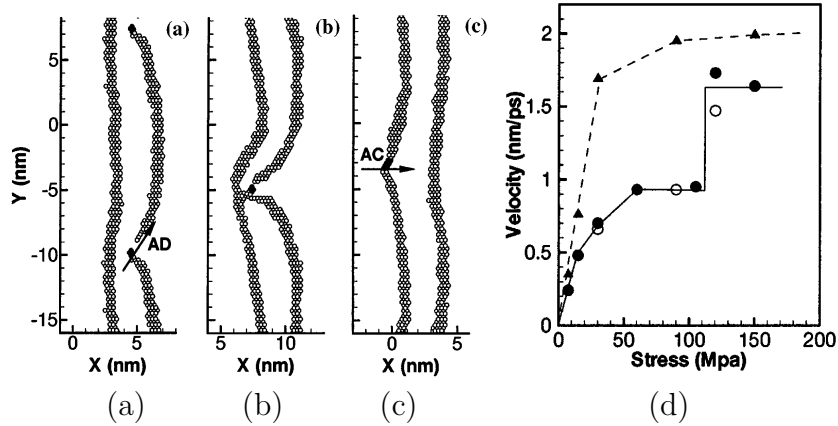
Figure 10: (a),(b),(c) MD snapshots of edge dislocation interaction with an interstitial loop in Ni. (d) Dislocation velocity as a function of stress. The dashed curve corresponds to free dislocation at $T = 100K$. Solid curve is for dislocation with an attached interstitial loop, with empty symbols for $T = 10K$, full symbols for $T = 100K$ [18].

is of course the notorious inaccuracy or, often, complete lack of interatomic potentials for atom-atom interactions in metals and alloys.

Considerable progress has been achieved recently in direct Molecular Dynamics modeling of dislocation interaction with interstitial and vacancy clusters in FCC metals Ni and Cu, for which reasonable interatomic potentials do exist [18, 37, 38]. Both vacancy and interstitial type defects were found to serve as pinning obstacles to dislocation motion and, in the short-range collisions, to be partially or completely absorbed or transformed. These mechanisms are especially important for understanding the mechanical behavior of irradiated materials where collision cascades produce a large number of displaced atoms whose subsequent motion results in gradual evolution of radiation-induced defect microstructure, from Frenkel pairs to a distribution of defect clusters. These defects offer considerable resistance to dislocation motion and are thought to harden or even shut down dislocation multiplication leading to a characteristic upper yield behavior followed by a sharp stress decrease at the lower yield point. At this point considerable shear localization is observed in the form of clear channels [39]. Shear localization results in high stress concentrations at the grain boundaries and can eventually lead to crack initiation.

24

The interaction between a moving edge dislocation and a small self-interstitial (SI) loop is considered in [18]. A four-interstitial cluster is introduced away from the glide plane of the dislocation. The interstitial cluster then relaxes into a prismatic dislocation loop that is highly mobile in the direction along its Burgers vector. The loop is observed to move to the glide plane of the dislocation and react with the leading partial. After the reaction, the loop flips its Burgers vector to direction AD, which is in the dislocation glide plane, but at 60° degrees to the dislocation Burgers vector, as shown in Fig. 10(a). This interstitial loop acts as a dragging point impeding dislocation motion. Fig. 10(d) shows the dislocation velocity as a function of stress with and without the attached interstitial loop. When the dislocation is free from the loop, its velocity is linear in stress at small stresses, with a friction coefficient $\nu_0 = \sigma b/v = 5 \times 10^{-6} \mathrm{Pa} \cdot \mathrm{s}$ $(T = 100K)$. At higher stress the velocity function bends and reaches a plateau at about 72% of the transverse sound wave velocity (2.9nm/ps). This behavior is similar to that of the edge dislocation in BCC metal Mo [40] (see Section 4).

When the loop is attached to the dislocation, as in Fig. 10(a), it increases the friction coefficient to $\nu = 8 \times 10^{-6} \mathrm{Pa} \cdot \mathrm{s}$ at low stresses. The dislocation velocity also saturates at a lower velocity of 0.9nm/ps. This appears to be in line with the fact that motion direction of the loop is at 60° degrees to that of the dislocation line, so that the terminal velocity of the dislocation with the loop attached is limited to half of that of a freely gliding dislocation. Upon further increase of stress, the trailing partial catches up with the leading one, as shown in Fig. 10(b). More core reactions take place resulting in the loop attachment to the trailing partial, with its Burgers vector rotated again in the direction AC, parallel to the direction of motion of the dislocation [Fig. 10(c)]. This allows the dislocation to resume motion at a higher speed, as shown in Fig. 10(d).

The vacancy clusters in irradiated FCC metals are found to form stacking fault tetrahedra (SFT) (see [41] and references therein). The interaction between an edge dislocation and a SFT is examined in [38]. Fig. 11 shows a series of MD simulation snapshots (in a near $[\bar{1}11]$ projection) of the interaction between a moving, dissociated edge dislocation and a perfect SFT that lies on its path. The simulation was performed at an initial temperature of 100K and under applied shear stress of 300MPa. Fig. 11(a) is a snapshot showing the edge dislocation dissociated into two Shockley partials and the SFT at $10ps$ after applying the stress. The next snapshot taken at $19.5ps$ shows the leading partial that has just bypassed the SFT shear-
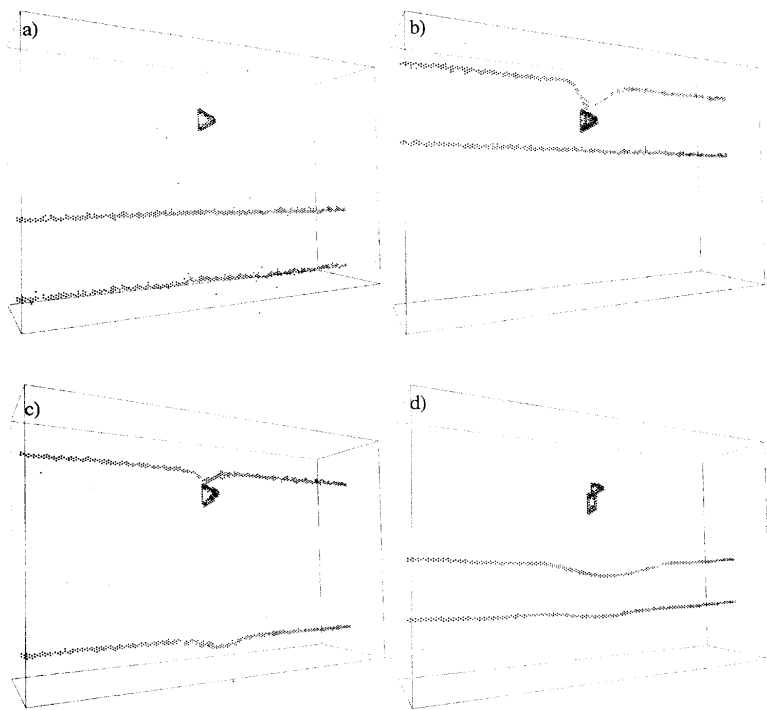
25

Figure 11: MD snapshots of edge dislocation interaction with a perfect SFT in Cu at (a) 10ps, (b) 19.5ps, (c) 23.3ps and (d) 115.0ps.

ing its top by $a/6\langle 112 \rangle$ in the process. The SFT is seen to act as a strong but shearable obstacle whose strength is expressed by the cutting angle of $\sim 80°$. At $23.3ps$ the trailing partial passes through the SFT that offers now significantly less resistance (Fig. 11(c)). Taking advantage of the periodic boundary conditions, the simulation was continued long enough to allow the dislocation to cut through the SFT five more times. Notably, the SFT was neither destroyed nor absorbed. Although considerably sheared, it remains largely intact (Fig. 11(d)). Qualitatively similar behavior was observed in other simulations performed in a range of applied stress from 50 to 300 MPa for varying SFT positions with respect to the glide plane. In all cases, the initially perfect SFT acts as a strong barrier that, although considerably sheared, remains intact following the dislocation passage.

However, a totally different behavior was observed in the case where the SFT is not initially perfect but consists of two overlapping, truncated SFTs [38]. The latter configuration has been predicted in the earlier MD and kMC simulations [42] and is more consistent with HREM images. It was found that upon contact the leading partial absorbs vacancies making up a part of the truncated SFT and climbs, forming a pair of superjogs that effectively pin this dislocation. The trailing partial eventually catches up with the leading partial, climbs and absorbs the remaining vacancies, and constricts with the leading partial at the superjogs. After that the constricted and jogged partials move together albeit with a decreased velocity. Eventually the climbed dislocation segment is seen to dissociate into separate partials again, apparently after spewing out a vacancy cluster from one of the superjogs. Although the detailed mechanism of SFT absorption has not been fully analyzed, it is clear that both perfect and truncated SFT offer considerable resistance to dislocation motion.

Similar dislocation climb behavior resulting from defect absorption was observed in [37] in molecular static simulations of the interaction between edge dislocations and self-interstitial clusters in Ni. In that case of course the dislocation climbs in the opposite direction. One of the superjogs produced after collision is initially constricted, presumably in the form of a Lomer segment. This superjog is sessile but can transform to a glissile configuration through the incorporation of three self-interstitials, as discussed in [37]. This mechanism could explain the vacancy cluster left by the superjog in the above simulation of dislocation - SFT interaction [38].

Recent TEM observations suggest that screw dislocation in irradiated FCC metals move faster than edges, and that the screws seem more effective

27

in both absorbing and producing the point defects [43]. In light of these observations it appears important to undertake a study similar to the one described above but for screw dislocations.

2.6 Outstanding issues

A number of outstanding issues concerning core effects on dislocation mobility in FCC metals and alloys could be mentioned. Mobility of dislocations containing extended jogs is one example. Unpinning from such obstacles involves, in some cases, non-conservative mechanisms that produce or absorb point defects or clusters. This may be true not only for screw dislocations but also for non-screws that are sometimes observed to engage in non-conservative processes [37]. Mechanisms of screw dislocation motion under high stress are poorly understood. In view of experimental indications that fast moving dislocations produce a large amount of debris [43], it appears possible that cross-slip mechanisms at high stress are very different from those at low stresses. The latter too may be a more complicated phenomenon than is currently recognized; continuum elasticity estimates and atomistic simulations both suggest that multiple mechanisms of cross-slip are likely to operate even under low stress conditions. The effect of junction nodes on the mobility of dislocations entering the node is interesting, due to the possibility of allowing glide of otherwise sessile dislocation junctions, such as extended LC locks. Finally, a major challenge for dislocation modeling is an accurate and realistic description of interactions between moving dislocations and impurity atoms and clusters. Such a description can provide the basis for understanding the thermodynamics and kinetics of co-evolution of dislocation and alloy microstructures.
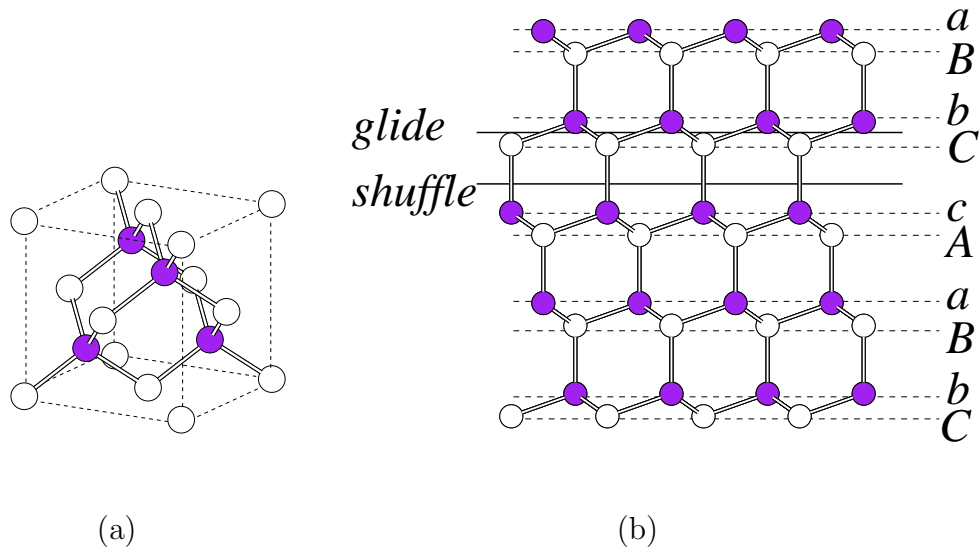
Figure 12: Diamond cubic structure of Si lattice. The two inter-penetrating FCC lattices are shown as white and black atoms, respectively. (a) A primitive cell of the diamond cubic lattice. (b) Glide and shuffle sets of (111) planes.

3 Diamond-Cubic Semiconductors

3.1 Introduction

For over 40 years dislocations in semiconductors, especially in silicon, have been an active field of research driven by the need for a better understanding of defect behavior in electronic components. At the same time, the relative ease of growing high purity single crystals with zero dislocation content makes silicon an ideal test-bed material for experiment, theory and modeling. The nucleation and migration of dislocations are of fundamental concern because their electrical activity can seriously degrade device functionality.

To a considerable extent, dislocation behavior is determined by the structure of the host crystal lattice. Here we focus on the group with diamond cubic structure among which are elemental Si and Ge and zinc-blende III-V (GaAs) and II-VI (InP) compounds. The structure of diamond cubic lattice,
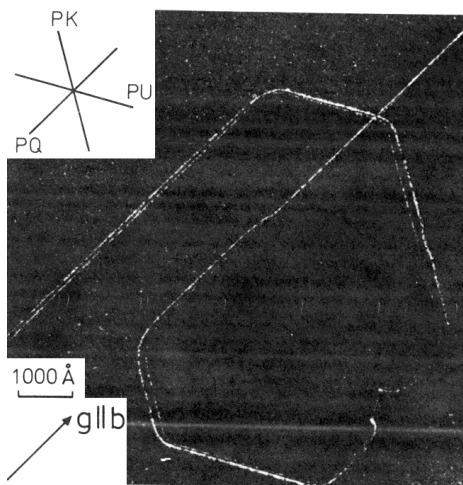
Figure 13: Weak beam micrograph of a dissociated loop in silicon [44] deformed for 45 min at $T = 420°C$ and $\tau = 256$MPa.

consisting of two inter-penetrating face-centred-cubic (FCC) lattices offset by $\frac{1}{4}[111]$ is shown in (Fig. 12(a)). A zinc-blende structure is obtained when the two sub-lattices are occupied by different atoms, such as Ga and As. The slip systems in diamond-cubic crystals are the same as in FCC metals (see the preceding section), i.e. $\frac{1}{2}[110](111)$. However, due to the coexistence of two FCC sub-lattices, there are two different sets of (111) planes (Fig. 12(b)). The closely spaced set, e.g. between atom layers b and C, is called the *glide* set. The widely spaced set, e.g. between atom layers C and c, is called the *shuffle* set. The set of (111) planes on which dislocations reside and move has been a topic of controversy for over forty years.

Stable stacking faults can exist only in the glide set. TEM observations have produced ample evidence that dislocations in DC crystals are dissociated both in motion and at rest, at least in the usual range of experimental conditions (e.g. $T = 800 \sim 1000$K, $\tau = 1 \sim 1000$MPa). A typical weak-beam micrograph is shown in Fig. 13. This and other similar observations have been used to argue for the preference for dislocations to reside on the glide rather than the shuffle set, on the grounds that by dissociating into partials, a dislocation reduces its elastic energy. However, a more detailed analysis shows that core reconstruction of the partial dislocations also has to be taken into account. At moderate temperature and strain the disloca-
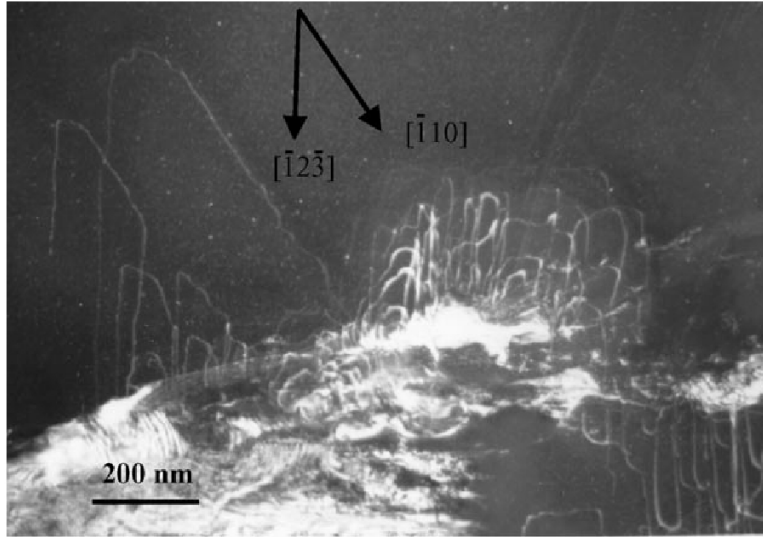
Figure 14: Dislocation microstructure at room temperature and under confining pressure of 5GPa. The dislocations are mostly aligned along [110] and [123] directions [45].

tions are observed to form hexagonal loops, as in Fig. 13. In these loops the dislocations line up along the [110] directions which suggests a high Peierls barrier for the motion of 0° (screw) and 60° (mixed) dislocations.

Recently non-dissociated dislocations have been observed after deformation at low temperature and under high confining pressure. The TEM micrograph in Fig. 14 shows perfect dislocations aligned along the [110], [112] and [123] directions. The latter two directions have not been seen previously in the conventional experiments, suggesting a different core structure under large pressure. The observation of wavy slip traces is still another indication that the observed dislocations cross-slip frequently and therefore are likely to be non-dissociated. All this evidence points to a transition from glide to shuffle core occurring under low-temperature, high-stress deformation conditions. This topic will be discussed in light of the atomistic simulation results presented below.

Fig. 15 shows a typical set of stress-strain responses of silicon single crystals at several test temperatures. A common feature is a pre-yield peak followed by a post-yield drop. This transient behavior reflects the delayed
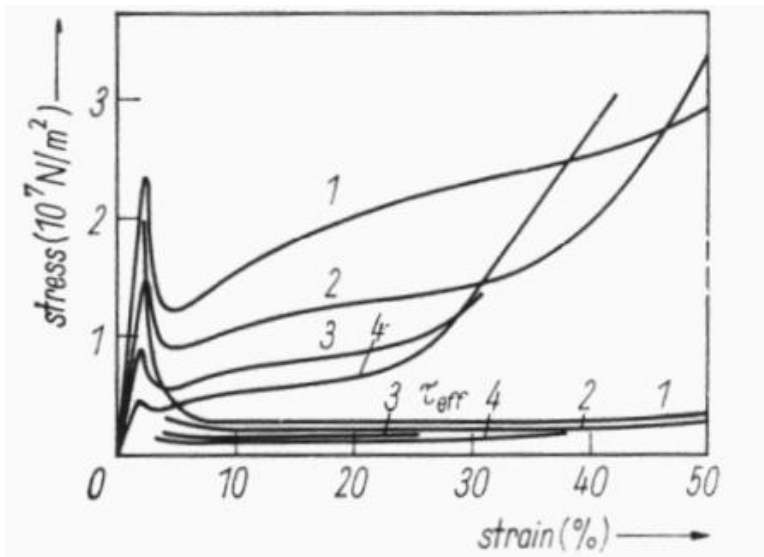
31

Figure 15: Stress-strain curve of Si for strain rate $\dot{\epsilon} = 1.2 \times 10^{-4}$ and initial dislocation density $N_0 = 2 \times 10^4 \text{cm}^{-2}$. (1) T=800, (2) 850, (3) 900, (4) 950°C. The effective stress τ_{eff} is also plotted, which is the external stress minus the (estimated) internal stress due to mutual interactions between dislocations [46].
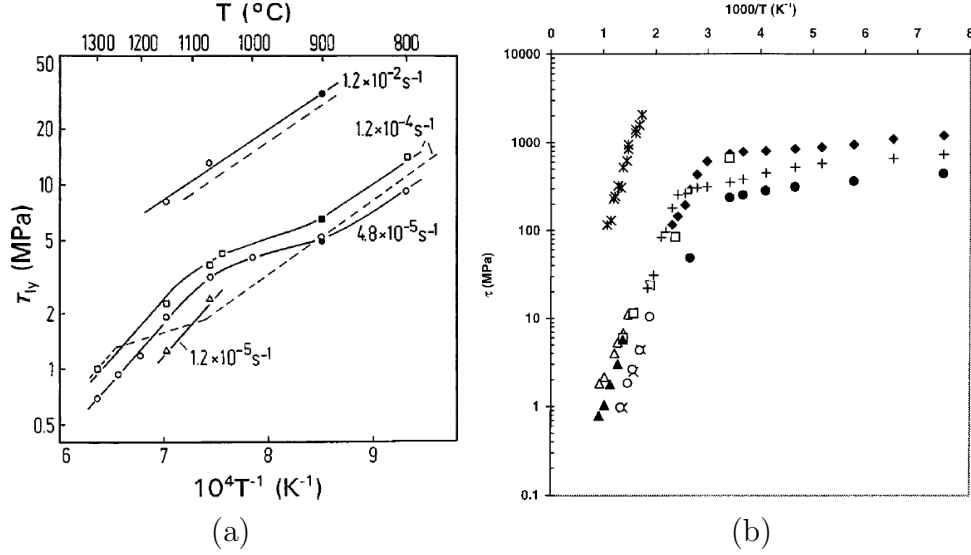
Figure 16: (a) Lower yield stress as a function of temperature for dislocation free Si samples [48]. (b) Yield stress of Si (∗), GaAs ($\square, \blacklozenge, \triangle$), InP ($+, \blacktriangle, \times$) and InSb ($\circ, \bullet$) as a function of temperature [49].

kinetics of dislocation multiplication and is a function of initial dislocation density. Eventually, the rate of dislocation multiplication settles to a steady-state flow value beyond the yield point. This stress value, called the lower yield stress τ_{ly}, is often used to characterize the plastic response of the material. It is found that over a wide range of temperatures ($T = 700 \sim 2000$K), τ_{ly} can be represented by an exponential function

$$\tau_{ly} = C_{ly}\dot{\epsilon}^n \exp(\frac{Q}{nk_BT}) \ , \tag{11}$$

where C_{ly} and n are constants independent of T and strain rate $\dot{\epsilon}$, and Q [47] is the activation energy ($Q \sim 2$eV). This observation suggests that dislocation motion and, hence, plastic deformation in silicon are thermally activated.

Deviations from Eq. (11) beyond the usual mid-temperature range have been reported recently. In particular, the effective activation energy was found to increase at temperatures above 1200K. This transition is also seen in dislocation mobility measurements although its origin remains controversial. It has been suggested that a change of self diffusion mechanism in silicon

at elevated temperatures is the cause [50, 48]. Alternatively, the effect of dislocation-dislocation interactions has been proposed as an explanation [51]. At the low temperature end, the yield deviates from the mid-temperature behavior but in a different sense; both the activation energy Q and the yield stress become lower than what Eq. (11) would predict. This low temperature behavior is observed in almost all diamond-cubic semiconductors, as shown in Fig. 16(b). The aforementioned change of the dislocation core structure from dissociated glide to perfect shuffle core is likely to be related to this macroscopic transition.

In the following we discuss the current understanding of dislocation core structure and the mechanisms of its motion. We will focus on those aspects of atomistic and mesoscopic theory and simulations that help in interpreting the experimental findings as well as give predictions.

3.2 Core structure and lattice resistance

3.2.1 Glide-set partial dislocations

Under moderate stress and temperature conditions the dislocations in silicon and other semiconductors are generally seen to stretch along the $\langle 110 \rangle$ directions forming hexagon-shaped loops on the (111) glide plane. The dislocations are dissociated into Shockley partials connected by an intrinsic stacking fault (SF), as in

$$\frac{1}{2}[1\bar{1}0] = \frac{1}{6}[1\bar{2}1] + \frac{1}{6}[2\bar{1}\bar{1}] \tag{12}$$

Given the predominant screw or 60° character of the full dislocations, the partials are either 30° or 90°, as shown in Fig 17. The SF energy can be estimated by comparing the separation between two partials observed in experiment [1] to that predicted by linear elasticity theory [5]. The resulting estimates range from 50 to $70 mJ/m^2$.

A low SF energy is usually taken to be a sufficient condition for the dislocations on the glide set to dissociate, given that dissociation lowers the elastic energy of the dislocation. However, recent atomistic calculations suggest that core reconstruction can significantly alter the energy balance of the dissociation reactions in silicon [52]. Using the Stillinger-Weber (SW) interatomic model, it has been shown that only after bond reconstruction in the cores of the two partials has taken place, does dislocation dissociation become more energetically favorable than the undissociated (perfect) state.
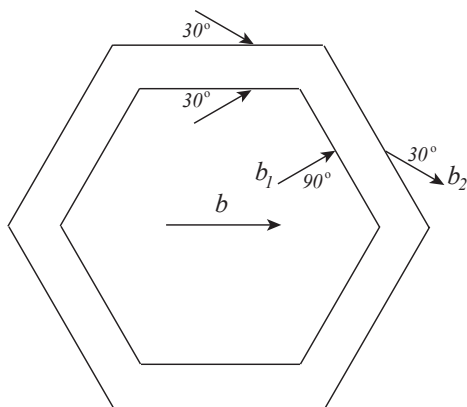
Figure 17: Preferred dislocation line directions in silicon.

That dislocations form hexagon-shaped loops by stretching under stress along the $\langle 110 \rangle$ directions is clearly a core effect. Since the elastic energy of dislocations is a smooth featureless function of the character angle and does not favor any particular character, except possibly screw, it must be the core energy or, even more likely, the anisotropy of dislocation mobility that is responsible for this behavior.

Fig. 18(a) shows two atomic layers in a perfect diamond-cubic lattice; atoms above and below the (111) glide plane are denoted by white and black circles respectively. For compound semiconductors with zinc-blende structure, the open and closed circles sites would be occupied by atoms of different species. In this projection, each atom layer forms a triangular lattice so that black atoms are situated at the centres of the white triangles. Similar to FCC metals, an intrinsic stacking faults can be formed by shifting the black atoms into unoccupied white triangles. There are three ways of doing this, as indicated in Fig. 18(a). When the boundary line between the stacking fault and the perfect lattice region is drawn along a $\langle 110 \rangle$ direction, the interface (line) becomes either a 30° or a 90° partial dislocation, depending on the angle between the line and the shift direction. Fig. 18(b) shows a 30° partial. This dislocation is produced by shifting every black atom above the line along the $\vec{b}_{30}$ direction. Fig. 18(c) shows a 90° partial obtained by shifting all black atoms above the line along the $\vec{b}_{90}$ direction. In both cases,

(a)

Stacking Fault

(b)

Stacking Fault

(c)
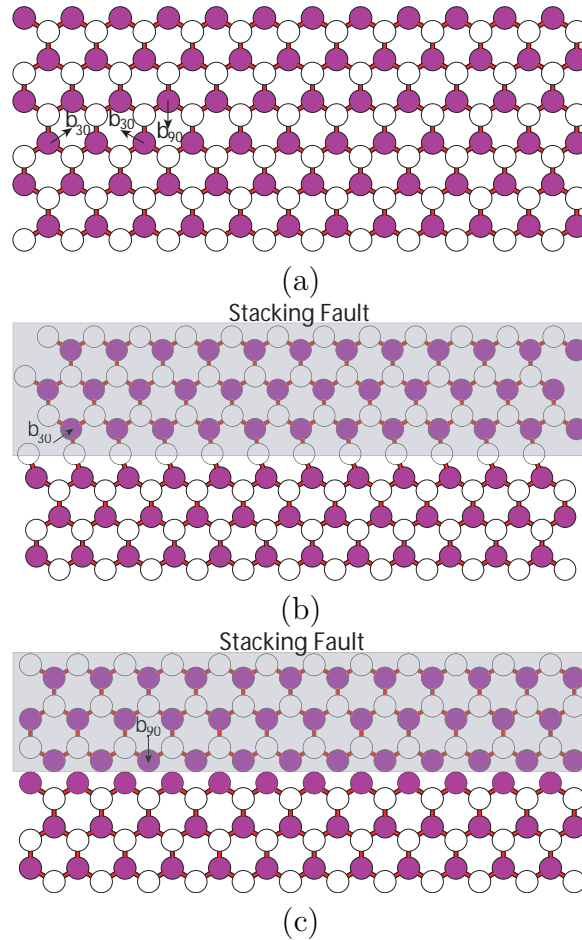
Figure 18: (a) Perfect diamond cubic lattice. Two layers of atoms, immediately above (white) and immediately below (dark) the glide-set (111) plane are shown. Each atom has four bonds, but the fourth bonds are out of the plane and are not shown. Stacking fault can be formed by dark atoms slipping into adjacent centres of the white triangular lattice in three ways. (b) The core of a 30° partial (unreconstructed), as an interface between the stacking fault and the perfect lattice. (c) The core of a 90° partial (unreconstructed).

36

the dislocation line separates the SF (top) from the perfect crystal (bottom).

It was shown that [52] a screw dislocation dissociated into two 30° partials having the core structures given in Fig. 18(b) actually may have a higher total energy than its perfect non-dissociated counterpart. Nevertheless dissociation is still favored because the cores of the partial dislocation can reconstruct to significantly reduce the final total energy. The final configuration requires some additional lattice distortions to bring the core atoms together, but this is more than off-set by a significant energy reduction associated with the pairing of the dangling bonds present in the unreconstructed cores (see Fig. 18). Removal of the dangling bonds by reconstruction is consistent with the experiments suggesting that less than 3% of the atomic sites in partial dislocation cores have unpaired orbitals [53].

In the reconstruction of the 30° partial dislocation, pairs of core atoms move towards each other to form bonded dimers, as in Fig. 19(a). As a result, the repeat distance along the dislocation core increases two-fold, from $b = \frac{1}{2}[110]$ to $2b$. *Ab initio* calculations confirm that this double-period (DP) reconstruction reduces the core energy very significantly, by 1.02eV per dimer according to [54]. Core reconstruction energies in units of eV/b from different calculations are listed in Table 1.

The 90° partial core can reconstruct in more than one way. In Fig. 19(b), two rows of atoms with dangling bonds form bonded dimers by bridging across the core. This entails some lattice distortion which, however, is more than compensated by the energy gain from the pairing of dangling bonds. The repeat distance along the dislocation line remains at b, but the mirror symmetry with respect to the plane perpendicular to the dislocation line is now broken. *Ab initio* calculations predict a lower energy gain for this single-period (SP) core reconstruction, at 0.42eV/b according to [54]. Alternatively, the dangling bonds in the 90° partial can be removed by a double-period (DP) reconstruction, such as shown in Fig. 19(c). This atomic rearrangement simultaneously breaks both mirror and translational symmetries of the unreconstructed core. Recent *ab initio* calculations [54, 55, 56, 57] show that the DP core has a slightly lower energy (by ~ 0.03eV/b) than the SP core. With the energy difference being so small, both core variants can co-exist at room temperature.

Core reconstruction is expected to have a strong influence on dislocation mobility [58], since it lowers the ground state dislocation energy and thus anchors the dislocation more strongly to the lattice. A simple measure of dislocation-lattice coupling is the Peierls stress, a minimal stress needed to
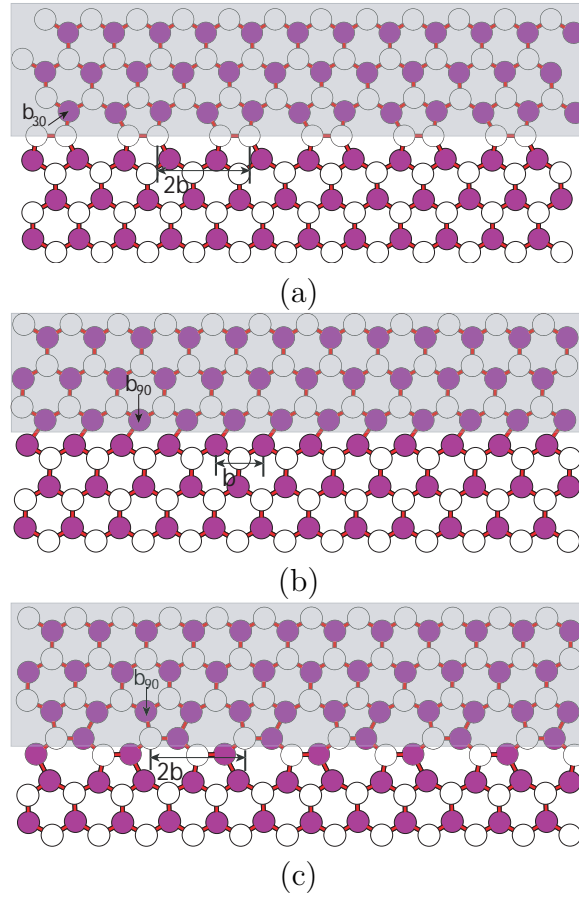
37

Figure 19: Reconstructed core structures of partial dislocations in silicon.
(a) Double-period core of 30° partial. (b) Single-period core of 90° partial.
(c) Double-period core of 90° partial.

move a straight dislocation at zero temperature. Atomistic simulations using SW potential have given [59] Peierls stress values for 30° and 90° partials at 21GPa and 17GPa, respectively; however, these results have to be taken with caution. First, the SW potential is known to have difficulty in properly describing the core reconstructions [60]. Second, the type of boundary conditions used in this study [59] has been found to have a large effect on the calculations of Peierls stress [52]. Nonetheless, it is generally accepted that the Peierls stress of the glide-set partials is quite high, of the order of 10GPa, which is consistent with the observed low mobility of dislocations in silicon and its brittle behavior at temperatures below 0.6 of the melting temperature [61]. A possible way to interpret this brittleness is to say that dislocation nucleation and propagation are insufficient to relieve the stress concentration at the crack tip [62].

Conceivably the levels of stress approaching the Peierls value for glide partials may never be achieved in a deformation experiment. This is because recent data suggest that low-temperature, high-stress plasticity is controlled by the shuffle dislocations. The highest stress of 2GPa so far achieved in the experiment [49] is in the range of the Peierls stress for shuffle partials, but is still considerably below the estimated 10GPa for the glide partials. On the other hand, the situation may change for compound semiconductors, given the strong influence of core reconstruction on dislocation mobility. As shown in Fig. 19, core reconstruction in the partials requires bonding of atoms of the same type. With the increasing polarity of compound semiconductors on going from IV-IV alloys, to III-V and II-VI compounds, the energy reduction by reconstruction is expected to decrease, and may eventually make core reconstruction unfavorable [63]. Consequently, the Peierls stress for partial dislocations may become much lower. Recent *ab initio* calculations suggest a strong relationship between the strength of partial reconstruction and the experimentally measured activation energy Q of dislocation mobility. As is shown in Fig. 20, Q decreases with increasing polarity, hand in hand with the decreasing reconstruction strength [64]. Additional complications arise in the compound semiconductors where two types of dislocation exist with two different types of atoms (e.g. Ga or As) residing in the core. The partials then may become charged, giving rise to strong electro-mechanical coupling.
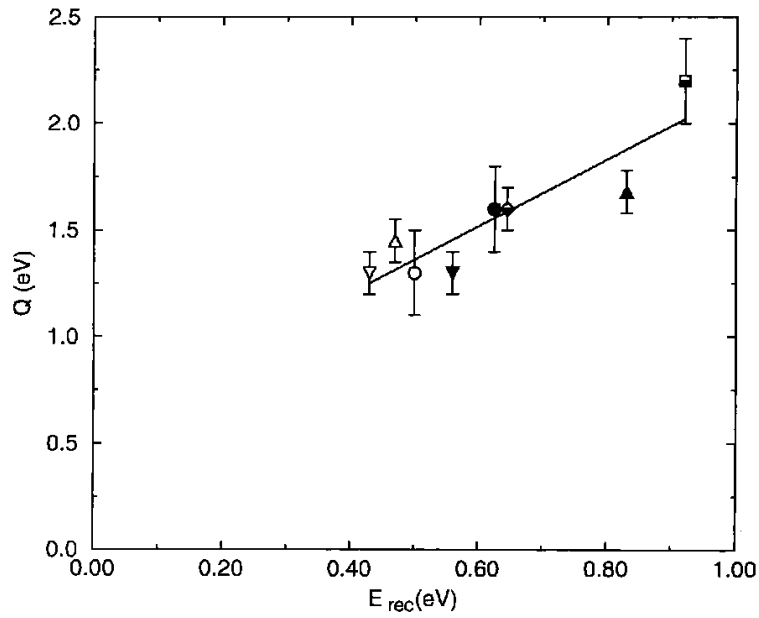
Figure 20: Calculated core reconstruction energies for 30° partials versus experimental activation energies of 60° dislocations in type IV, Si(□) and Ge(◇), and type III-V, GaP(△), GaAs(∇) and GaSb (○), semiconductors. Open and closed symbols represent α and β dislocations respectively. Half-filled symbols are for type IV materials [64].

Table 1: Core reconstruction energy (in eV/b, $b = 3.84\mathring{A}$) of 30° and 90° partials from different calculations. The energy of double-period (DP) core of 90° partial is given relative to that of the single-period (SP) core.

		30°	90° SP	90° DP
SW	[65]	0.81		
Tersoff	[66]	0.54	0.46	
EDIP	[58]	0.45	0.80	
TB	[67]	1.38	0.69	
DFT	[68]	0.53†		
DFT	[54]	0.52		
DFT	[54]	0.44		
TB	[69]		0.69	
DFT	[70]		0.88	
DFT	[54]		0.42	
TB	[56]			E_{SP} - 0.21
DFT	[56]			E_{SP} - 0.26
DFT	[57]			E_{SP} - 0.042
DFT	[54]			E_{SP} - 0.19

† free energy at 930K

3.2.2 Shuffle-set perfect dislocations

Recent experiments indicate a change of deformation mechanism in semiconductors with decreasing temperature. The signatures of this transition include a bend in the yield stress - temperature curves, such as in Fig. 16(b), as well as a change in the dislocation microstructure, as in Fig. 14. Wavy slip lines can be interpreted as indications of frequent cross slip events; they also suggest that the shuffle-set perfect screw dislocations play an important role in low temperature deformation.

Two different core structures can be considered for the perfect screw dislocations in silicon on the shuffle-set plane, as shown in Fig. 21(a) and (b). Core A [71] is centred in the 6-member ring of atoms, while core B [52] is centred on the bond between two atoms. These two different core structures allow the following interpretation. Of the two {111} planes on which the screw dislocation can potentially move, core A is centred at the intersection

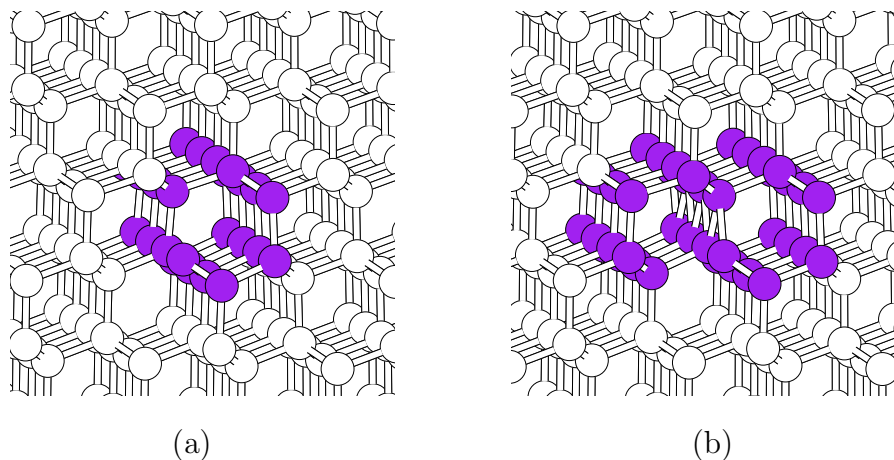(a)   (b)

Figure 21: Core structures of shuffle-set screw dislocation in Si. The high energy core atoms are shown in dark color. (a) Core A resides in a hexagonal ring. (b) Core B resides at the boundary between two hexagonal rings.

of two shuffle-set planes, while core B is at the intersection of a glide-set with a shuffle-set of planes. Core A, while on shuffle-set planes, is likely to be involved in cross-slip often observed in the low temperature - high stress experiments. Core B, being in the glide set, can dissociate into glide partials and may be involved in transitions between the glide-set and shuffle-set dislocations. To understand the various possible behaviors associated with the perfect screw dislocations, an examination of the energetics of the various core configurations is in order.

Recent atomistic simulations based on the SW potential [72] predicted that core B has lower energy than core A by 0.14eV/b [52]. However, still more recent *ab initio* calculations show that core A is the ground state of a perfect screw dislocation in Si, while core B is metastable, with an energy 0.38eV/b higher than that of core A [73]. This is consistent with another independent study giving $E(B) - E(A) = 0.32$eV/b [74]. In addition to being metastable with respect to core A, core B is likely to be unstable at finite temperatures with respect to dissociation into glide partials. Core A, on the other hand, may be reasonably stable at lower temperatures and can contribute to plastic response.

Several attempts have been made to determine the Peierls stress of a perfect shuffle-set screw dislocation using the SW potential. The value of

5GPa [59] first reported appears to be inaccurate, possibly due to inadequate boundary conditions. A second calculation produced a lower value of 2GPa, which was then confirmed by still another study, this time using periodic boundary conditions [75]. Recent *ab initio* calculations predict the Peierls stress to be 3.3 ± 0.2GPa[73] (at zero pressure). This is reasonably consistent with the low temperature yield stress measurements, which approach 1GPa at 300K [49]. Furthermore, compilation of low temperature data on the shear stress in semiconductors produced an estimate of 0.05μ [76], where μ the shear modulus. For silicon, this would correspond to 3.4GPa ($\mu = 98$GPa), in agreement with the *ab initio* results. Given that the experiments are performed at high pressure ~ 10GPa, it is of considerable interest to compute the pressure dependence of Peierls stress *ab initio*.

3.3 Secondary core defects

The dislocation cores we have considered thus far are "perfect" one-dimensional defects. In reality, secondary point-like defects should naturally exist in the dislocation cores. Reconstruction defects (RD) are expected at the boundaries separating two core segments which have undergone atomic rearrangements in the opposite sense. They are also known as anti-phase defects, or topological solitons. Another type of point defect is a vacancy or an interstitial bound to the core, which is the unit of dislocation climb between shuffle-set and glide-set planes. Perhaps the most important core defects are dislocation kinks, the nucleation and migration of which control the mobility of dislocations at finite temperatures. In this subsection, we discuss these three types of core defects and their possible combinations, as well as the role they play in facilitating dislocation motion.

Our discussion focuses exclusively on core defects in the glide-set partial dislocations because very little is known about the shuffle-set dislocations. We should emphasize, however, that given the importance of the shuffle-set perfect dislocations in low-temperature deformation that has been recently established, the investigation of their core defects warrants attention. We may speculate that because the core structure of the shuffle-set dislocations is simpler than that of the glide-set partials, these defects are likely to be less complex thus presenting an opportunity for a definitive study.

Much of the current understanding of the structure and energetics of core defects has come from computer simulations that rely on the use of empirical interatomic potentials and, more recently, on *ab initio* methods. Experimen-

tal evidence, while useful, has been scarce and subject to the limits of HREM. Atomistic simulation results have provided information on the various types of core defects in the glide-set partials and their topological characteristics. On the other hand, the energies of these defects are still uncertain. For various reasons, there is considerable discrepancy among the calculations reported by different groups, sometimes using the same computational models. These differences remain the major obstacles to a quantitative and predictive modeling of dislocation mobility (see next subsection) based on atomistic mechanisms. With increasing computing capabilities allowing the use of more accurate methods and larger simulation cells, many of the calculations should be repeated to obtain converged results on the core defect properties.

3.3.1 Reconstruction defects

When a symmetry-breaking reconstruction takes place, symmetry is traded for degeneracy, but it is not completely "lost" in the sense that different degenerate variants of the reconstructed core are related to each other by this symmetry operation. As an example, consider the reconstruction of the 30° partial, from Fig. 18(b) to Fig.19(a) where the translational symmetry along the core with repeat period b is broken. As a result of reconstruction the repeat distance along the core is doubled to $2b$. At the same time, each core atom in Fig. 18(b) can choose to bond with either of its two neighbors. This leads to two variants of core reconstruction that are energetically degenerate and related to each other precisely by the broken-symmetry operation, namely translation by b. The boundary between these two reconstruction domains, a reconstruction defect (RD), is an atom that has no partner with which to bond, as shown in Fig. 22(a).

The reconstruction defects in the 90° partial appear in more varieties and are more complex. In the single-period (SP) core, the broken symmetry is the mirror symmetry with respect to the plane perpendicular to the dislocation line. Hence there are two degenerate variants of the SP core that are mirror reflections of each other. As can be seen in Fig. 22(b), there are two RD's at the boundaries between the two variants. In the alternative double-period (DP) reconstruction of the 90° partial both the translational symmetry and the mirror symmetry are broken. To observe the breaking of the mirror symmetry, notice that the bonds parallel to the core centre (dashed line) connect either white to black atoms or black to white, on going from left to right. Given that each of the two broken symmetries is a two-fold operation,

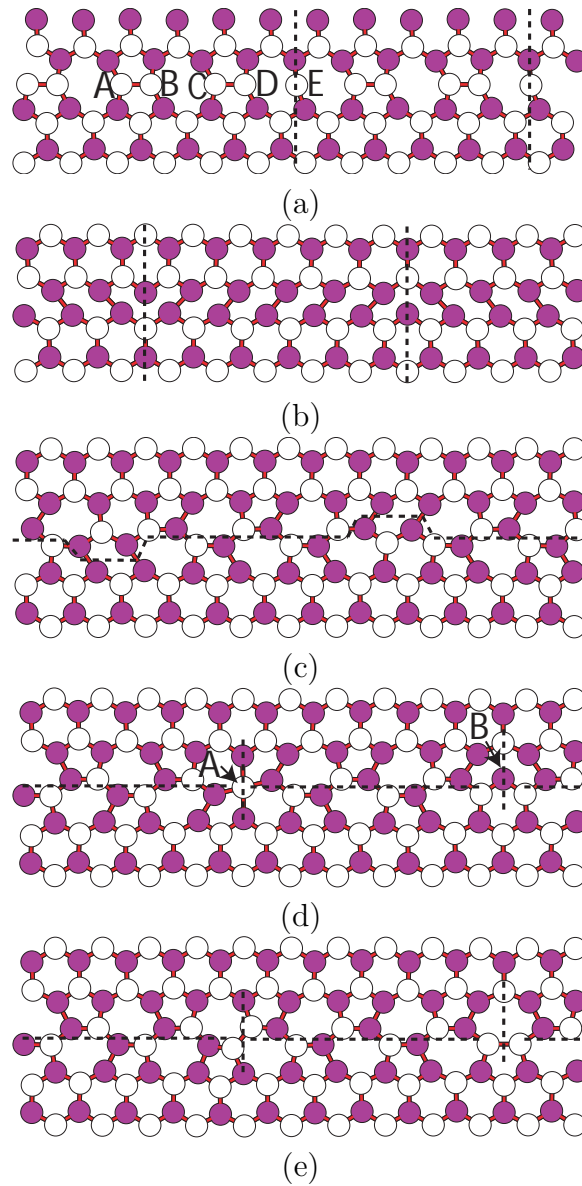Figure 22: Reconstruction defects (RD) in the partial dislocation cores in silicon, indicated by vertical dashed lines. (a) RD's on 30° partial. (b) RD's on single-period 90° partial. (c) RD's connecting double-period 90° partial cores that are related by translation symmetry. (d) RD's connecting double-period 90° partial cores that are related by mirror symmetry. (e) Combination of RD's in (d) with interstitial and vacancy.

the ground state of the DP core is four-fold degenerate.

Fig. 22(c) shows two DP cores that are related by translation symmetry separated by RD's. These types of RD's can be considered as short segments of the SP core, the energy of which has been calculated to be around 0.4eV [55]. Two more reconstruction defects are shown in Fig. 22(d) separating two DP cores related to each other by the mirror symmetry. Notice that defect A has an over-coordinated atom while defect B has an under-coordinated atom (with a dangling bond). To restore four-fold coordination, one can remove the atom at B and insert it into A. The resulting configuration can be considered as composed of complexes of two RD's with a vacancy and an interstitial, respectively (22(e)). The energies of these two complexes, computed using tight-binding methods, are 0.65eV [55]. Complexes like these are likely to be less mobile than those in Fig. 22(d) since their motion requires that an interstitial and or a vacancy has to diffuse along with the RD's.

3.3.2 Core vacancies and interstitials

Experiments have shown that plastic deformation in semiconductors produces an elevated density of point defects [77, 78, 79, 80]. The latter can be detected by the electron paramagnetic resonance (EPR)technique, also known as electron spin resonance - ESR. The g tensor of the line centres was found to be of dangling bond type, because it is almost axially symmetric. Several line centres in the spectrum, such as Si-K3 and Si-K7, were attributed to bulk vacancies and vacancy clusters, due to their comparable intensity in all crystallographically equivalent orientations. It was also observed that the production of such point defects does not seem to involve dislocation interactions, because the signal was insensitive to single slip or multi slip orientation [77].

On the other hand, line centres such as Si-K1, Si-K2 and Si-Y were attributed to vacancies inside the dislocation core, because they are not observed for all crystallographically equivalent orientations. By means of an analysis of the orientation symmetry of the signal and energy spectrum, these three line centres were identified with different vacancy configurations along the 30° partial [79, 80]. Annealing the sample at $T > 800°$C was found to lead to the disappearance of K1, K2 and Y lines. Electric dipole spin resonance (EDSR) signals are also detected under such conditions, suggesting complete elimination of dangling bonds in the core [80].

Consider an imperfectly reconstructed 30° partial dislocation core as

shown in Fig. 22(a). Atom E in the RD is bonded with three atoms (the vertical bond with an atom immediately above is not shown). Removal of atom E creates a vacancy with three neighboring atoms, or V_{3c}. The symmetry of this defect, which is the combination of an RD and a vacancy, is found to be consistent with the Si-Y line of EPR. If, on the other hand, a reconstructed atom such as A is removed, the resulting vacancy has four neighboring atoms, i.e. V_{4c}. This defect is consistent with the Si-K1 line of EPR. If we remove a string of core atoms, such as A, B, C, D, etc, the result is a linear chain of V_{3c} defects. This corresponds to the Si-K2 line, which was identified as a linear chain of spin centres [79].

Ab initio calculations have been carried out to study the energetics of V_{3c}, V_{4c} and V_{3c} clusters in the 30° partial dislocation core [81], corresponding to the Si-Y, K1 and K2 lines of EPR. The formation energies of such defects are 0.9eV, 2.4eV and 1.9eV per vacancy, and their formation entropy is around $2k_B$. In comparison, the formation energy of a bulk vacancy is 3.6eV. Therefore, it is energetically favorable for bulk vacancies to agglomerate into 30° partial dislocation cores. Furthermore, they are likely to bind either with the RD or among themselves to form short segments of "hollow" dislocations. Because of its considerable formation energy, vacancy concentration in the 30° core still should be negligible at thermal equilibrium. However, this no longer needs to be the case when dislocations are driven to move by external stress, which is a highly non-equilibrium process. Complicated dislocation - point defect interactions can be expected under such conditions, where a moving dislocation core can collect vacancies from the bulk, or inject point defects into the bulk. The point defects can also facilitate or obstruct the motion of dislocations, as discussed in the next subsection.

High resolution electron microscopy (HREM) observations of dislocation cores provide valuable information [63], although the resolution is not high enough to draw definitive conclusions. Images of 90° partials are found to agree with computer models of perfectly reconstructed core atoms, indicating a low concentrations of vacancies and interstitials in the 90° partial. On the other hand, the HREM contrast in the 30° partial core is rather weak, suggesting a density of core atoms to be between 0.5 to 1.5 per core site. This suggests that the 30° partial could have a complex core structure with alternating vacancy and interstitial segments.

The conglomeration of vacancies or interstitials in the glide-set partial dislocations may give rise to structures that are equivalent to partial dislocations on the shuffle-set [63]. Such partials, produced by the climb of glide-set
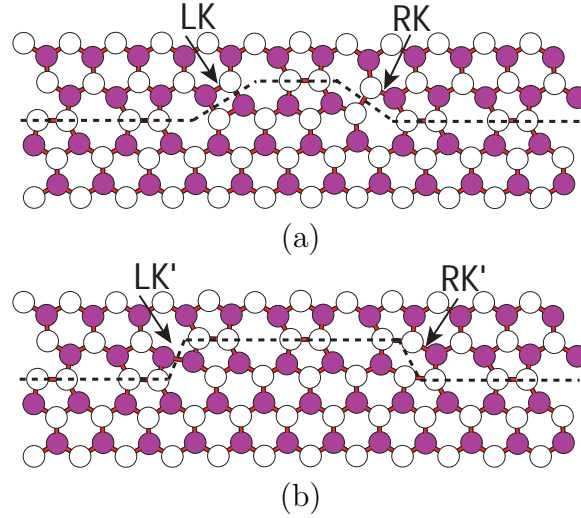
Figure 23: Kink pairs on 30° partial, (a) LK and RK, (b) LK′ and RK′.

partials through the absorption or emission of vacancies or interstitials, round out the possible types of dislocations in diamond cubic semiconductors.

3.3.3 Kinks

The most extensively studied defects in the dislocation core are kinks. Their importance derives from the widely accepted belief that their nucleation and migration along the dislocation line are the primary mechanisms of dislocation motion at finite temperatures [5]. Atomic-sized kinks connect dislocation segments lying in the adjacent Peierls valleys separated by the smallest translation period. A kink-pair on a 30° partial [65] is shown in Fig. 23(a). The width of this kink-pair is 3b. This defect is formed by shifting three black atoms (under the hump delineated by the dashed line) from their perfect lattice positions. Notice that the atomic configurations of the left (LK)and right (RK) kinks are topologically different from each other.

The kink-pair shown in Fig. 23(a) is not the smallest possible. The most narrow kink-pair is obtained by shifting just one black atom to form a configuration where LK and RK are immediately adjacent to each other. Subsequent migration of LK to the left and RK to the right, such as under the influence of external stress, increases their separation in discrete steps, eventually resulting in the translation of the entire partial upward by one repeat

Table 2: Kink and APD formation energy E_k and migration barrier W_m (in eV) in 30° partials in silicon. Experimental estimates of kink energies are also listed. Note that experiments do not differentiate the various kink species. Instead effective kink energies are estimated.

| | | E_k | | | | | W_m | | | | |
		LK	RK	LC	RC	APD	LK	RK	LC	RC	APD
SW	[60]	1.2				0.84					
SW	[65]	0.82	0.82	1.12	0.79	0.81	0.82	0.74	0.22	1.04	0.17
SW	[54]	0.98	0.65	1.29	0.63						
EDIP	[58]	0.65	0.39	0.90	0.83	0.49	1.46	0.89			
TB	[67]	0.35	1.24	0.88	2.15	1.33	1.53	2.10			0.3
DFT	[82]					0.65					
DFT	[83]							2.1			
TEM	[84]						1~1.2				
HREM	[1]	0.8					1.55				
TEM	[85]	0.9					1.3				
IL†	[86]	0.62					1.58				

† intermittent loading of 60° dislocations

step from its original position. Fig. 23(b) shows the double-kink obtained by moving LK to the left and RK to the right, both by one b, from their positions in Fig. 23(a). Notice that the bonding configuration of the resulting left kink (LK$'$) and right kink (RK$'$) are different from their respective counterparts in Fig. 23(a). This is a consequence of the doubled periodicity in a reconstructed 30° partial core. Only after the left kink (or right kink) moves by $2b$ along the dislocation line is its original bonding configuration restored. A detailed discussion of the relationship between kink multiplicity and symmetry breaking was given in [87].

Additional species of kinks can be formed by combining those we have just identified, LK, RK, LK$'$ and RK$'$, with the reconstruction defect RD, thus leading to kink-RD complexes. When the core of a kink overlaps with an RD the resulting configuration has significantly lower energy. This means that these two defect species will tend to bind and form a new type of core defect. The following two reactions have been found to be energetically favorable, resulting in the formation of a left kink complex (LC) and a right kink complex (RC),

$$LK + APD \quad \rightarrow \quad LC \tag{13}$$
$$RK + APD \quad \rightarrow \quad RC \ . \tag{14}$$

The energy gains of the LC and RC reactions are 0.51eV and 0.84eV respectively [65] computed using the SW potential, and 0.80eV and 0.42eV using a TB model [67]. The complexes formed by combining LK$'$ and RK$'$ with RD are not energetically stable [67]. The two important kink energy parameters that affect dislocation mobility are their formation energies E_k and migration energy barriers W_m. Their values calculated for different kink species and complexes are given in Table 2. By binding with kinks, RD's are seen to either lower or raise the kink migration barrier. It was found that RD can facilitate kink-pair nucleation and pre-existing kinks can also serve as preferential sites for RD-pair nucleation [65]. Thus, the complex interaction between kinks and RD's is expected to play a role in dislocation mobility.

The family of kink species is even more extended in the 90° partials, given that it has two competing core reconstructions (SP and DP), each with several species of RD's that can combine with kinks. The unreconstructed 90° partial is symmetric under mirror inversion with respect to the plane normal to the dislocation line. Therefore, in the unreconstructed 90° partial, left and right kinks are exact mirror images of each other. However, since
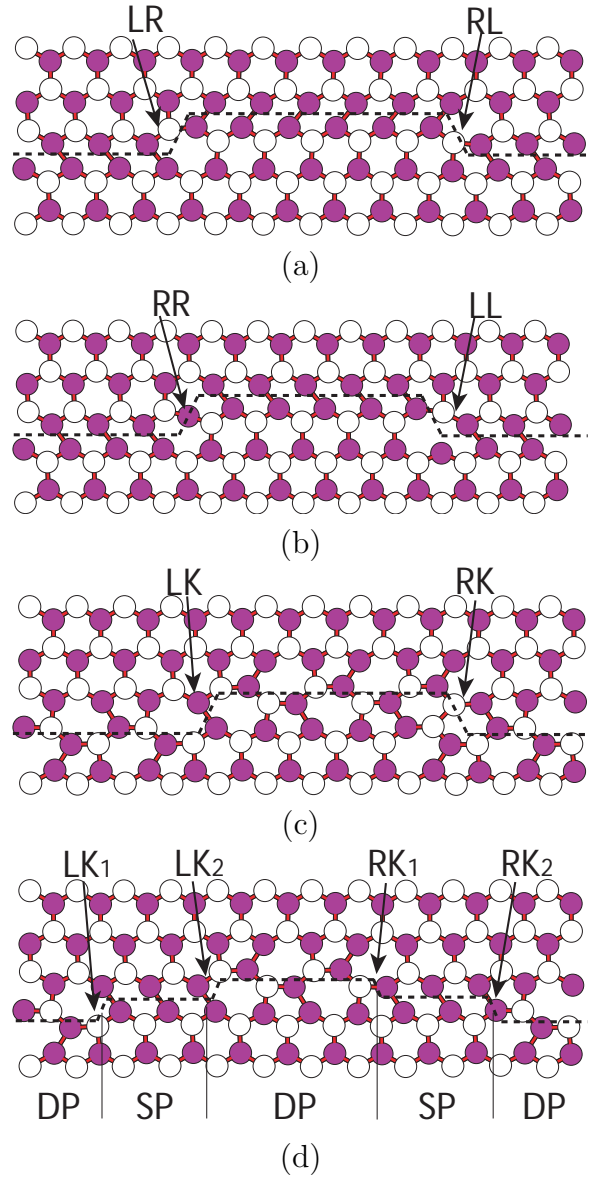
50

Figure 24: Kinks in 90° partial. (a) Kink pair LR and RL in a single-period (SP) 90° partial. (b) Kink pair RR and LL on (SP) 90° partial. (c) A kink pair on double-period (DP) 90° partial. (d) Dissociation of kinks shown in (c) into partial kinks bounding short segments of SP core.

51

both (SP) and (DP) reconstructions break the mirror symmetry, multiple kink species are formed. At the same time, every left kink finds an exact mirror image in one of the right kinks.

By convention, different types of kinks in the SP core are labelled according to the geometric characteristics of their right kinks representatives [67]. All the left kinks then can be obtained by a mirror reflection. The kinks are named by the sense of core reconstruction on both sides of the kink. Consider the right kink in Fig. 24(a) as an example. Going from left to right side of the kink, the reconstruction bonds first tilt to the right and then to the left. This kink was therefore denoted as a right-left kink (RL). To label the left kink in Fig. 24(a) according to the nomenclature first proposed in [67], one should first mirror-invert this kink. The resulting right kink will have a left-right sequence of tilts and is called left-right (LR) kink. Similarly, the two kinks in Fig. 24(b) are called right-right (RR) and left-left (LL). Tight-binding (TB) calculations [67] predicted the formation energies for LR and RL kinks to be about 0.12eV. The LL and RR kinks can be considered as complexes of LR and RL kinks with RD's but were found to be unstable in finite temperature simulations: the LL and RR kinks spontaneously dissociated into LR and RL kinks while emitting RD's.

In the DP core of the 90° partial, there must be five different species of RD's and eight topologically distinct species of kinks [54]. These have not been examined and we will not attempt to enumerate all of them here. Instead, we want to point out an interesting possibility in which a conventional (full) kink dissociates into two partial kinks enclosing a segment of the SP core. This is analogous to the dissociation of a perfect dislocation into two partials, bounding an area of the stacking fault, except that kink dissociation involves two 0D defects (partial kinks) and a 1D stacking fault (the SP segment). An example of such dissociated kinks in the DP core is shown in Fig. 24(c). Here we arbitrarily call the left and right kinks LK and RK, respectively. Let us first observe that the minimal spacing between two SP and DP cores in a 90° partial is only half of the full translation period. Therefore, both the left and right kinks on a DP core can split into partial kinks bounding a segment of the SP core, shown in Fig. 24(d), through the following reactions,

$$LK \quad \rightarrow \quad LK_1 + SP + LK_2 \tag{15}$$
$$RK \quad \rightarrow \quad RK_1 + SP + RK_2 \tag{16}$$
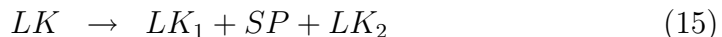
Here the partial kinks are arbitrarily marked LK_1, LK_2 and RK_1, RK_2 to

Table 3: Kink and APD formation energy E_k and migration barrier W_m (in eV) on 90° partials with SP core reconstruction in silicon. Experimental estimates of kink energies are also listed. Note that experiments do not differentiate different kink species. Instead effective kink energies are estimated.

		E_k				W_m			
		LR/RL	LL	RR	APD	LR/RL	LL	RR	APD
EDIP	[58]	0.70	0.84	1.24	0.65	0.62			
Tersoff	[66]	0.12							
Tersoff	[60]	0.90			0.37				
TB	[89]	0.50†	1.74*	2.04*	1.31	1.87			0.04
TB	[67]	0.12	*	*	1.45	1.62			0.04
DFT	[90]				1.2				
DFT	[91]	0.1				1.8			
DFT	[92]	0.04				1.09			
TEM	[93]	≥0.4				≤1.2			
TEM	[84]					1∼1.2			
HREM	[1]	0.74				1.55			

∗ approximate energy, defect unstable
† not fully converged [67]

acknowledge that many species of full and partial kinks can exist in the 90° partial.

Assuming that an SP core has slightly higher energy than a DP core [55], an SP segment acts here as a "one-dimensional stacking fault", exerting a force on the partial kinks LK_1 and LK_2 (also between RK_1 and RK_2), which, by themselves, repel each other through elastic interactions. The width of a dissociated kink is dictated by the balance between elastic repulsion and the stacking-fault attraction forces. For the Tersoff [88] potential, the equilibrium partial kink separation between LK_1 and LK_2 was found to be $2b$, with a total energy reduction of 0.04eV due to dissociation [54]. While no systematic study of the partial kink energies in 90° partial has been undertaken, it is reasonable to expect that dissociation can reduce the kink energy, suggesting that more kinks can be available on the 90° partial for dislocation motion. The existence of two types of Peierls valleys can be yet another possible reason why the 90° partials have higher mobility than the 30° partials.

Unfortunately, there is still a sizeable gap between the resolution of com-
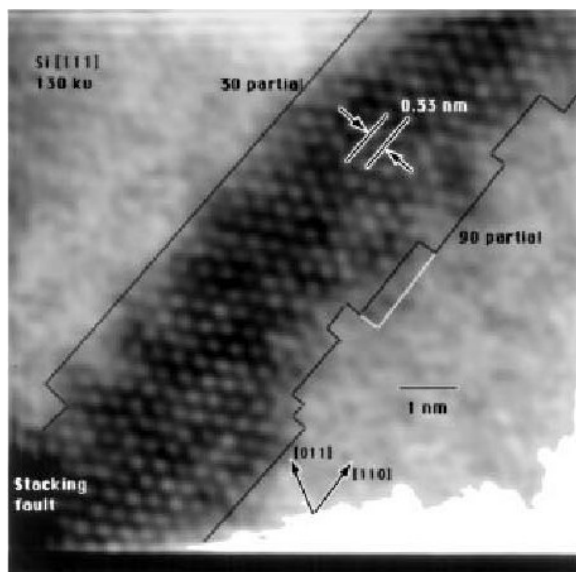
Figure 25: Kinks on 30° and 90° partials of a 60° dislocation observed in HREM [1].

puter models and that of HREM observations. Direct observation of kinks has been reported only recently using a new technique [1] that allows a "plane-on" view of stacking faults using forbidden reflections. Shown in Fig. 25 are two partial dislocations bounding a dark stacking fault. In this case, dissociated 60° dislocations were examined to enable simultaneous observation of 30° and 90° partials.

Due to limited resolution, it was not possible to determine the exact positions of the kinks, let alone the detailed atomic arrangements in the core of kinks and partial dislocations. Nonetheless, this experiment is the most direct observation of kinks to date. It provided useful information about kinks spacing that can be compared with theoretical models. The sample was initially deformed under high stress and temperature and subsequently quenched so that the partials were trapped at non-equilibrium separations. The sample was then heated in an electron microscope. Only the 90° partials moved in the measurements and their kink density was consistently about 3 times higher than in the 30° partials. Measurements of kink velocities *in situ* indicated that the kink migration barrier on 90° partial was $W_m = 1.24 \pm 0.07$eV. However, kink pinning at invisible obstacles was also observed.

These obstacles have been postulated to be oxygen atoms. The energy barrier for overcoming the obstacles was estimated to be 2.4eV. An analysis of the width distribution of kink pairs led to an estimate of kink formation energies of $E_k \approx 0.81$eV for 30° partials and $E_k \approx 0.74$eV for 90° partials (free energies were estimated to be 0.797eV and 0.727eV, respectively). However, the estimates of E_k could have large error bars due to the scarcity of data points (only 7 kink pairs were counted for the 90° partial). Also, given that the kinks might have been pinned at invisible obstacles, the observed kink-pair width distribution could be a reflection of the obstacle spacing rather than a function of the kink formation energy.

Tables 2 and 3 show various calculated and measured values of the formation energies E_k and migration energy barriers W_m for different kink species and RD's on 30° and 90° partials in silicon. A conclusion that can be drawn from these data is that, despite decades of effort, there is not a single converged data point in these two tables. Computations based on empirical interatomic potentials, tight-binding methods, and *ab initio* methods, produced very different results. In a few cases, different groups using the same potential models have reported significantly different values for the same parameter [59, 52]. This makes us think that, for the calculations of dislocation properties to be accurate, one should use not only an accurate description of interatomic interactions, but also a proper treatment of boundary conditions. The boundary condition issue is much more serious for DFT and TB simulations that employ relatively small computational cells. Possibly, some of the *ab initio* calculations reported so far [94] have produced results that are less accurate than the interatomic potential simulations.

Despite the limited accuracy, some qualitative trends can be seen in Tables 2 and 3. In cases when data for the same defect are available from several models, we tend to trust *ab initio* results more than that of tight-binding methods, and more than the data obtained using empirical potential models.[2] Considering the most accurate results to date, the kink formation energies on 90° partials are generally smaller than those on 30° partials. In this regard, tight binding results seem to agree with *ab initio* data in giving very low kink energy (about 0.1eV) for the kinks on the 90° partials. Unfortunately, no *ab initio* data are available for kinks on 30° partials. The smallest kink energy on 30° partial from tight-binding calculations is 0.35eV.

---

[2]This is on the condition that in all calculations the boundary effects have been properly taken care of, and the convergence with respect to the simulation cell size has been reached.

All the kink results given in Table 3 refer to the SP core of the 90° partial. It is now generally accepted that this partial can also undergo the DP core reconstruction that results in a slightly lower core energy than the SP core. At present, there is little information on the kinks on DP core and the partial kinks linking a DP core and an SP core. What is available are only results from atomistic simulations using empirical potentials. Nonetheless, if one accepts the fact that dissociation of full kinks into partial kinks further reduces kink formation energies, then the arguments in favor of higher mobility of the 90° partials become even more compelling.

It is not surprising that more data for different kinks species are available from empirical potential calculations than from *ab initio* calculations. The technical difficulties and computational expense of the latter are the reasons why very few types of kinks have been studied. On the other hand, experimental estimates for kink energies cannot differentiate kink species at all. Instead, an effective value describing the average effect of all kinks is estimated. Therefore, it would be misleading to directly compare *ab initio* results for a given kink species with experimental estimates.

So far we have discussed kink mechanisms of dislocation motion that are purely conservative, i.e. do not involve mass transport by diffusion. Diffusional mechanisms could play an important role at high temperatures. It has been suggested that [63] vacancy pipe diffusion along dislocation core can facilitate kink-pair nucleation and kink migration. This is because these kink mechanisms entail either bond switching or exchange. If one of the sites involved in the atomic rearrangement is occupied by a vacancy, then switching of the bond can also be accomplished simply by a vacancy jump. At high temperatures, such non-conservative kink mechanisms may well be competitive with the conservative mechanisms discussed earlier.

3.4   Dislocation mobility

The main purpose of studying dislocation core and secondary core defects is to understand how dislocations move. In principle atomistic simulations, such as those discussed above, are capable of giving results that not only enable the understanding of existing data on dislocation mobility, but also lead to further predictions outside the range of experimental conditions. At present, quantitative predictions of dislocation motion from first principles are not feasible. At the same time, different measurements of dislocation velocity show considerable scatter to such an extent that there is little con-
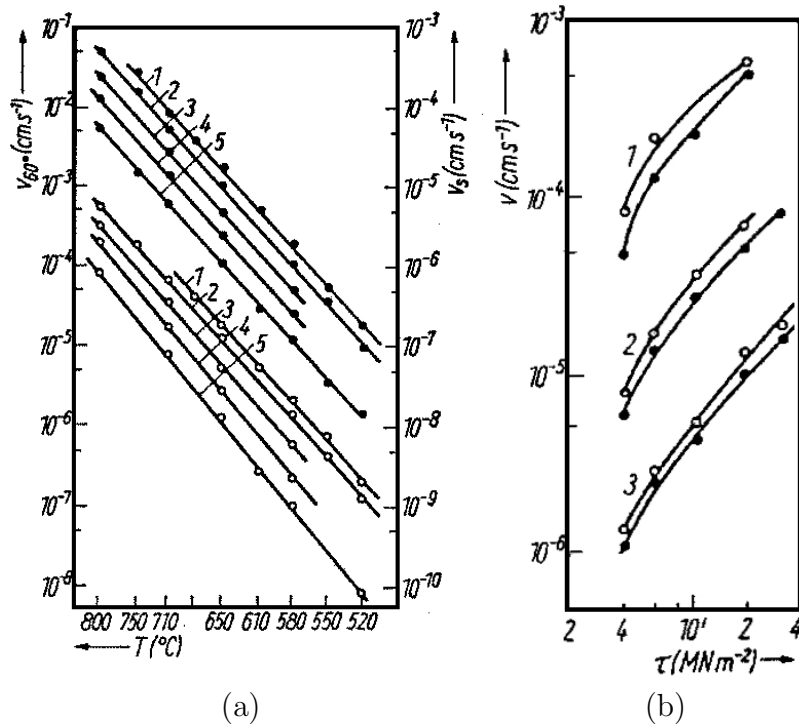
Figure 26: (a) Temperature dependence of velocity of screw ($\bullet$) and 60° ($\circ$) dislocations in intrinsic Si at stresses (1) $\tau = 30$, (2) 19, (3) 10, (4) 6, (5) 4 MPa. (b) Stress dependence of velocity of screw ($\bullet$) and 60° ($\circ$) dislocations in intrinsic Si at temperatures (1) $T = 800$, (2) 710, (3) 650 °C [95].

sensus on what is the controlling mechanism for dislocation motion in semi-conductors. Despite these problems, there are certain trends that may be considered established and theoretical models that have found support from the experiments.

3.4.1   General behavior

A set of experimental data on dislocation mobility in silicon is shown in Fig. 26. The dislocations were imaged using X-ray topography and the velocities v of screw and 60° dislocations were measured over a range of resolved shear stress τ and temperature T conditions. Following [96] we refer to the temperature and stress range of these experiments as the "central" range,

i.e. $0.45T_m < T < 0.65T_m$, $5 \times 10^{-5}\mu < \tau < 10^{-3}\mu$, where $T_m = 1693$K is the melting temperature and $\mu = 68$GPa is the shear modulus of silicon. A number of measurements in this parameter range using various techniques have been reported [84, 86, 93, 95, 97, 98, 99, 100, 101, 102, 103, 104, 105, 106, 107]. While their general trends, particularly with regard to temperature dependence, are consistent, the absolute values of the velocities can differ by about a factor of two [96].

Dislocation mobility in this "central" range is often described using the following empirical relationship

$$v(\tau, T) = C(\tau) \exp\left(-\frac{Q(\tau)}{k_B T}\right). \tag{17}$$

The Arrienus plots of dislocation velocity versus the inverse temperature, such as in Fig. 26(a), show straight lines whose slopes are the activation energies Q. In this series of measurements [95], a Q_s value (for screw dislocations) around 2.2eV was obtained over the entire stress range, while $Q_{60°}$ (for 60° dislocations) increases from 2.16eV to 2.43eV as the stress decreases from $\tau = 30$MPa to 4MPa. A later experiment [104] using *in situ* X-ray topography together with presumably purer silicon samples gave $Q_s = 2.35$eV and $Q_{60°} = 2.2$eV for stresses ranging from 2 to 20MPa. The effective activation energy Q having a value 2.2 to 2.3eV has been verified by several groups and is now widely accepted. All the experiments indicate that 60° dislocations (comprised of a 90° and a 30° partials) are generally more mobile than screws (comprised of two 30° partials). This is also in agreement with TEM observations showing that 90° partials are more mobile than 30° partials [53].

The stress dependence of dislocation velocity is by comparison more controversial. For a given temperature the variation of dislocation velocity with stress is empirically described as $v \sim \tau^m$. The standard kink diffusion model [5], to be discussed later, predicts a linear relationship between stress and velocity, i.e. $m = 1$. From Fig. 26(b) it is clear that this behavior is not seen at low stress. Also, m is found to depend on temperature [95] suggesting that the intrinsic mechanism of kink diffusion cannot account for the details of the experimental findings. In order to explain this discrepancy a concept of weak obstacles was invoked. On the other hand, later *in situ* X-ray topography experiments [104] reported that the relationship between stress and velocity remains linear from 2MPa to 20MPa.

In the range of resolved shear stress τ between 30MPa to 300MPa, it has been found that dislocation velocity can be expressed as $v = v_0(\tau/\tau_0)^m$, with $1.2 \leq m \leq 2.2$ [102]. However, the actual value of m appears to depend not only on the type of dislocations, but also on the orientation of Burgers vector with respect to the compression axis. This observation suggests a breakdown of the Schmid's law in silicon at high stresses. We would argue that Schmid's law is also violated at low stresses, as shown by the large scatter in the velocity data measured at the same resolved shear (Schmid) stress. Mitchell et al. [108] have shown that velocity dependence of the type observed in [104] can be fitted by the kink diffusion model [5] if one includes the stress dependence in the free-energy of kink-pair formation.

At temperatures higher than $0.7T_m$ the dislocation mobility exhibits another transition [102]. Fig. 27 shows that, as the temperature increases above $0.7T_m$, the behavior of dislocation mobility undergoes a change. The effective activation energy increases to $Q \approx 4.0 \pm 0.1$eV, accompanied by a corresponding increase in the pre-exponential factor. This behavior shows up in the velocity plots as a characteristic bend. Mechanistic understanding of this transition is still lacking even though it has been proposed that, at such high temperatures, vacancies can facilitate kink-pair nucleation and migration [63].

In analyzing the experimental data one can observe considerable scatter among the different measurements that cannot be explained within a single theoretical model. To establish a consistent picture of dislocation motion, it is important to recognize the limitations and possible artifacts of the different techniques used to measure dislocation velocity. Three approaches are widely used to observe dislocations, selective etching [109, 103], X-ray topography [95, 104], and transmission electron microscopy (TEM) [101, 93, 84].

In the case of etching the intersection between a dislocation line and the free surface, an etch pit, is exposed. To measure the dislocation displacement from the etch pit position, one has to assume the dislocation remains straight beneath the surface. Although this can be verified by observing the shape of the etch pit and by repeated etching, the confirmation is indirect. Chemical solutions used in etching could introduce impurity atoms to the surface which then can pin the dislocation. This can be the reason why a starting stress effect (existence of a critical stress below which dislocations cease to move) has been observed in etching experiments [109] but not in X-ray experiments.

The resolution of X-ray topography is about 2.5μm, comparable to that of selective etching. Hence, only large scale behavior of dislocation motion
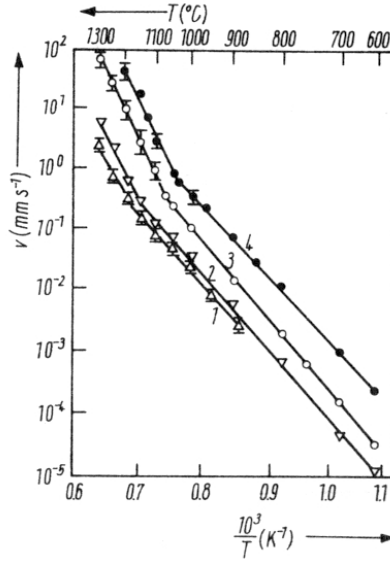
Figure 27: Temperature dependence of 60° dislocation velocity in Si [103] for different stresses (1) 2MPa, (2) 5MPa, (3) 10MPa, (4) 45MPa.

can be observed. Smaller scale details, such as impurity clusters, jogs, etc, are not observed, as these effects are smeared out in the overall dislocation velocity that is measured. The exposure time in the X-ray topography is long so that it is difficult to image dislocations *in situ*, unless a strong X-ray source is used. If the measurements are not performed *in situ*, dislocation and point defect microstructures can change during heating and cooling cycles between loading, which may affect the measured dislocation velocity [104].

Because a small concentration of impurity atoms (such as oxygen) can have a large effect on dislocation mobility, careful characterization of all impurity species in the specimens is a requirement for all experiments. For example, it was found [104] that boron has essentially no effect on dislocation mobility up to a concentration of 1.4×10^{19} atoms·cm^{-3}, while earlier measurements seemed to show a pinning effect associated with boron. It was argued [104] that the discrepancy could be a result of an unnoticed oxygen impurity concentration in other experiments.

Non-Schmid behavior also has been observed in silicon. The dislocation velocity was found to have a dependence on stress components other than

the Schmid (or glide) stress τ_s. In particular, the velocity of the 60° dislocation is dependent on the climb stress (τ_c). Which of the two partials, 30° or 90°, is leading also seems to make a difference. As we will explain in the next subsection, it can be expected that the Escaig stress component (τ_e), which exerts opposite glide forces on the two partials, can play an important role in dislocation mobility. These observations suggest that it is necessary to take the other stress components (besides the glide stress) into account when comparing two experimental reports. This may resolve some of the discrepancies among the different experiments. Parenthetically, the discrepancy between the two mentioned X-ray topography measurements [95] and [104] may be attributed, at least partly, to differences in loading conditions. In [95] a tensile load was applied along $[\overline{1}2 3]$ direction while in [104] the tensile axis was $[11\overline{2}]$.

In situ TEM measurements offer a unique opportunity to observe dislocation motion in detail but the method has its own disadvantages. The application and measurement of stress are difficult. Stress is usually estimated from the local curvature of dislocations, or from the width of the stacking fault between the partials. This makes any reported stress value only approximate. Because very thin films are used in TEM, surface effects are more serious than in other techniques. Examples of surface effects include the image stress on dislocations and enhanced kink nucleation at the free surfaces which can significantly increase the dislocation velocity [101]. Dislocations under TEM are often seen to be pinned by invisible strong obstacles [93, 1], possibly impurity atoms (clusters) diffused from the surface of the thin film, or produced as a radiation damage by-product of the electron beam itself. At the same time, the electron beam increases the dislocation mobility by producing excitations, e.g. electron-hole pairs, that enhance the rate of kink-pair nucleation and kink migration. All in all, the dislocations may behave differently in the bulk than under the electron microscope.

3.4.2   Stochastic discrete kink model of dislocation mobility

In this subsection we discuss a mesoscale model that overcomes the computational limitations of direct atomistic simulations to reach the length and time scales of dislocation motion in the laboratory experiment. To provide a reference point for the model development, we briefly recall a few relevant features of a well known kink diffusion model due to Hirth and Lothe [5], referred to here as the HL model.
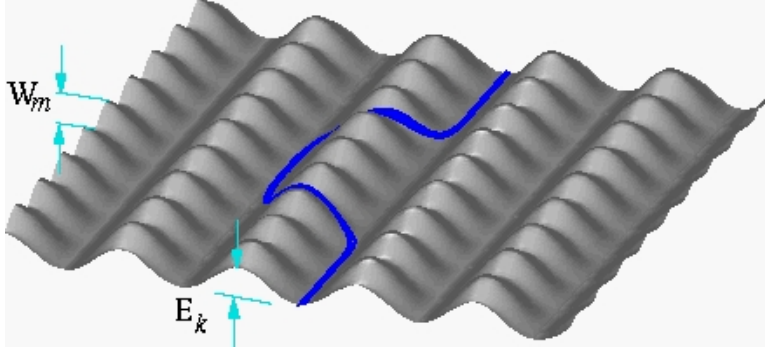
Figure 28: Schematic of the Peierls barrier and kink mechanism for dislocation motion. Dislocation is represented as a continuous line, which resides mostly at the bottom of the Peierls energy surface except at kinks.

The basic assumption of the HL model is that a dislocation moves in a stochastic sequence of thermally activated, random kink-pair nucleation and migration events. The rate of kink-pair nucleation is defined by the nucleation barrier that depends on the kink-pair formation energy, kink migration barrier, elastic attraction between two kinks of the same pair and the applied stress. Once nucleated, kinks diffuse along the dislocation line and either recombine with other kinks or pile up at the ends of the line. By considering the balance of kink-pair nucleation and migration rates under stress, it is relatively straightforward to obtain (in the limit of long dislocations)

$$v = \nu_D \frac{\tau a b h^2}{k_B T} \exp\left(-\frac{E_k + W_m}{k_B T}\right) , \qquad (18)$$

where v is the dislocation velocity, ν_D is the Debye frequency, τ is the resolved shear stress on the dislocation, a, b and h are the dislocation period, Burgers vector and kink height, respectively, E_k is the kink nucleation energy and W_k is the kink migration barrier. Experimental data on the temperature and stress dependence of dislocation mobility in the "central" range is generally consistent with Eq. (18). Furthermore, the estimates for kink formation and migration energies based on this equation are in reasonable agreement with the atomistic simulation results.

Overall, despite reports of its shortcomings and given its analytical simplicity, the HL model is remarkably successful in describing dislocation mobility in silicon. As an example, let us consider the claim that experimental

data presented in [104] can not be explained by the HL model. By comparing Eq. (18) with the empirical relationship found in [104],

$$v = v_0 \tau \exp\left(-\frac{Q}{k_B T}\right) , \tag{19}$$

one can readily see that

$$v_0 = \nu_D \frac{abh^2}{k_B T} \tag{20}$$

$$Q = E_k + W_m . \tag{21}$$

Using their own experimental data Imai and Sumino obtained $v_0 \approx 10^4 \mathrm{m \cdot} s^{-1}\mathrm{\cdot MPa}^{-1}$ whereas by plugging into the right hand side of Eq. (20) the values appropriate for silicon, one obtains $v_0 \approx 10\mathrm{m \cdot} s^{-1}\mathrm{\cdot MPa}^{-1}$ which is lower by three orders of magnitude than the measured value.

However, this discrepancy is only apparent, because the entropy factors in double kink nucleation and kink migration processes have been ignored in [104]. In Eq. (18) E_k and W_m should be replaced by free energies, $E_k - TS_k$ and $W_m - TS_m$, where S_k and S_m are entropies for the nucleation and migration processes. Therefore, Eq. (20) should be replaced by

$$v_0 = \nu_D \frac{abh^2}{k_B T} \exp\left(\frac{S_k + S_m}{k_B}\right) \tag{22}$$

To account for the difference in three orders of magnitude, $S_k + S_m \approx 7k_B$ would be needed. This is actually not unreasonable considering the estimate of $3k_B$ for both S_k and S_m obtained in the earlier atomistic calculations [110]. Therefore, the experimental data of [104] should not be viewed as evidence of the failure of the HL model, but instead as confirmation of the importance of the entropy factors.

The HL model is nevertheless a simplification that ignores, for example, the fact that dislocations in silicon, at least in the "central" parameter range, are dissociated. Although the values for E_k and W_m used in the HL model refer to partial dislocations, the process where two partials interact strongly with each other and move together is usually not considered. When the applied stress is much larger than the interaction stress between the partials, the partials are likely to be relatively independent of each other, in which case this simplification is justified. The simplification is also valid for materials with a small stacking fault energy γ_{ISF}, in which case the separation

between partials X_0 is large and their coupling becomes weak. If, on the other hand, the applied stress is small, then the coupling between partials can have a significant effect on dislocation mobility in silicon. In other words, the mobility of two interacting partials forming a bound state may not be well described by the generic HL model. There have been a number of reports of anomalous behavior of dislocation velocity at low stress [95]. It appears possible to attribute such low-stress anomalies to the coupling between partial dislocations.

The effect of coupling between the partials on their mobility has been examined by Möller [111]. It was assumed that nucleation of kink-pairs on two partials becomes correlated when stress is lower than a critical value τ_c, while it is not correlated at higher stress. Below the threshold stress kink-pairs have to nucleate simultaneously on both partials in close vicinity, which makes kink-pair nucleation considerably less frequent than what the HL model would predict. Using this model Möller attempted to explain the experimental mobility data at low stress without the need for the *ad hoc* postulate of weak obstacles which had been previously introduced for this purpose. Unfortunately, the model was not successful in accounting for the experimental data, making it necessary to re-introduce some obstacles back into the description. Besides this inconsistency, the model was unable to resolve another controversy. While some experiments found a non-linear stress-velocity behavior [95], other experiments found a linear relation down to very low stress [104].

To make his model analytically tractable, it was necessary for Möller [111] to introduce simplifying approximations. Recently a different approach, one based on kinetic Monte Carlo (kMC) simulation, has given new insights into the effects of partial dislocations interacting with each other on their mobility [112]. In the kMC description, two partial dislocations move together via kink-pair nucleation and kink migration while interacting through the Peach-Koehler forces. The simulations reveal a rather subtle coupling effect between the partials.

To understand the effect, assume for a moment that there is no Peierls barrier and consider the equilibrium separation X_0 between the partial dislocations. This distance is determined by a force balance between two competing terms. One is the repulsion between the partials, an elastic interaction with a force inversely proportional to their separation. Another arises from the stacking fault which exerts a constant attractive force between them. X_0

is the separation at which these two forces balance each other, i.e.

$$X_0 = \mu b^2 \alpha / (\gamma_{ISF} - \tau_e b \beta) \ , \tag{23}$$

where $\alpha = [1/4 - 1/12(1 - \nu)]/(2\pi)$, $\beta = \sqrt{3}/6$ for screw dislocations dissociated into two 30° partials, μ is the shear modulus, τ_e is the so called Escaig stress, i.e. the resolved shear stress along the edge components of the partial Burgers vectors, which exerts equal but opposite forces on the two partials. Therefore, X_0 is a continuous function of the stacking fault energy and the Escaig stress τ_e. However, because of a very high Peierls barrier in silicon, the actual separation X between the partials can only be an integer multiple of $h = b\sqrt{3}/2$. If X_0/h happens to be an integer, then the ideal spacing is commensurate with the lattice period. Any perturbation of this ideal spacing, such as kink-pair nucleation, will incur additional energy cost. However, this cost is significantly reduced if kink-pair nucleation takes place on both partials simultaneously so that the ground state spacing X_0 is preserved between the two kink-pairs. Such correlations are suppressed when the stress driving kink-pair formation and motion becomes high enough to overcome the interaction between kinks on the two partials.

The situation is different when X_0/h is a half-integer, in which case the ground state of the two partials becomes doubly degenerate, i.e. $X = X_\pm = X_0 \pm 1/2$. When the partials are separated by X_-, forward kink-pair nucleation and propagation on the leading partial extends the stacking fault width to X_+, which is another ground state. Likewise, in the state X_+, forward kink-pair nucleation on the trailing partial does not require any kink activity on the leading partial. In this case, there is no commensurability barrier and mobility of the whole assembly should be relatively high because the two partials can now move sequentially through alternate contraction and expansion of the stacking fault.

Fig. 29 shows the simulated velocity of a dissociated screw dislocations as a function of Schmid stress. Two sets of data are shown with X_0 equal to $10.0h$ and $10.5h$, respectively. The change of X_0 can be realized by either changing the stacking fault energy (by 5%) or by applying an Escaig stress of 25MPa. When X_0/h is a half-integer, the function remains linear down to very low stresses. On the other hand, when X_0/h is an integer, the mobility drops super-linearly below 20MPa. Also plotted in Fig. 29 are two sets of conflicting experimental data [100, 104] resembling the two simulated curves. While a linear velocity-stress relationship was reported in [104], a non-linear
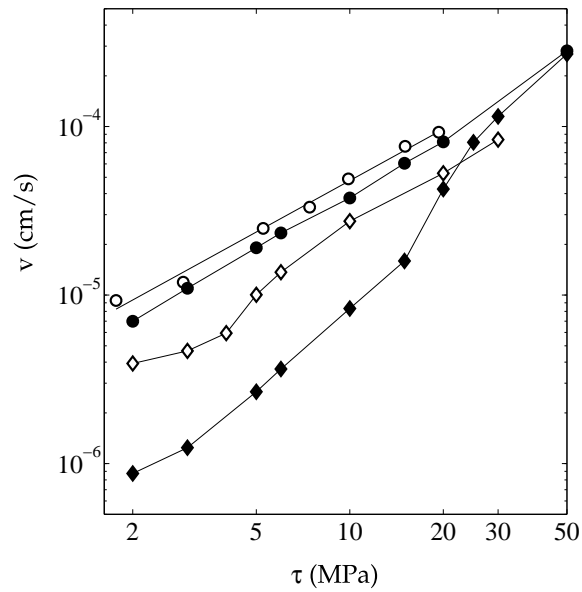
Figure 29: Velocity of a screw dislocation in Si as a function of stress. kMC prediction at temperature $T = 1000$K for a commensurate case ($X_0 = 10.0h$) is shown as ♦, with a "starting stress" at about 20MPa. Experimental data from [100] at temperature $T = 983$K shows similar velocity variation, plotted as ◊. kMC results for a non-commensurate case ($X_0 = 10.5h$) are plotted as •, demonstrating linear stress-velocity relationship, in agreement with other experiments, at temperature $T = 1005$K plotted as ∘ [104].

velocity reduction was observed in [100], albeit at a smaller critical stress. The magnitude of this mobility reduction is also smaller than in the simulated case of $X_0/h = 10$.

It was argued in [104] that the discrepancy between the two experiments was due to a higher purity of samples used in [104]. However, given that a small change of X_0 can have a large effect on the low-stress mobility, another explanation could be the different averaged values of the parameter X_0 in the two experiments. Assuming that both measurements used similar materials with the same stacking fault energy (albeit unknown to within an accuracy of 5%), then the difference in X_0 could potentially come from the different values of Escaig stress. Indeed, the experiment [100] was conducted with a tensile axis $[1\bar{2}3]$. The corresponding primary slip system was $(1\bar{1}1)[10\bar{1}]$, with a Schmid factor of $s = 0.4667$. By analogy to the Schmid factor, let us define an Escaig factor as the ratio of Escaig stress to the tensile stress. The Escaig factor was $e = 0.1347$ in [100] while the ratio of Escaig and Schmid factors in this experiment was $\tau_e/\tau_s = 0.2887$.

The tensile axis in [104] was $[11\bar{2}]$, with the primary slip system $(\bar{1}11)[01\bar{1}]$. The corresponding Schmid and Escaig factors were $s = 0.4082$, $e = 0.0786$, respectively, and their ratio was $\tau_e/\tau_s = 0.1925$. We notice that the velocity data points reported were plotted against Schmid stress only, although Escaig stresses in these two experiments were markedly different. For example, for a Schmid stress of 4MPa, X_0 for these two loading conditions can be different by $0.008h$. This is not large, compared with the two extreme cases studied in the kMC simulation in which X_0 changes by $0.5h$. However, it is reasonable to expect that such a change of X_0 could lead to a noticeable change of dislocation mobility, comparable to the discrepancy that exists between these two experiments.

It appears possible to directly observe the effect of Escaig stress on dislocation mobility through the modulation of stacking fault width by experiments. Evidently this effect should be more pronounced when the Escaig stress is large. For example, when the loading condition is such that the ratio of Escaig and Schmid stresses is $\tau_e/\tau_s = -6.25$, kinetic Monte Carlo simulations [112] predict that the variation of dislocation velocity plotted with Schmid stress should exhibit oscillatory behavior with a period of about 8MPa. This is consistent with the fact that it takes 25MPa of Escaig stress to change X_0 by $0.5h$. A possible set up for the experiments to verify this effect has been proposed [113].

3.4.3 Kink diffusion versus obstacles

While the HL kink diffusion model and its extensions have been quite widely adopted, alternative views on the mechanisms controlling dislocation mobility in semiconductors also have been put forth. The basic assumption of the HL model has been called into question (see for example [114]) and point defects, instead of dislocation kinks, were suggested as being responsible for the lattice resistance to dislocation motion [115, 116]. As was already discussed, the generic HL model can not explain the low stress dislocation mobility behavior, which shows significant non-linearity. To remedy this situation the idea of "weak obstacles" was proposed as an extension of the HL model in order to explain such behavior [117, 47]. These obstacles are assumed to impede kink migration along the dislocation line; they must be weak so that at high stress they are no longer effective and the dislocation velocity-stress relationship becomes linear. The weak-obstacles theory, on the other hand, has its difficulties; to fit the experimental data a very high density of obstacles is required. In pure silicon, it is hard to imagine what kind of extrinsic defects can fit the description [114]. As mentioned above, the HL kink diffusion model, when extended to account for the coupling between the partials, can explain the low stress mobility behavior without the need for any additional entities, such as weak-obstacles.

One way to make use of the HL kink diffusion theory is to extract values of kink formation and migration energies from velocity measurements which are normally inverted to give the sum of the two energies. The results can be tested against TEM data which can give the two energies separately. For example, it is found that dislocation velocity is proportional to dislocation length for lengths smaller than $0.2 \sim 0.4 \mu$m. [93], a behavior which is given by the HL model. From this value one can estimate the kink migration energy (see previous subsections). In other experiments, the samples were first deformed at high stress and temperature and then quickly cooled down, so that dislocations were trapped at non-equilibrium configurations with large stacking fault widths and high density of kinks. Subsequent annealing under the electron microscope allows direct observation of dislocation motion via migration of pre-existing kinks[84], from which kink migration energy was estimated ($W_m = 1 \sim 1.2$eV). These findings are in general agreement with the HL model and atomistic calculations of kink energies.

Kink nucleation and migration contributions can be also isolated in the

intermittent loading experiments [86, 107][3], where a stress pulses of length t_i are separated by pause periods of length t_p. Kinks of the kink-pairs nucleated during the pulse period may become unstable during the pause period and may recombine with each other. In such conditions, the dependence of dislocation velocity on t_i and t_p can be used to estimate kink formation and migration energies. The data reported in [86] leads to $W_m = 1.58$eV for the kink migration energy and to $E_k = 0.62$eV for the kink formation energy, consistent with the atomistic models. Alternatively, if one adopts the obstacle theory, the same data can be used to estimate the strength and the length distribution of obstacles.

The authors [86] present their data as evidence against the HL model on the basis of the following argument. From the estimated value of E_k, one can also estimate the dislocation Peierls stress according to [86],

$$\tau_{PN} = \frac{\pi^3 E_k^2}{2a^2 b^4 \mu} \approx 760\text{MPa} \tag{24}$$

where a is the kink height, b is the Burgers vector, and μ is the shear modulus. This value is indeed too low compared with other experiments that clearly show that $\tau_{PN} > 1$GPa. On the other hand, recent atomistic calculations show that kink energy of $E_k \approx 0.6$eV is fully consistent with very high values of the Peierls stress for partial dislocations, at $\tau_{PN} > 5$GPa. This suggests that Eq. (24) is inaccurate and should not be used for quantitative comparison.

While we argue that much of the observed phenomenology of dislocation motion in semiconductors can be explained quite well within the HL kink diffusion model, there is no doubt that point defects, such as vacancies, interstitials, and impurity atoms, interact with dislocations and can affect dislocation mobility under certain conditions. Intrinsic point defects can also be produced by dislocations during deformation, making for rather complex interactions between point defects and dislocations.

In situ high resolution TEM experiments [1] provide possibly the most direct observation of obstacles for dislocation motion in showing that kinks can be trapped by invisible strong pinning centres. Yet, such obstacles may well be experimental artifacts, produced, for example, by impurity atoms

---

[3]Internal friction [118, 114] measurements were also performed earlier that could achieve the same effect, but they became less popular because of the difficulty of relating the data on absorption peak to kink energies[101].

69

diffusing in from the surface, or by the high energy electron beam itself. Thus they may be irrelevant for bulk semiconductors.

Certain types of impurity atoms are found to have a strong effect on dislocation mobility while others do not. *In situ* X-ray topography [104] data suggests that impurity atoms, such as nitrogen, oxygen, phosphorus and boron, tend to make dislocations immobile at stress below certain critical value, $3 \sim 5$MPa, depending on impurity type and concentration. Above the critical stress, these impurities are reported to have different effects. Nitrogen is seen to have no effect after reaching the threshold stress, while oxygen causes dislocation velocity-stress relationship to become non-linear in the low stress regime. Likewise, boron (in p-type Si) does not seem to have much effect once dislocations begin to move, but phosphorous (in n-type Si) is known to enhance dislocation mobility. Because it is difficult to ensure that there is only one type of impurity in the sample, the above conclusions must be taken with caution. The effect of electrically active impurities (B and P) on dislocation mobility was explained by the electron hole transfer between bulk crystal and dislocation levels [119].

Selective etching experiments also showed that phosphorous doped silicon sample has a starting stress of about 2MPa for dislocation motion [107]. This was explained by kink expansion through randomly distributed obstacles. This result too may be subject to experimental artifacts due to surface effects. Starting stress behavior was also observed in SiGe crystals with different Ge concentrations[120]. It was proposed, that at small Ge concentration, dislocations drag a Cottrell atmosphere, while at large Ge concentrations kinks drifting along a dislocation would interact with random obstacles.

While the dragging effect of impurity atoms is expected, the effect of intrinsic point defects on dislocation mobility in pure silicon remains unclear. It was found that $60°$ dislocations, when subject to climb forces, may become unstable during motion, i.e. some segments move faster than others so that the dislocation line becomes ragged [97]. It was postulated that this is due to vacancy absorption or emission by a dislocation, which in turn modifies the dislocation core. However, detailed atomistic mechanism is lacking. Double cross slip of screw dislocations also has been proposed as a mechanism for dislocation point defect interaction[116]. The motion of screw dislocations after double cross slip requires jog dragging which depends on the rate of emission or absorption of point defects. Interaction with intrinsic point defect and climb also seem to be necessary to explain the forward-backward asymmetry of dislocation mobility observed in [105].

3.5   Outstanding issues

Although silicon has been a favorite material for theoretical and experimental investigations on dislocation mobility, many issues still remain unresolved. It appears that dissociated glide-set dislocations and perfect shuffle-set dislocations control the plastic deformation of semiconductors at high and low temperature regimes, respectively. However, a satisfactory explanation of the origin of this transition is lacking. Specifically, the atomistic pathways for a shuffle-set dislocation to transform into the glide-set are poorly understood. Atomistic modeling coupled with experimental observations should be able to resolve this issue.

The disagreement among theoretical values for the formation and migration energies of kinks on the glide-set partial dislocations reported by different groups is a serious concern. While some of the disagreement can be attributed to the multiplicity of kink species, the fidelity of the atomistic models themselves is an issue. *Ab initio* DFT calculations are the most accurate among the approaches currently in use, but they suffer from the artifacts of boundary conditions in small computational volumes. The situation is expected to improve with the increasing availability of more powerful computers and algorithmic improvements. One particular aspect ripe for theoretical exploration is kink mechanisms in the perfect shuffle-set dislocations. Recent experimental data provide ample evidence for their importance. In fact, given the relative simplicity of the shuffle dislocations compared to the glide partials, it may be possible to establish a consistent picture of kink dynamics in the shuffle-set perfect dislocations first.

Better mechanistic understanding of interactions between intrinsic point defects and the dislocation core is needed. These include climb and cross slip, as well as point defect generation as a result of dislocation motion, such as by jog dragging. There are still debates on whether kinks or point defects are the controlling factor for dislocation motion. The effect of electrically active dopants on dislocation core, i.e. the electro-mechanical coupling, is a promising area where *ab initio* calculations and experiments can be combined to address technologically important questions. Atomistic mechanisms of dislocation nucleation in misfit layers and surface effects on dislocation mobility and multiplication are two more issues of significant technological importance and theoretical interest.

Evidently, the complexity of atomistic mechanisms in the dislocation core is nearly "bottomless". A "bottom-up" approach, in which one attempts to

predict the complete behavior of dislocations after mastering "all" the atomistic mechanisms, seems to be impractical. Instead, a "top-down" approach could be more promising where a larger scale dislocation model is used to provide guidance on which of the atomistic mechanisms are important and under what conditions. Once this is established, high-accuracy calculations can be performed to determine a selected set of important parameters.

4 BCC Metals

4.1 Introduction

BCC metals and alloys have been heavily used by humankind since the Iron Age. Their most useful property is high strength over a wide range of temperature and straining conditions. Combined with the abundance of the iron ores, the relatively straightforward technologies for metal extraction and the high formability at reasonable temperatures, iron alloys naturally became and continue to be the kings of structural materials. BCC metals, e.g., the refractory metals Mo, W, Nb, Ta and others, also served as important elements for more specialized applications; when used in combinations with Fe, they can greatly improve the quality of structural materials.

Although there are considerable variations in the plasticity behavior of BCC materials, it is well recognized that certain generic behavior can be attributed to their common lattice crystallography. Among these characteristics are the prominent temperature and strain-rate dependence of the yield stress, features of slip crystallography, and the existence of a ductile-to-brittle transition at low temperatures. This last property is a manifestation of the inability of dislocations to multiply and/or move fast enough, at low temperatures, to relieve the stress concentrations that are the causes of cracking.

As shown in Fig. 30(a) [121], TEM micrographs of deformed specimens show characteristic features of long screw dislocations often stretching along many microns, with no or very little deviation from the perfect screw orientation. This anisotropy of dislocation microstructure directly reflects the anisotropy of dislocation mobility. In situ TEM observations [122] show very clearly that at low and moderate temperatures screw dislocations move much slower than edge and mixed dislocations. For example, in pure molybdenum at room temperature the velocity of screw dislocation has been estimated to be 40 times lower than that of edge dislocations [123]. The pre-strained microstructure dominated by long screw segments is produced by rapidly moving edge dislocations under stress. Some early dislocation velocity measurements have suggested that screws actually move faster than edges [124, 125, 126]; however, such behavior could be due to surface related enhancement of screw mobility or even the artifacts of chemical etching used to monitor dislocation motion, and in any event it is unlikely that such data are representative of dislocation behavior in the crystal bulk.

Another common element of the microstructure in BCC metals is a high
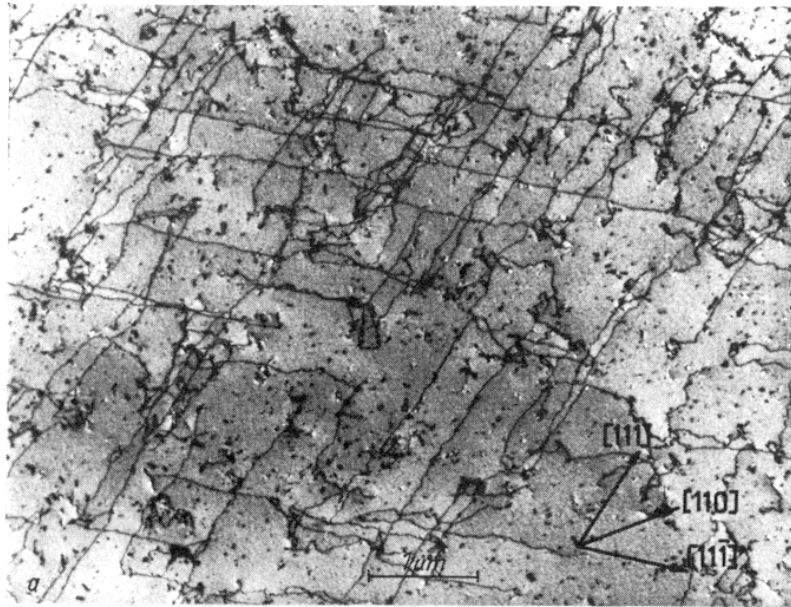
(a)
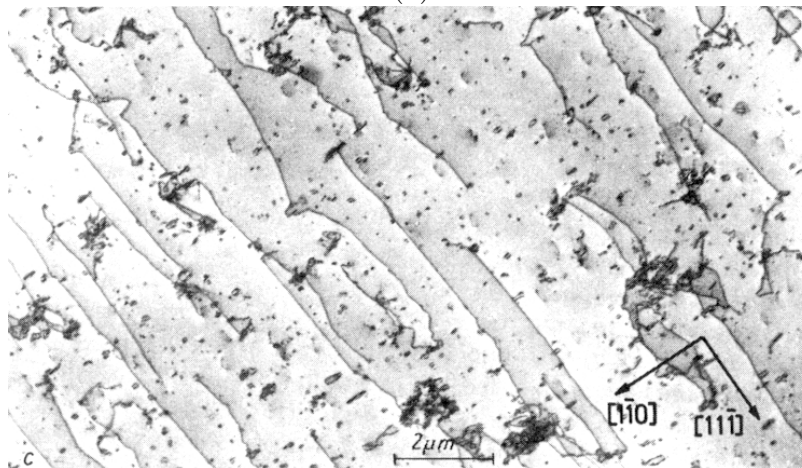
(b)

Figure 30: (a) Dislocation microstructure in Mo under 2% tensile strain along [110] at 77K. (b) Dislocation microstructure in Mo under 5.8% tensile strain at 293K [121].

concentration of debris in the form of vacancy and interstitial loops, which are often observed after deformation, as shown in Fig. 30(b) [121]. The debris concentration typically increases with increasing straining rate. While mechanisms of such debris production are not entirely clear at present, a possible explanation for this behavior will be discussed later in this section.

The dominant dislocation type has Burgers vector $\frac{1}{2}\langle 111 \rangle$, which is the smallest repeat vector of the BCC lattice. $\langle 100 \rangle$ dislocations are also observed. The latter are thought to be products of reactions between $\frac{1}{2}\langle 111 \rangle$ dislocations. Slip trace analysis reveals slip in $\{110\}$, $\{112\}$ and even $\{123\}$ planes of the $\langle 111 \rangle$ zone [127, 5]. At higher temperatures, the so-called pencil or non-crystallographic slip is observed such that the slip plane, on average, follows the maximum resolved shear stress (MRSS) plane, with the slip traces having a wavy appearance [128, 129, 130]. The zonal character of dislocation slip and the mentioned TEM observations underscore the prominent role of screw dislocations in the plasticity of BCC metals. In the kinematical sense, at low and moderate temperatures (below ~ 400K) the non-screw dislocations behave as "slaves" to the dominant screws.

Both calculations and experimental observations suggest that there are no stable stacking faults in BCC metals, at least in ambient conditions. If so, then the dislocations in these solids should not dissociate in a planar, FCC-like fashion. Combining this with the fact that the BCC dislocation cores are observed to be rather compact and the pre-dominance of screw dislocations already mentioned, one sees that plasticity in BCC metals should be strongly influenced by cross-slip processes. The very term "cross-slip" coined to describe rather infrequent events where the dislocation changes glide plane in FCC metals, could be somewhat misleading when used to describe the motion of screw dislocations in BCC metals. Given its compact core, a screw dislocation does not have to first constrict in order to change its glide plane; there would be always more than one glide plane that is available. The selection of glide plane and resulting slip crystallography are likely to be governed by rather more subtle effects in the core of the screw dislocation than the planar dissociation invariably observed in FCC metals. As recently emphasized by Duesbery and Vitek [131], existing perceptions about dislocation behavior in BCC metals are heavily influenced by the views developed earlier for FCC and HCP metals. Since the extrapolation of these views beyond these crystallographic classes has not been well justified, the "FCC ideology" should not be applied to BCC metals without a sound basis.
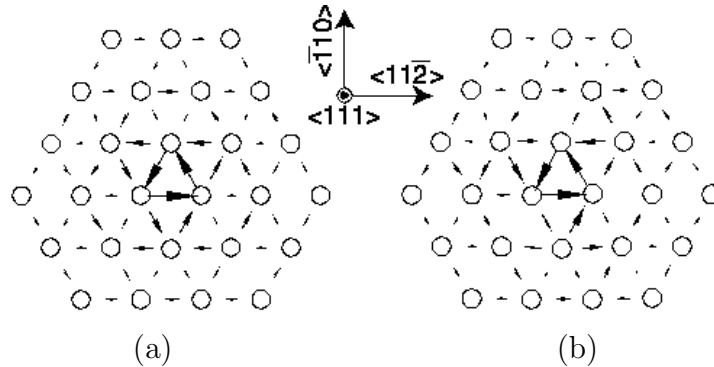
Figure 31: Differential displacement map of screw dislocation core in BCC metals, (a) symmetric core, (b) asymmetric core [139].

4.2 Core structure and lattice resistance

4.2.1 Screw dislocations

The early ideas about the structure of screw dislocation core are centred around the hypothesis of FCC-like planar splitting for explaining the observed slip phenomenology [132, 133, 134]. In a drastic departure, Hirsch suggested that screws can dissociate in more than one plane and that such a non-planar dissociation can explain the observed high Peierls barrier and the strong temperature dependence of the yield stress [135]. Initially, various variants of screw dislocation splitting were considered (for a review see [136]). Eventually, with the help of computer simulations, the thinking converged to the well-known three-way dissociation into three equivalent {110} planes. Vitek et al [137, 136] and Duesbery et al [138, 131] have clearly shown that such a dissociation can occur even when no plane of the {111} zone contains a stable stacking fault. Still, the use of the term "dissociation" implies that the perfect screw dislocation somehow splits into several partials or, fractional dislocations. We think that such a picture is not necessarily appropriate for describing the screw dislocation core in BCC metals as it could lead to complications and even misunderstanding. In the following, we will refer to dislocation core spreading as "polarization", resulting from a symmetry-breaking core reconstruction.

Fig. 31 shows differential displacement maps (DDM) [140] of screw dislocations. Each circle represents a column of atoms. The dislocation line and

Burgers vector are parallel to the atom columns, i.e. along z direction (out of the plane). The DDM map is constructed by first computing the atom displacement (along z direction) with respect to perfect lattice for each column. The arrows then indicate the difference between displacements of neighboring columns. The length of the arrow is proportional to the magnitude of displacement difference and the direction of the arrow indicate the sign of the displacement difference, i.e. the column that the arrow points to has a larger displacement than the column on the other end of the arrow. Because the lattice is periodic in z direction by Burgers vector b, the displacement difference, i.e. the differential displacement, between any two columns can be only defined *modulo b*. By convention, the differential displacement is always mapped into the domain of $(-b/2, b/2]$ by adding or subtracting multiples of b. Among the three atoms in Fig. 31(a) that surround the centre of dislocation, the DDM arrows form a closed circuit. The differential displacement between any two atoms out of these three, going counterclockwise, is $b/3$. By going around any circle containing the dislocation centre, one accumulates a total displacement b. We should emphasize that while the arrows in the DDM are all in the plane for convenience of visualization, the displacement component they represent is strictly out of the plane.

It should be noted that, regardless of the details of misfit distribution, the core is rather compact. That the core spreads is a consequence of elastic-energy reduction; any such spreading can be interpreted as fractional splitting of the perfect screw dislocation core into the planes of the {111} zone. Less obvious is which directions and planes the spreading entails. The fine structure of the core would depend on subtle details of atomic interactions in the core. Some atomistic models predict nearly equal core extensions in all directions while others show a characteristic splitting into three directions on three {110} planes of the zone. The latter can be interpreted as a core reconstruction that also spontaneously breaks the symmetry of the host lattice.[4] The atomistic meaning of this core reconstruction is very simple: three rows of atoms immediately bounding the geometric centre of the screw dislocation shift in the same direction along the Burgers vector [141]. This shift can take place in either of the two directions along the dislocation line, giving rise to

_____

[4]The symmetric core configuration is sometimes unfortunately referred to as six-fold symmetric, whereas the symmetry-broken structure is described as three-fold symmetric. This description is incorrect and misleading. The symmetry around the {111} zonal axis remains three-fold, regardless of the core reconstruction. The symmetry that is broken is that with respect to 180°-rotation around any of three {110} axes of the zone [5](p. 370).

two energetically equivalent but geometrically distinguishable core variants. We will discuss the possible consequences of such core reconstruction, aka polarization, later on in this section.

The detailed structure of screw dislocation core in BCC metals has been examined through atomistic simulations [142, 143, 144, 145, 146, 147, 139], particularly with regard to the effects of in-core relaxation. Most of the earlier calculations predicted a polarized core structure that was seemingly observed in HREM experiments [148]. Polarization was a significant issue since the details of the atomic rearrangement in the core were thought to have an effect on the lattice resistance to dislocation motion. Specifically it has been an almost universal belief that the high Peierls stress of the screw dislocation is a direct consequence of their non-planar core structure. According to this view, the mobility of the screw dislocation must be limited because, by spreading into several planes of the zone, the dislocation effectively anchors itself to the lattice, such that in order to translate through the lattice it has to retract some of its extension, a process that requires considerable energy. The anchoring effect of non-planar dissociation is thought to be more pronounced when the core is polarized, since then the core extension would be maximum [149]. Recently this belief has been called into question by *ab initio* calculations [139] which presented evidence that even non-polarized screw dislocations in Mo and Ta have high Peierls stress, of the order of 1GPa. On the other hand, it has also been observed that the Peierls stress is a sensitive function of core polarization [150]. In view of the these contradictory results, it seems prudent to conclude that high Peierls stress is not necessarily caused by non-planar core dissociation or polarization, and yet, with all things being equal, core polarization may have an effect on the Peierls stress. That core polarization may not be the dominant factor for the magnitude of Peierls stress is consistent with the observation that, under shear stress approaching the maximum (Peierls) sustainable level, the dislocation core undergoes profound changes that effectively wipe out the features of core structure observed at zero stress [151, 152].

That the compactness of the core gives rise to a large Peierls stress is also an effect described by the Peierls model of dislocation core. It is evident that, for a dislocation to translate from one lattice position to the one adjacent, the more extended the core the less each atom in the core has to move relative to its neighbors. While clearly more atoms take part in the translation of a wider core, the Peierls barrier for the wider core is lower because of the highly non-linear character of interatomic interactions in the core. This effect is also

seen from a well known correlation between the core width and Peierls stress in FCC metals [6]. The opposite effect can also occur - a dislocation with narrow core, notably in Si, can have very high Peierls stress, approaching the ideal shear resistance of the crystal [59] (see the preceding section).

In atomistic simulation when the applied stress reaches the Peierls value, a screw dislocation responds by moving along one of the crystallographic planes of the $\frac{1}{2}\langle 111 \rangle$ Burgers vector zone, most often a $\{110\}$ plane closest to the MRSS plane. Depending on the interatomic potential, the translation plane can be $\{112\}$ [152] as well. For example, the FS model potential predicts that screw dislocations in Mo move along $\{110\}$, but in Ta they move along $\{112\}$ [131]. Also, screw dislocations simulated by using Finnis-Sinclair's model of bcc-Fe are observed to move on either a $\{112\}$ or a $\{110\}$ plane depending on the orientation of the MRSS plane [33]. The slip-plane selection and critical stress condition for screw dislocations are clearly in violation of the Schmid law [153]. For example, in cases where the screw dislocations show a definite preference to glide, say, on $\{110\}$ plane the Schmid law specifies which of the three $\{110\}$ planes of the zone will be selected, as well as the level of applied stress σ_{ij} at which the dislocation should begin to move, the latter being given by

$$\sigma_{ij} s_{ij} = \tau_{PN} \ , \tag{25}$$

where τ_{PN} is the Peierls stress and s_{ij} is the Schmid tensor of the given plane. For a pure shear stress σ applied along the Burgers vector, the relation reduces to

$$\sigma = \tau_{PN} / \cos(\chi), \tag{26}$$

where χ is the angle between the MRSS plane and the nearest $\{110\}$ plane. Relative to the Peierls stress for $\chi = 0$, the Peierls stress variation specified by the Schmid law is shown in Fig. 32. The variation simulated using an atomistic model of Mo, also shown, is clearly in considerable disagreement with the Schmid law [154, 153]. This and almost all other atomistic calculations reported so far showed that the motion of screw dislocation in BCC metals at low temperature does not follow the prescriptions of Schmid law [153]. The origin of the non-Schmid behavior is largely due to the twining-antitwining asymmetry of the BCC lattice, which makes $\chi = 30°$ and $\chi = -30°$ drastically different from each other. In addition to the non-Schmid χ-dependence, other stress components have been found to affect the critical stress, most notably the components perpendicular to the Burgers vector [155, 156]. Duesbery and Vitek [131] traced such non-Schmid effects to a coupling between

the applied stress and a small but resolvable edge components of displacement observed in the core of the screw dislocations. An extensive and thorough analysis of various non-Schmid couplings affecting the motion of screw dislocations in BCC metals was presented by Duesbery in volume 8 of this series. An alternative to coupling with edge components is that the activation energy for motion couples to other stress components via the activation strain. A specific case would be coupling of isostatic stress to a variation in the nonlinear dilatometric field of the dislocation, which could vary during kink formation.

Given that the Peierls stress of a screw dislocation is considerably higher than that of non-screw components, it is usually assumed that the macroscopic yield stress at low temperatures is closely related to this stress, a reasoning that finds support in the results of Dislocation Dynamics simulations [157]. As we have just discussed, the well-documented violations of the Schmid law in the yield behavior of BCC metals are in general agreement with atomistic simulations [143, 145, 147, 139]. In this context, the current discrepancy between the computed and experimental estimates of the Peierls stress is puzzling. The atomistic calculations consistently overestimate the yield stress (see e.g. [121, 158]) by a factor of 2-4. For example, the zero-temperature limit of yield stress for Mo is 750MPa [121] while the Peierls stress for screw dislocation from atomistic calculations is around $2 \sim 3$GPa [146, 147]. Attributing the discrepancy to the inadequacy of interatomic potentials, while seemingly reasonable, is not supported by recent DFT calculations [139] which also gave Peierls stress values for Mo and Ta several multiples of the experimental estimates. Another hypothesis suggests that the lower experimental values reflects the collective motion of dislocations in groups and amplification of the applied stress through the mutual interaction of dislocations in each group [159]. This explanation appears tenuous and does not provide a mechanistic interpretation. At present the consistently lower values of the experimental yield stress point to a fundamental aspect of dislocation behavior in BCC metals that remains to be explained. In the next subsection concerning secondary core defects, we will discuss simulation findings that relate the yield-stress discrepancy to particular features of interaction between screw dislocations.
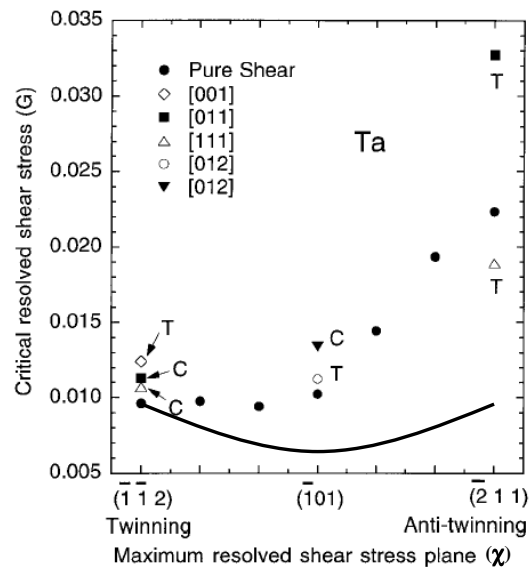
Figure 32: Screw dislocation Peierls stress for different loading stress directions in the {111} zone. The solid line shows the prediction of Schmid law and the symbols show typical atomistic simulation results [145].
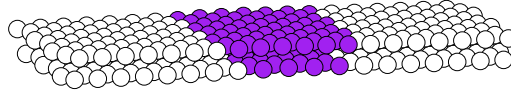
Figure 33: Core structure of an edge dislocation. Two layers of atoms immediately above and below the glide plane are shown. Atoms with local energy 0.1eV higher than the bulk are plotted in black to show the dislocation core.

4.2.2 Non-screw dislocations

The core structure of edge (Fig. 33) and other non-screw dislocations, is relatively unremarkable when compared to the screws. The core shows moderate spreading in the glide plane although no clear planar dissociation can be detected. The Peierls stress of non-screw dislocations in BCC metals is commonly assumed to be low. Duesbery and Xu [160] have challenged this belief by presenting atomistic simulations that gave a high Peierls stress for pure edge dislocations in Mo (FS potential), of the order of 0.5 GPa. The authors assumed that mobility of edge dislocations at non-zero temperatures should be controlled by kink mechanisms, similar to the ones operating in screw dislocations. This interpretation was in turn called into question by another simulation study giving more attention to the effects of boundary conditions as a source of error in determining the Peierls stress [40]. The present status is that a converged Peierls stress value for pure edge dislocations, obtained using the FS model of Mo, is just 25 MPa, more than an order of magnitude lower than that reported in [160]. Although different boundary conditions, fixed and periodic, respectively, were used in the two studies, it is evident that finite-size simulation cell effects, if not properly treated, can lead to serious errors.

An implication of the above noted discrepancy is that the relation between Peierls stress and the dislocation character remains to be clarified. There is an indication from atomistic calculations that some non-screw dislocations have much higher Peierls stress than the others [161]. In contrast to the
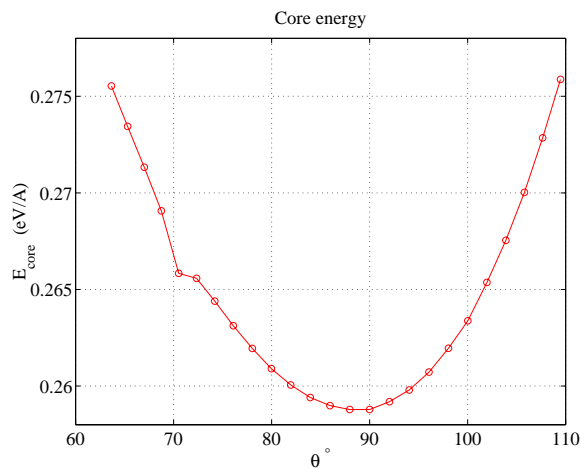
Figure 34: Core energy of non-screw dislocations in BCC Mo as a function of character angle, with core radius $r_c = 1b$.

earlier work [160], it is not the pure edge dislocations that have exceptionally high Peierls stress but the 71°-mixed dislocations denoted M111 in [162, 161]. For the latter the fully converged Peierls stress value for the same FS model potential is 320 MPa, whereas for the other non-screw dislocations on {110} planes the stress is generally 20-30 MPa. These values are in contrast to the value of 2.4 GPa obtained for screw dislocations using the same potential model. That the M111 dislocations are special is indicated by the observation of a cusp-like dependence of the dislocation core energy on the character angle, with the cusp centred precisely on the M111 character angle (Fig. 34). This cusp resembles the well-known behavior of the grain boundary energy as a function of the misorientation angle, near a special low-Σ boundary [163]. The essential difference here is that dislocations, unlike grain boundaries, produce long-range elastic fields; their energy is dominated, in most cases of interest, by the elastic energy. Since the dominant elastic component of the dislocation energy is generally a smoothly varying function of the character angle, the cusp-like feature shown in Fig. 34 is not as distinct as that seen in the grain-boundary energy. It takes a special effort and the use of very accurate methods [164] to observe cusp-like features in atomistic calculations of dislocation energies.

The observation of dislocation energy cusps implies that the two orienta-

83

$$[\bar{1}2\bar{1}]$$
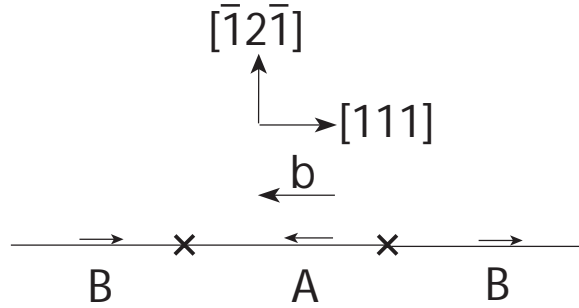
$$\rightarrow [111]$$

b

B A B

Figure 35: Schematics of reconstruction defects (RD) on screw dislocation core in BCC lattice. The arrows indicate the direction of reconstruction displacements of the three atom columns in the core. They are opposite in A and B type cores, forming two types of RD's, AxB and BxA [141].

tions (screw and M111) correspond to particularly favorable packing of atoms in the dislocation core. Analogous to special grain boundaries, at both orientations the dislocation displays special properties, notably a high Peierls stress. It would be useful to examine whether kink mechanisms operate in the M111 dislocations at non-zero temperatures and if the cusp-like behavior can result in experimentally detectable features of dislocation microstructure.

4.3   Secondary core defects

4.3.1   Reconstruction defect

It has been already noted that polarization of the screw dislocation core in BCC metals is a special case of symmetry-breaking core reconstruction. Symmetry arguments in fact provide a unique perspective from which to analyze the core structure. This particular core reconstruction breaks a dyadic symmetry with respect to 180°-rotation around a $\langle 110 \rangle$ axis, resulting in a two-fold degenerate core, i.e. there exist two geometrically distinguishable but energetically equivalent variants of the reconstructed (polarized) ground-state core structure. This suggests that reconstruction defects (RD), or anti-phase defects should appear where the dislocation core divides into two segments, each with a different reconstructed core. As noted in [141, 165] there are two types of RD in a reconstructed $\frac{1}{2}\langle 111 \rangle$ screw dislocation in BCC lattice, denoted as AxB and BxA flips. The meaning of these terms is easy to

understand by observing that the core reconstruction involves moving three central rows of atoms together in the same direction with respect to their immediate neighbor rows. One variant of the core reconstruction produces a shift in, say, positive Z direction (along the Burgers vector), while the other variant results in an identical shift in the opposite direction. When two adjacent core segments shift in opposite directions, they will either shift towards each other or move apart, to produce respectively a compressed region (BxA-flip, positive pressure), as shown in Fig. 35, or an extended region (AxB-flip, negative pressure). If the displacement of three central rows is equal to $b/6$, the maximum possible value, then a BxA-flip is an interstitial-like defect while the AxB-flip defect is vacancy-like. In atomistic calculations smaller displacements leading to partial interstitial or vacancy-type defects have been observed [166].

Given that core degeneracy can affect screw dislocation motion, it is appropriate to examine if and how this degeneracy can be removed by stress. Using the Finnis-Sinclair potential model, we find [73] that energy degeneracy of the two variants of a polarized screw dislocation core in Mo is indeed removed by either one of the two glide stress components, shear stresses applied along the Burgers vector on any plane of the zone. Furthermore, the non-glide stress component, called "edge" stress, also removes the degeneracy. This means that under the action of an appropriate stress component, one of the polarization variants of a screw dislocation core becomes energetically favored relative to the other, and occupies a larger fraction of the core length. Furthermore, if the "wrong" core variant were somehow created, it would have a tendency to convert to the low energy variant, most probably by the stress-induced drifting of RD's. In other words, the motion of RD's along the screw dislocation core could be coupled to the external stress. Activation of one or the other core variant and the conversion rate will depend on the magnitude of the degeneracy splitting and the kinetics of flip nucleation and motion. This effect contributes further to the already complex picture of how the glide and non-glide stress components can affect the choice of slip planes of screw dislocation.

4.3.2   Kinks

A Peierls stress of the order of 1 GPa signifies a correspondingly high energy (Peierls) barrier and motion of screw dislocation at non-zero temperature, via thermally and stress-activated kink-pair mechanisms (see the preceding

section). Early calculations by Duesbery showed that nucleated kinks experience very low resistance to their motion along the screw line [141], consistent with the observation of very long and geometrically straight screw dislocations [122]. Therefore, the overall rate of dislocation motion seems to be controlled by kink-pair nucleation events. Later calculations confirmed that the kink migration barrier [40] is indeed low relative to the kink-pair nucleation barrier and the energy of a stand-alone kink [143]. For example, the FS model potential for Mo predicts that kink-pair nucleation energy is 1.2 eV while the Peierls stress for kink motion along the line is 20 MPa, quite similar to the Peierls stress of pure edge dislocations [40].

Historically, various continuum models have been used to model kinks in screw dislocations in BCC metals. Dorn and Rajnak [167] have applied a line tension model to examine analytically the transition state for kink-pair nucleation. This model provides a useful relationship between the Peierls stress, Peierls barrier, and kink-pair formation energy, which is given earlier in Eq. (24). Early in the 70's several other continuum models were proposed based on the understanding at the time of the structure of screw dislocation core [168]. Recently, Ngan developed a Peierls-Nabarro model that accounts for the observed non-planar extension of the screw core [169, 170]. This model allows numerical evaluation of kink energies using the γ-surface data as an input. In comparison, direct atomistic calculations of kinks to be discussed below, are still too expensive and/or inaccurate and have so far produced relatively few data points for kink energetics. The continuum models, although approximate, provide an inexpensive alternative to atomistic calculations for a general study of variation of kink-pair energy with stress. By matching the continuum models to suitable atomistic counterparts at selected data points, one can hope to achieve results valid over a wide range of temperature and stress conditions.

An interesting continuum model of kink-pairs in screw dislocations in BCC metals was suggested by Edagawa et al [171] which departs completely from the FCC-inspired notion of the γ-surface as the core misfit potential. Instead it is assumed that the dislocation-lattice coupling (Peierls potential for the screw dislocation) can be specified as a 2D surface in the XY plane perpendicular to the direction of the Burgers vector:

$$E[x(z), y(z)] = \int_{-\infty}^{\infty} \left\{ \frac{\Gamma}{2} \left[\left(\frac{dx}{dz} \right)^2 + \left(\frac{dy}{dz} \right)^2 \right] + V_p(x, y) - \tau b(x \cos \chi + y \sin \chi) \right\} dz,$$

$$(27)$$

where E is the total-energy of the dislocation having the configuration $\mathbf{r}(z) = [x(z), y(z)]$ with respect to the initial equilibrium configuration at $\mathbf{r}_0 = (x_0, y_0)$, Γ denotes the line-tension of the dislocation and $\Phi(x, y) = V_p(x, y) - \tau b(x \cos \chi + y \sin \chi)$ is the effective Peierls potential including the work done term. The dislocation containing a kink-pair is represented by a continuously curved line in 3D whose shape is obtained by the variation of the total energy containing three terms: (1) a positive elastic (line tension) self-energy of the curved dislocation, (2) a positive Peierls energy per unit length integrated over the entire dislocation line, and (3) a negative mechanical work by the applied stress causing the line to bow out from its initially straight configuration. This model appears to be most appropriate for describing screw dislocations in BCC metals, accounting correctly for their non-planar core structure and motion. The model also provides a reasonable description of the kink-pair nucleation barrier and its dependence on stress, and even the χ-dependence of Peierls stress discussed above is correctly reproduced [171]. Consequently, such a formulation may be suitable for parametrization against atomistic calculations, in which case just two parameters are sufficient to fully define the non-planar misfit potential (equation above). One may use, for example, an atomistic value of the kink-pair energy at zero stress and, in the opposite limit, a value of the Peierls stress, say, for $\chi = 0$. The misfit potential thus produced can be used to compute and tabulate the kink-pair nucleation barrier in the entire range of applied stress. Used in this manner, the model serves as an interpolation function for kink-pair nucleation barrier between two limits, a state of zero stress and that of Peierls stress.

However useful, the continuum models nevertheless cannot account for salient atomistic features of the dislocation core structure and dislocation motion. Only calculations taking into account explicitly the atomic degrees of freedom can properly describe the subtleties of dislocation behavior in BCC metals in their full complexity. These are discussed below.

Fig. 36 shows the schematics of core atoms in screw dislocations with kinks on the (110) plane. Because the BCC lattice is not symmetric with respect to 180° rotation along $\langle 111 \rangle$ directions, the left and right kinks on the screw dislocation are not degenerate, even when the core is not polarized [87]. For the polarized core, there are six different kink types in various combinations of two RD's and two original kinks [87]. Duesbery has referred to the kinks with the same sense of polarization on each side and the kinks separating two segments of opposite polarization as homokinks and heterokinks respectively [141]. In view of the possible kink pairs on {110} planes, there
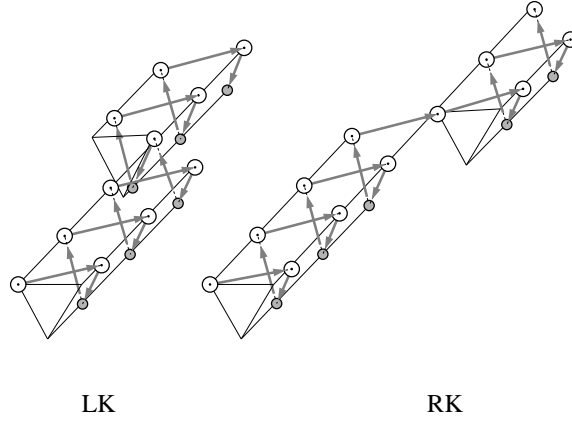
LK   RK

Figure 36: Core atoms of a screw dislocation in BCC lattice with left kink (LK) and right kink (RK). LK and RK are different because of the lack of 180° rotation symmetry along ⟨111⟩ direction of the BCC lattice.

are several distinct combinations of homo- and heterokinks that may contribute to dislocation motion [159]. Atomistic calculations performed so far indicate that one particular kink-pair, namely the pair called $BnApB$ in [159], has the lowest nucleation barrier. When the dislocations move by nucleating and expanding this kink pair, its core polarity will be reversed each time it moves by a unit step on the (110) planes. As shown in [159], this kink pair provides a 3D atomistic path for dislocation translation that is consistent with the zig-zagging motion of straight screw dislocations observed in the earlier 2D simulations [152]. Thus, a case can be made for this particular kink pair as the dominant translation mechanism below the Peierls stress. As a cautionary note, we observe that, just like in the case of kinks in glide partials in Si (see the preceding section), the flips that must be present in the core may facilitate the nucleation of other kink-pairs that can compete with this pair. If this is the case, dislocation motion under stress can proceed through a complex sequence in which several types of kink-pairs contribute simultaneously. Later on, we will discuss yet another possible contribution of flips to the "rough" motion of screw dislocations under high stress.

Atomistic simulations have found that the centre of the dislocation has to
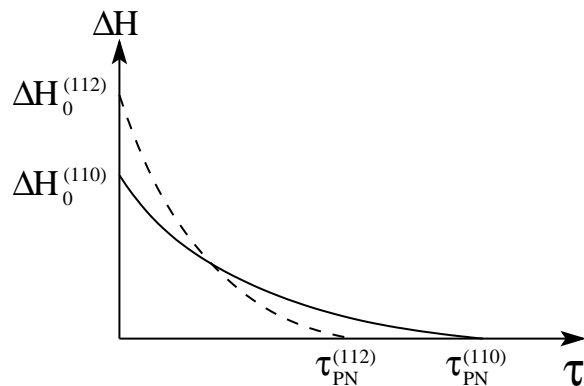
Figure 37: Double kink nucleation barrier as a function of stress. Solid and dashed curves represent kinks on (110) and (112) planes respectively.

reside in one type of the triangles (either $\triangle$ or ∇, depending on the Burgers vector) in the triangular lattice of atom rows when looking along the Burgers vector direction (Fig. 31). Centering the dislocation in the "wrong" triangle will result in three core atoms sitting on top of each other, resulting in the high energy "hard core" configuration, instead of the low energy "easy core" configuration [143]. For this reason, translation of the dislocation core on the $\{110\}$ plane, or equivalently along the $\langle 112 \rangle$ direction requires a minimum core displacement from one "easy" position to another. Translation on the $\{112\}$ plane, or equivalently along the $\langle 110 \rangle$ direction requires a displacement that is $\sqrt{3}$ times larger. Therefore, most atomistic simulations have focused on kinks on the $\{110\}$ plane. Duesbery has shown that at zero stress the $\{112\}$ kink pairs, being unstable, dissociate into shorter $\{110\}$ kinks. In this as yet unpublished work, Duesbery used the NEB technique [172, 173] to explore the atomistic paths for kink-pair nucleation in which the final (destination) state of the dislocations contains a $\{112\}$ kink pair. The search showed that the dislocation, although forced to make a large $\{112\}$ step, preferred to do it in two smaller $\{110\}$ steps. On the other hand, Seeger considered kink-pairs in the $\{112\}$ plane and developed a theory that agrees well with experimental data on internal friction. Therefore, which kink matters in what conditions is still an open issue.

According to the elasticity theory kinks on $\{110\}$ plane should have 1/3 the energy of those on $\{112\}$ plane simply because kink energy is proportional to the square of its height. Atomistic simulations of straight screw disloca-

tions at zero temperature show that, depending on the interatomic potential, dislocations can move on {112} planes under stresses equal to or exceeding the Peierls value [131]. Such motion can be viewed as a limiting case in which the stress is sufficiently high to overcome any effect of the kink-pair nucleation barrier. That dislocations move along the {112} planes at stress equal to the Peierls stress implies that as the stress levels approaches this critical value from below, the effective barrier for {112} kink-pair nucleation must have been greatly reduced to allow this mechanism to operate. At low stress the {110} kink-pairs should be still favored given their lower nucleation energies at zero stress. The overall stress dependence of kink-pair nucleation barrier can be one which connects smoothly the the high-stress limit favoring the {112} kink-pairs with the low-stress limit where the {110} kink-pairs dominate, as depicted schematically in Fig. 37. A crossover between the two regimes offers a possible resolution of the current controversy.

Recently Wen and Ngan presented an exploration of atomistic mechanisms of kink-pair nucleation in α-Fe [174]. Their results show that the $BnApB$ kink-pair has the lowest activation barrier among all possible candidates. Seen in Fig.7 in their paper [174] are signs of a degeneracy-removing coupling between the glide stress and the core polarization. This work is a definitive description of atomistic mechanisms of kink-pair nucleation in the relevant range of applied stress, from zero to Peierls, which should pave the way for similar future studies. The main conclusion that core polarization favors pencil glide, however, appears to be questionable. The mixing of two different translation directions, as required for pencil glide, is more likely when the core is not polarized so that the screws can translate by any of the six {110} kink-pairs. In this case, the ratio of glide stress resolved on two neighboring {110} planes can be anywhere between 0.5 and 1.0. In the case of a strong core polarization considered by the authors, i.e. when translations can take place only by three kink pairs of the $BnApB$ type, the resolved stress ratio spans a significantly wider range from -0.5 to 1.0. Most of this range is far from the ratio of 1.0 ideal for the pencil glide mixing.

4.3.3 Junction Nodes

The junction node where three dislocation segments meet is a special (point-like) entity which can play a significant role with regard to the above mentioned discrepancy between the Peierls stress determined atomistically and the observed low temperature limit of the yield stress. Matsui et al. [175]
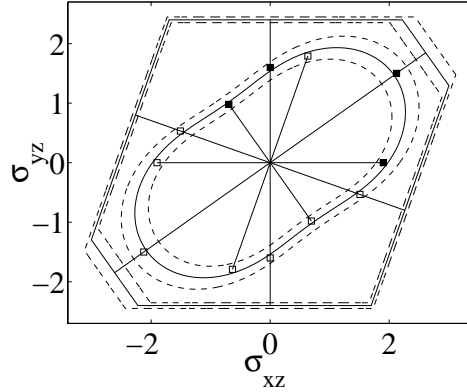
90

Figure 38: Peierls stress of the dislocation network as a function of stress orientation. Filled symbols show the values of critical stress for the four directions actually tested. Open symbols are obtained by symmetry. Dashed lines indicate the range of error in the computed Peierls stress [179].

have suggested that the 3-nodes at the ends of a dislocation junction can act as sources of dislocation kinks, thereby explaining the anomalous slip behavior observed in some high-purity BCC metals at low temperatures [176]. According to the proposed Co-planar Double Slip (CDS) mechanism, the enhanced kink nucleation at the nodes can more than compensate for a low resolved stress on the anomalous slip system which then becomes more active than other more highly stressed systems. Subsequently, Saka et al. [177] observed motion of co-planar junction networks using *in situ* TEM. However, this observation was challenged by Garratt-Reed and Taylor [178], who noted that dislocations had to move against the applied stress in some stage of the CDS glide and therefore such a mechanism was unlikely to operate. Garratt-Reed and Taylor suggested an alternative mechanism for facilitating screw dislocation motion in the glide plane [178]. In their mechanism the dislocations approaching each other do not need to form a junction to move faster; they can exert torques on each other causing them to bend in the anomalous {110} plane. While such trajectory change may prevent the dislocation from getting any closer, it can also be an efficient source of kink nucleation. The two hypotheses, although differing in details, both emphasize that dislocation interactions, whether local as in CDS or remote as in Taylor's mechanism, can enhance dislocation mobility rather significantly.

91

Recently, direct atomistic simulations of the motion of a screw dislocation network have been performed to verify the feasibility of the CDS mechanism in BCC metals [179]. As two sets of $\frac{1}{2}\langle 111 \rangle$ screw dislocations zipped together to form $\langle 001 \rangle$ junctions, a dislocation network is generated on the $\{110\}$ plane. It was found that the network can move conservatively in any direction in the $\{110\}$ plane, provided the stress direction and magnitude are chosen appropriately. It was also found that the network begins to move at stress levels well below the Peierls values for its constituent dislocations, for all directions of stress in the $\{110\}$ plane. The results of these calculations are shown in Fig. 38, in terms of the critical stress required to move the junction network as a function of stress direction, expressed in polar coordinates with stress magnitude and direction angle as variables. The nodal effect on dislocation mobility is seen here in the clustering of the data points from atomistic calculations inside the envelope formed by the Peierls stress values computed for each of the three constituent dislocations in isolation.

While kink nucleation at the nodes appears to be the mechanism for enhanced mobility, contrary to the original hypothesis of Matsui and Kimura the kinks were observed to nucleate at the trailing node of the moving junctions and then to converge on their leading nodes. Otherwise, the CDS mechanism seems to be supported by the atomistic calculations. It was also confirmed that such a nodal enhancement of dislocation mobility requires two conditions to be satisfied simultaneously, a high barrier for kink-pair nucleation on a straight screw dislocation, and a low kink migration barrier. In these calculations using the Finnis-Sinclair model of Mo, the Peierls stress value of 2.4 GPa obtained indeed indicates a high nucleation barrier. At the same time, the Peierls stress for kink migration is 20 MPa, two orders of magnitude lower. We expect that when these energetic conditions are met, the nodal effect on dislocation mobility will be even more dramatic at finite temperature. Even though the atomistic study confirms the CDS mechanism, it is possible that the mechanism suggested in [178] also can be important. Similar simulations examining the effect of torques on dislocation mobility would be instructive.

4.4 Dislocation mobility

4.4.1 Experiments

Experimental measurements of dislocation mobility in BCC metals are more difficult compared to the case of Si (see the preceding section), mainly due to the problem of obtaining samples with low dislocation density. Early experimental results on screw and edge dislocation mobility may be contaminated by the interaction of moving dislocations with grown-in dislocations and the free surfaces. For example, it was reported that edge dislocations [124] have a lower mobility than screw dislocations [125, 180, 181, 182]. This has led to the conclusion [126] that kink mechanisms do not play a role in screw dislocations, which is in contradiction with the current understanding.

More recent *in situ* TEM observations have established that edge dislocations move much faster than screw dislocations [122], consistent with TEM observation of dislocation microstructures dominated by screw dislocations. Unfortunately, it is difficult to estimate the actual stress exerted on dislocations in *in situ* TEM experiments. This can be seen from the large difference between the applied stress and the estimated local stress on dislocations in Fig. 39 [122].

In addition to the large mobility difference between edge and screw segments, TEM observations have provided ample evidence that dislocation motion by itself can produce high density of point defects and point defect clusters, in the form of prismatic dislocation loops. This behavior is similar to FCC metals, where large density of Stacking Fault Tetrahedra (SFT) is observed in pure material deformed at high strain rate [183]. Generally, the higher the strain-rate the larger the observed concentration of defect debris [184]. The resolution of TEM observations of defect size distribution is limited to about 2 nm; defects at smaller sizes are not visible. The defect spectrum appears to be similar to the microstructures found in the same materials after irradiation. These observations also reveal characteristic shapes of screw dislocations with extended cusp-like features, as shown in Fig. 30(b). Although some of these features are likely to be due to dislocation interaction with extrinsic defects (impurities, precipitates), a large density of debris is also observed in very pure metals. The implication is that such behavior is intrinsic to high strain-rate deformation of metals. Recent simulation results revealing the underlying mechanisms of debris production will be discussed in later this subsection.
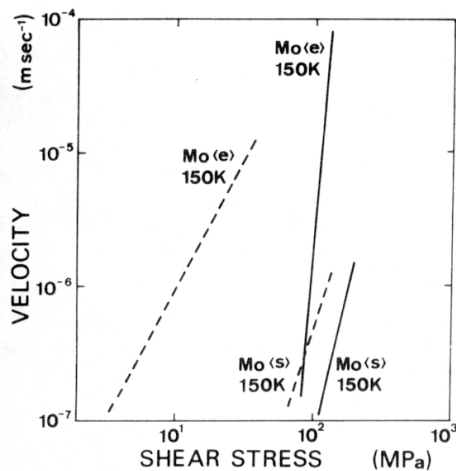
Figure 39: Velocity of edge (e) and screw (s) dislocations in Mo as a function of stress by *in situ* high voltage electron microscopy [122]. Solid lines represent external stress, and dashed line represent estimated local stress on dislocations taking into account mutual dislocation interactions.

Atomistic simulations have been carried out to make direct contact with measurements of dislocation mobility. While it is still too early to expect quantitative comparisons with experiments (which show large error bars as well), the simulations have been helpful in elucidating the qualitative behavior and mechanisms of dislocation motion. In the following we will discuss a number of recent results of direct Molecular Dynamics simulations of screw and edge dislocations in BCC metals.

4.4.2 Screw dislocations

Fig. 40 shows two snapshots from a series of MD simulations of screw dislocation motion in BCC Mo (Finnis-Sinclair model [185]) at 10K [186]. The simulations are quasi 2-dimensional in that the simulation cell is periodic along the dislocation line of length equal to five Burgers vectors. A constant strain rate is imposed to move the dislocation at the average velocity 200m/s on the (110) plane. The internal stress fluctuates with considerable amplitude about the Peierls value as the dislocation moves intermittently, with bursts over several atomic spacings. This behavior, reminiscent of the Portevin-LeChatelier (PLC) effect in crystal plasticity [187], is likely due to
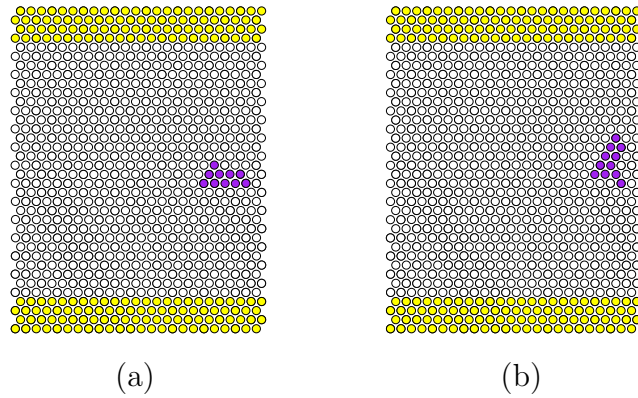
94

(a)   (b)

Figure 40: Snapshots of quasi-2D MD simulation of screw dislocation motion in BCC Mo at 10K. Atoms with local energy 0.1eV higher than that of the perfect lattice atoms are plotted in dark color to show the dislocation core. The simulation cell is periodic along the horizontal direction (along which dislocation moves) as well as along the dislocation line (out of plane). The gray atoms in the upper and lower layers of the cell are forced to displace at a constant velocity corresponding to a fixed strain rate.

the small size of the simulation cell and the constant strain rate boundary-conditions. Nonetheless, certain qualitative features observed from these simulations may be relatively free from simulation artifacts. First, the dislocation core under stress, at rest and in motion, looks very different from the core under zero stress. The three-way splitting is not observed, instead, the core structure seems rather planar, as shown in Fig. 40, similar to earlier calculations of static relaxation under high stress [151]. Second, several cross-slip events were detected, prior to each the core was seen to fork or bifurcate onto the two candidate cross-slip {110} planes at 60° to the horizontal plane, as shown in Fig. 40(b). In all cases, cross-slip occurs in the upward direction even though the resolved stress on both potential cross-slip planes is the same. On reversing the straining direction, the cross-slip direction remains upward, which can be understood as a manifestation of the twinning-antitwining asymmetry on the atomistic level.

While capturing certain mechanistic aspects of screw dislocation motion, the foregoing simulations are not expected to be able to adequately account for the three-dimensional motion of a screw dislocation. An obvious constraint is the short dislocation length of 5 Burgers vectors which cannot accommodate even a single kink. According to previous simulations, a minimal kink would have to be at least $5b$ to $10b$ in width. Extending the simulations to much longer screw dislocations, one finds a greater complexity of kink mechanisms during dislocation motion.

A series of MD simulations of a $100b$ long screw dislocation moving in α-Fe (Finnis-Sinclair model [188]) has been performed [33]. The boundary condition is similar to that in Fig. 40 except that surface traction forces are applied to top and bottom layers of atoms to impose a constant-stress condition. As a point of reference, the Peierl stress for this dislocation is 900MPa. At 300K and under applied stress of 400MPa, dislocation motion via a sequence of kink-pair nucleation and kink migration events was observed. Almost equal number of kinks were nucleated on the horizontal {110} plane as on the "cross-slip" {110} plane inclined at 60°. This possibly reflects the twinning-antitwinning asymmetry in BCC lattice, just as in the 2D simulation above. During the simulation the dislocation was resting most of the time, whereas the kinks moved rapidly along the dislocation line once nucleated. On average, the dislocation moved at a velocity 88m/s at 25° to the horizontal (MRSS) plane.

A high mobility of the nucleated kinks is to be expected given that the applied stress (400MPa) far exceeds the Peierls stress for kinks (20MPa), so that

kink motion is limited only by the phonon drag mechanisms. The interplay between the rate of kink-pair nucleation and the kink migration velocity gives rise to a particular length scale λ such that, when a dislocation is shorter than λ, kink-nucleation would be rare and existing kinks will tend to glide along the dislocation line through the periodic boundary and recombine, before the next kink-nucleation event occurs. Under this condition, the dislocation velocity should be proportional to its length, since the number of double-kink nucleation sites is proportional to its length. This behavior has been reproduced in mesoscale kinetic Monte Carlo simulations [189]. For the simulation conditions described above, taking $v_k \sim 2000 \mathrm{m/s}$, $J \sim 3 \times 10^{17} \mathrm{m}^{-1} \mathrm{s}^{-1}$, one can estimate that $\lambda = \sqrt{v_k/J} \sim 300b$, which is consistent with the actual observation of at most only one kink pair on the dislocation line.

On dislocations with length longer than λ, another kink-pair can form while the previously nucleated kinks are still gliding along the line. Kinks from the same pair will not be able to recombine with each other while encountering kinks from the subsequent nucleation events. It is then generally expected that the dislocation velocity will reach a plateau value and become length-independent [5]. However, results of both atomistic and mesoscale simulations reveal the possibility of a much more complex behavior for screw dislocations in BCC metals due to their ability to cross-slip easily.

The characteristic length λ can be readily varied by setting the temperature and/or applied stress. This is because stress and temperature have very different effects on the thermally activated kink-pair nucleation and phonon-drag controlled kink migration. In particular, kink migration velocity should be proportional to stress and must decrease with increasing temperature. At the same time, the kink-pair nucleation rate should rise very quickly with increasing stress or temperature. Thus λ must be a sensitive function of σ and T. For example, the condition of $\lambda < 100b$ is reached in a similar simulation at the temperature of 100K and a stress of 750 MPa. A snapshot of such a simulation is shown in Fig. 41. The dislocation is seen to leave a significant amount of debris in its wake. This observation of debris formation confirms our earlier hypothesis [189] that, given the ease of cross-slip, a moving screw dislocation can contain both "glide" kink-pairs and "cross-slip" kink pairs, provided $l > \lambda$. A collision of glide and cross-slip kinks produces non-planar defects which have been called "cross-kinks" in the context of TiAl [191], as shown in Fig. 42(a). Such collisions create topological conflicts that, according to [191], can be resolved by one of two ways, sweeping the cross-kinks along the line akin to the pinning-unpinning mechanisms suggested in [191],
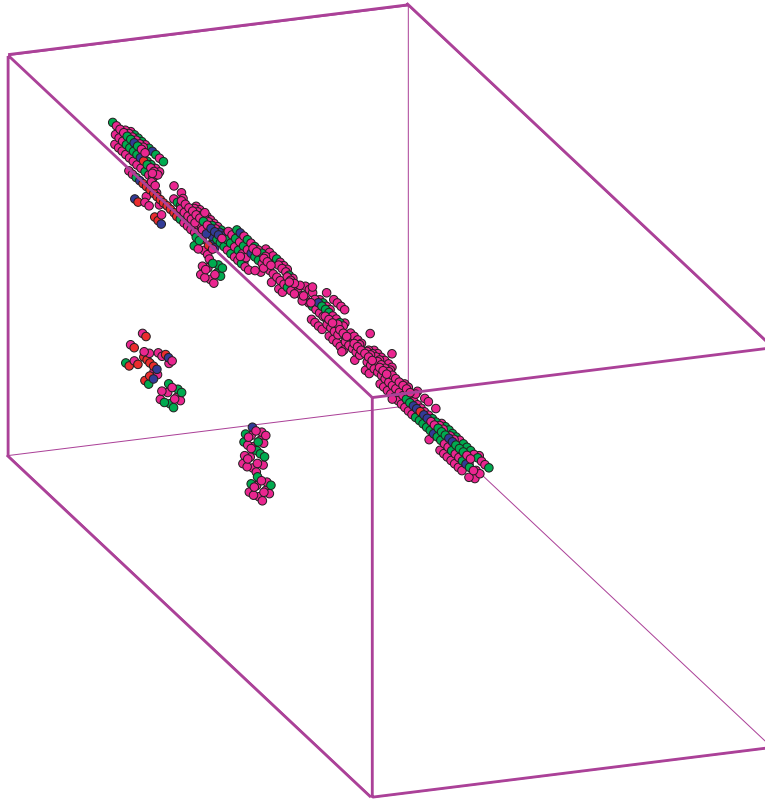
97

Figure 41: Snapshot of MD simulation of screw dislocation motion in BCC Fe at temperature 100K and 750MPa shear stress. Only atoms with central symmetry parameters [190] significantly deviate from that of perfect BCC lattice are shown. Debris in the form of vacancy and interstitial loops are left in the wake of the moving dislocation.
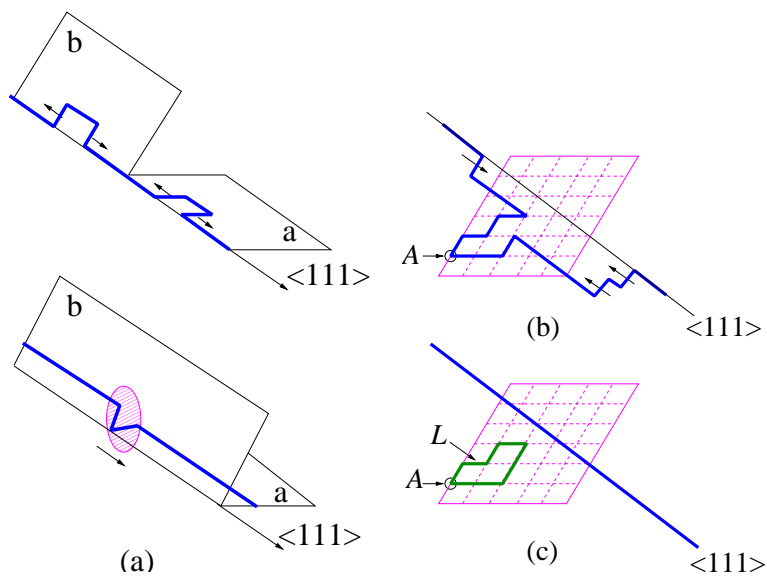
Figure 42: Schematic representation of the formation of (a) two kinks forming a cross-kink, (b) more kinks joining the cross-kink at point A, and (c) debris loop L formation with the primary dislocation breaking away from the self-pinning point A.
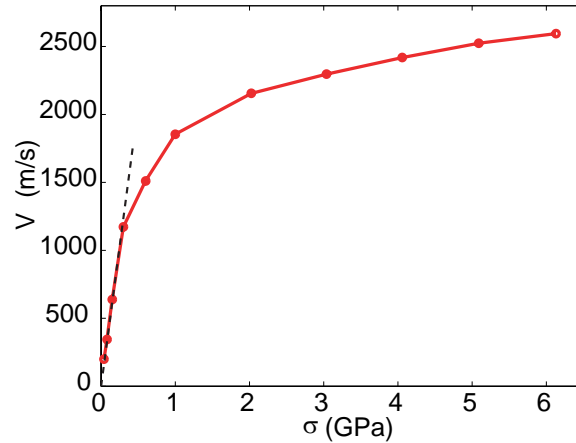
Figure 43: Edge dislocation velocity (●) as a function of stress in MD simulations of BCC Mo at 300K [40]. Linear relationship is observed at low stress - low velocity regime, indicated by the dashed line.

or non-conservative jog-dragging previously suggested in [192]. Our MD simulations show that the way the conflict is resolved is completely different. Similar to a previously suggested mechanism [189], the dislocation extracts itself from the conflict by moving by purely conservative double-kink nucleation, leaving behind prismatic loops, as shown in Fig. 42(b) and (c). No diffusional transport of vacancies or interstitials is involved in this process. That diffusion-less jog-dragging is possible was also suggested in [5] (p. 596).

The results just discussed show how important it is to let dislocations evolve freely in 3D and to probe the mechanisms of dislocation motion by large-scale MD simulations. In the 2D simulations shown in Fig. 40, such observation would not have been possible. In fact, the very same simulation depicted in Fig. 41 but repeated for a dislocation that is just 50b long, shows no roughening transition: the dislocation glides smoothly through nucleation and propagation of kink-pairs. These observations suggest that one must exercise caution in interpreting the data of 2D simulations that, thus far, have greatly outnumbered 3D simulations.

4.4.3 Edge dislocations

The mobility of the non-screw dislocations has been observed to be much higher than that of the screws. It is then generally expected that the velocity of non-screw dislocations is limited only by the viscous drag due to their interactions with the lattice vibrations. While this belief was challenged by Duesbery and Xu [160], who found a rather high Peierls stress for edge dislocations in Mo (~ 0.5GPa) and were then compelled to postulate the kink mechanisms to account for the known high mobility, more recent Peierls stress calculations found that this result is probably inaccurate. The value of the Peierls stress for an edge dislocation obtained using the same potential [40] is predicted to be only 25MPa. Subsequent direct MD simulations [40] confirm that the mobility of edge dislocations is indeed controlled by phonon drag, and that kinks do not play a significant role.

The simulations made use of a simulation cell with a periodic boundary condition containing an edge dislocation dipole [40]. A constant stress is applied by the Parrinello-Rahman method [193]. The shape of the cell is chosen such that the interaction between the two dislocations and their periodic images is negligible. Fig. 43 shows the stress variation of dislocation velocity at 300K. The two edge dislocations moved readily and smoothly at 100MPa stress, consistent with their low Peierls stress. The velocity-stress relationship remains linear at velocities up to 1000m/s. From the ratio between stress and velocity in this linear regime one can extract the phonon drag coefficient $B = \sigma/v = 0.7$MPa $\cdot$ s/m. The drag coefficient is found to increase with increasing temperature. All of these features indicate that edge dislocation mobility is controlled by the phonon drag mechanism. Similar simulations were repeated for edge dislocations with a pre-existing kink, which gave essentially the same results, thus providing direct evidence that kinks play no significant role in edge dislocation motion.

At stresses above 500MPa, the dislocation velocity starts to level off, possibly due to relativistic effects, as shown in Fig. 43. In simulations using sufficiently large cells, the velocity value was found to be always lower than the transverse sound speed (3000m/s). Recent MD simulations of edge dislocation motion have been focused mostly on very fast motion in which dislocation velocity can approach the sound speed [194]. Whether dislocations can move with velocities exceeding the sound velocity is still an open question. On the one hand, it has been argued that supersonic motion is impossible [195]. On the other hand, several direct MD simulations show that

dislocations can move trans-sonically (between transverse and longitudinal sound velocities) and even supersonically, provided that they are nucleated directly into such a fast moving state [194]. In the above set of simulations, trans- and super-sonic dislocation motion were observed, when a small simulation cell was subjected to a high shear rate. However, such high speed dislocation motion was not observed in larger cells, in which the dislocation could not keep up with the shear rate and the crystal undergoes a shear collapse. Given that the effective dislocation density in the smaller cells is unrealistically high, in the range of $10^{16} - 10^{17} \mathrm{m}^{-2}$, the behavior observed in the larger cells is more convincing, in which the dislocation density approaches more realistic values, around $10^{15}\mathrm{m}^{-2}$.

It is generally believed that there should be a transition from kink mechanism to phonon drag for dislocation motion as the applied stress increases. Interestingly, this transition has not yet been observed by direct MD simulations for either screw or edge dislocations. For screw dislocations, their ease of cross-slip introduces a new mechanism at high stresses, i.e. the formation of "cross-kink" and debris loops, which significantly limits the dislocation velocity even above the Peierls stress. For edge dislocations, their exceedingly small Peierls stress makes the kink mechanism unlikely under most temperature and stress conditions. In the search for a direct realization of such a transition, we note that the mixed 71° (M111) has a much higher Peierls stress (320MPa), and being non-screw, is not able to cross-slip. Therefore, the 71° dislocation is a promising candidate to reveal the transition from kink mechanisms to phonon drag in dislocation motion. One interesting question that can be raised in this regard is, does the Peierls stress indeed define the transition?

4.5   Outstanding issues

The above discussions centred on the core effects on dislocation mobility in BCC metals. One of the key uncertainties yet to be settled is whether, in what sense and how much core polarization affects the motion of screw dislocations. The idea that polarization is the reason for the high Peierls barrier is well ingrained into the thinking about plasticity of BCC structures. Recent results [144, 139] obtained with DFT methods suggest that both in Ta and Mo the ground state of the core is not polarized, while previously most empirical potentials models predicted substantial core polarization in Mo [143, 145] and, with some exceptions, also in Ta [196]. At the same time,

some of the same recent calculations show that, despite the observed absence of polarization, the Peierls stress is high, of the order of 1-2 GPa. Although these latest calculations may contain some errors from the necessary use of small supercells, the notion that a high Peierls stress can be sustained in the absence of polarization seems to be well grounded. It is tempting to conclude that high lattice resistance to screw motion is a generic property of all BCC materials. Supporting this assertion is the observation that, under high stresses approaching the Peierls value, the structure of the dislocation core looks unpolarized. Thus, it is not clear how the zero-stress structure, even when it shows a strong polarization, can affect the magnitude of the Peierls stress.

Recent MD simulations indicate that the mechanisms of dislocation motion in the vicinity of the Peierls stress may be more complex than previously assumed. A common expectation is that below the Peierls stress level dislocations move via kink-pair nucleation and migration, while above the Peierls stress the motions are controlled by phonon-drag. This view now has been called into question by simulations which show that the screw dislocation motion becomes rough below Peierls stress and continues to be rough at and above the Peierls stress, with no visible signs of a transition to phonon drag. Furthermore, the screw motions produced large quantities of debris, both isolated defects and clusters. There is little or no mass transport associated with this defect production. Instead, the debris seemed to be formed entirely via conservative mechanisms. Given the singular character of the screws, it will be important to investigate if and how the transition takes place for non-screw dislocations.

The discrepancy between calculated and experimental estimates of the Peierls stress is a lingering issue despite attempts to reconcile the two values. Recently, Moriarty et al [197] presented calculations for Ta using a newly developed potential based on the Generalized Pseudopotential Theory. The Peierls stress computed using the new MGPT potential is 500 MPa, considerably closer to the experimental estimates of 260 MPa, whereas all the previous calculated results were around 1.5 GPa. This "convergence" could be taken to mean that it was the inaccuracy of the previous potential models that is responsible for the discrepancy. On the other hand, recent calculations based on the DFT method, which are presumably more accurate, produced Peierls stress values which are still around 0.7 GPa [139]. In light of these results, the discrepancy is still a fundamental issue that reflects an incomplete understanding of the mechanisms of dislocation motion in BCC

metals.

The cross-slip of screw dislocation, with its compact core, must be sufficiently frequent to make the dislocation motion fully three-dimensional, especially in the so-called pencil glide regime. When this is the case, both screw and non-screw dislocations may find themselves in almost any plane of the $\langle 111 \rangle$ zone. Hence, it is important to examine dislocation mobility as a function of its generalized character, by which we mean a combination of two angles defining the orientation of the dislocation line with respect to the Burgers vector. One of these angles is the usual character angle, while the other one defines the angle between the glide plane and some reference plane of the zone. For BCC materials, it would be appropriate to re-examine the mechanisms and resistance to dislocation motion for different combinations of the two character angles. So far, attention has focused mostly on the $\{110\}$ plane with occasional emphasis on the $\{112\}$ plane. However, even within one plane, say $\{110\}$, the mechanisms and magnitude of resistance to dislocation motion can vary significantly. Our recent results for the M111 dislocation is just one example. All these considerations indicate that dislocation mobility in BCC metals is a more complex phenomenon than it appeared some 10 years ago.

5 Concluding Remarks

The discussions presented in this chapter focused on the intimate connection between the structure and energetics of dislocation core and dislocation mobility mechanisms. From the theory standpoint, the ultimate objective is to be able to compute dislocation mobility from the underlying atomistic processes, preferably with no adjustable parameters. The feasibility of this program depends on a successful resolution of several issues, each posing a challenge in and of itself. A foremost concern is our ability to compute accurately. The increasing use of more reliable descriptions of interatomic interactions is expected to continue in the future, gradually making it possible to study dislocation behavior in increasingly more realistic physical environments. A second challenge is to connect predictive theory and simulation with experiments. A gap still exists between the time and length scales accessible to simulation and those pertinent to experiments. Recent and continuing advances in various experimental techniques for microscopic analysis, including *in situ* and subatomic scale resolution methods, create much excitement in the materials theory and modeling community. In response, new and more powerful computational methods spanning multiple time and length scales are being developed to deal with microstructural effects which need to be incorporated into our understanding. The core effects on dislocation mobility and crystal plasticity considered here are a microcosm of these more general developments in the physics of materials.

Multiscale modeling has come to symbolize the emerging notion of linking simulation models and techniques across the micro-to-macro length and time scales. The expectation is that by combining the different methods of calculation, one can attack a fundamental problem in a more comprehensive manner than where the methods are used individually. As we unravel the structural complexities of the dislocation core and begin to understand how it responds to stress and temperature effects at the local (atomistic) level, it would be important to transfer the "unit process" description of nucleation and migration to the microstructural (mesoscale) level where the collective behavior of dislocation interactions dominate. Work is on-going to feed the results of atomistic calculations into dislocation dynamics simulations of the evolution of a large collection of dislocation lines, and into finite-element and continuum models capable of dealing with system behavior on length and time scales appropriate for measurements. This is a vision that has considerable appeal to the community as can be seen from recent conferences

[for example, the Workshop on Multiscale Modeling of Materials Strength and Failure, Bodega Bay, CA, Oct. 7-10, 2001, and International Conference on Multiscale Materials Modelling, Queen Mary, Univ. London, June 17-20, 2002], special issues of journals, and funding initiatives. In view of the current interest and activities, one can look forward to significant advances in the microscopic understanding of the dislocation core and its effects on dislocation mobility.

Acknowledgements

References

[1] H. R. Kolar, J. C. H. Spence, H. Alexander, Phys. Rev. Lett. 77 (1996) 4031.

[2] S. S. Brenner, in: R. H. D. et al. (Ed.), Growth and Perfection of Crystals, Wiley, New York, 1958, p. 3.

[3] S. Suresh, T.-G. Nieh, B. W. Choi, Script. Mater. 41 (1999) 951.

[4] A. Gouldstone, H.-J. Koh, K.-Y. Zeng, A. E. Giannakopoulos, S. Suresh, Acta Mater. 48 (2000) 2277.

[5] J. P. Hirth, J. Lothe, Theory of Dislocations, 2nd ed., Wiley, New York, 1982.

[6] V. V. Bulatov, D. Richmond, M. V. Glazov, Acta Mater. 47 (1999) 3507.

[7] A. S. Argon, private communication.

[8] H. B. Huntington, Proc. Phys. Soc. B 68 (1955) 1043.

[9] R. E. Peierls, Proc. Phys. Soc 52 (1940) 23.

[10] F. R. N. Nabarro, Proc. Phys. Soc. 59 (1947) 526.

[11] A. H. Cottrell, Dislocations and Plastic Flow in Crystals, Clarendon Press, Oxford, 1953.

[12] F. R. N. Nabarro, Philos. Mag. A 75 (1997) 703.

[13] T. Vegge, J. P. Sethna, S. A. Cheong, K. W. Jacobsen, C. R. Myers, D. C. Ralph, Phys. Rev. Lett. 86 (2001) 1546.

[14] W. Benoit, M. Bujard, G. Gremaud, Phys. Stat. Solidi A 104 (1987) 427.

[15] G. Schoeck, Script. Metall. Mater. 30 (1994) 611.

[16] V. I. Alshits, V. L. Indenbom, Sov. Phys. Usp. 18 (1975) 1.

[17] V. I. Alshits, V. L. Indenbom, in: F. R. N. Nabarro (Ed.), Dislocation in Solids, Vol. 7, North-Holland, Amsterdam, 1986, p. 43.

[18] D. Rodney, G. Martin, Phys. Rev. Lett. 82 (1999) 3272.

[19] J. Chang, W. Cai, V. V. Bulatov, S. Yip, Comput. Mater. Sci. 23 (2002) 111.

[20] Y. Ashkenazy, I. Kelson, G. Makov, D. Mordehai, Abstracts, APS Annual Meeting, Seatle, Washington .

[21] V. V. Bulatov, F. F. Abraham, L. Kubin, B. Devincre, S. Yip, Nature 391 (1998) 669.

[22] M. I. Baskes, R. G. Hoagland, T. Tsuji, Modelling Simul. Mater. Sci. Eng. 6 (1998) 9.

[23] D. Rodney, R. Phillips, Phys. Rev. Lett. 82 (1999) 1704.

[24] V. B. Shenoy, R. V. Kukta, R. Phillips, Phys. Rev. Lett. 84 (2000) 1491.

[25] J. Friedel, Dislocations, Pergamon, Oxford, 1964.

[26] A. Korner, H. Schmid, F. Prinz, Phys. Stat. Solidi A 51 (1979) 613.

[27] M. Elkajbaji, H. O. Kirchner, J. Thibault-Desseaux, Phil. Mag. A 57 (1988) 631.

[28] A. Korner, H. P. Karnthaler, Phil. Mag. A 44 (1981) 275.

[29] J. Bonneville, B. Escaig, Acta Metall. 27 (1979) 1477.

[30] T. Rasmussen, K. W. Jacobsen, T. Leffers, O. B. Pedersen, S. G. Srinivasan, H. Jónsson, Phys. Rev. Lett. 79 (1997) 3676.

[31] T. Rasmussen, K. W. Jacobsen, T. Leffers, O. B. Pedersen, Phys. Rev. B 56 (1997) 2977.

[32] T. Vegge, T. Rasmussen, T. Leffers, O. B. Pedersen, K. W. Jacobsen, Phys. Rev. Lett. 85 (2000) 3866.

[33] J. Marian, unpublished.

[34] F. Ercolessi, J. B. Adams, Europhys. Lett. 26 (1994) 583.

[35] C. Woodward, S. I. Rao, D. M. Dimiduk, JOM - J. Min. Met. Mat. S. 50 (1998) 37.

[36] J. Huang, M. Meyer, V. Pontikis, Phil. Mag. A 63 (1991) 1149.

[37] D. Rodney, G. Martin, Phys. Rev. B 61 (2000) 8714.

[38] B. D. Wirth, V. V. Bulatov, T. D. de la Rubia, J. Eng. Mater. Tech. 124 (2002) 329.

[39] M. Victoria, N. Baluc, C. Bailat, Y. Dai, M. T. Luppo, R. Schaublin, B. N. Singh, J. Nucl. Mater. 276 (2000) 114.

[40] J. Chang, W. Cai, V. V. Bulatov, S. Yip, unpublished.

[41] B. D. Wirth, V. V. Bulatov, T. D. de la Rubia, J. Nucl. Mater. 283-287 (2000) 773.

[42] K. Norlund, F. Gao, Appl. Phys. Lett. 74 (1999) 2720.

[43] Y. Dai, M. Victoria, Acta Mater. 45 (1997) 3495.

[44] K. Wessel, H. Alexander, Phil. Mag. 35 (1977) 1523.

[45] J. Rabier, P. Cordier, T. Tondellier, J. L. Demenet, H. Garem, J. Phys. Condens. Matter 12 (2000) 10059.

[46] I. Yonenaga, K. Sumino, Phys. Stat. Solidi A 50 (1978) 685.

[47] H. Alexander, in: F. R. N. Nabarro (Ed.), Dislocation in Solids, Vol. 7, North-Holland, Amsterdam, 1986, p. 113.

[48] H. Siethoff, H. G. Brion, W. Schroter, Appl. Phys. Lett. 43 (1999) 1505.

[49] J. Rabier, J. L. Demenet, Phys. Stat. Solidi B 222 (2000) 63.

[50] M. Tang, L. Colombo, J. Zhu, T. D. de la Rubia, Phys. Rev. B 55 (1999) 14279.

[51] J. Rabier, A. George, Revue Phys. Appl. 22 (1987) 1327.

[52] H. Koizumi, Y. Kamimura, T. Suzuki, Phil. Mag. A 80 (2000) 609.

[53] H. Alexander, H. Teichler, in: P. Haasen, E. J. Kramer (Eds.), Materials Science and Technology, Vol. 4, VCH Weinheim, 1991, p. 249.

[54] V. V. Bulatov, J. F. Justo, W. Cai, S. Yip, A. S. Argon, T. Lenosky, M. de Koning, T. D. de la Rubia, Phil. Mag. A 81 (2001) 1257.

[55] J. Bennetto, R. W. Nunes, D. Vanderbilt, Phys. Rev. Lett. 79 (1997) 245.

[56] R. W. Nunes, J. Bennetto, D. Vanderbilt, Phys. Rev. B 58 (1998) 12563.

[57] N. Lehto, S. Öberg, Phys. Rev. Lett. 80 (1998) 5568.

[58] J. F. Justo, V. V. Bulatov, S. Yip, J. Appl. Phys. 86 (1999) 4249.

[59] Q. Ren, B. Joos, M. S. Duesbery, Phys. Rev. B 52 (1995) 13223.

[60] M. S. Duesbery, B. Joos, D. J. Michel, Phys. Rev. B 43 (1991) 5143.

[61] R. Hull (Ed.), Properties of Crystalline Silicon, INSPEC, London, 1999.

[62] B. J. Gally, A. S. Argon, Phil. Mag. A 81 (2001) 699.

[63] F. Louchet, J. Thibault-Desseaux, Revue Phys. Appl. 22 (1987) 207.

[64] J. F. Justo, A. Antonelli, A. Fazzio, Solid State Communications 118 (2001) 651.

[65] V. V. Bulatov, S. Yip, A. S. Argon, Phil. Mag. A 72 (1995) 453.

[66] M. I. Heggie, R. Jones, Inst. Phys. Conf. Ser 87 (1987) 367.

[67] R. W. Nunes, J. Bennetto, D. Vanderbilt, Phys. Rev. B 57 (1998) 10388.

[68] T. D. Engeness, T. A. Arias, Phys. Rev. Lett. 79 (1997) 3006.

[69] L. B. Hansen, K. Stokbro, B. I. Lundqvist, K. W. Jacobsen, D. M. Deaven, Phys. Rev. Lett. 75 (1995) 4444.

[70] J. R. K. Bigger, D. A. McInnes, A. P. Sutton, M. C. Payne, I. Stich, R. D. King-Smith, D. M. Bird, L. J. Clarke, Phys. Rev. Lett. 69 (1992) 2224.

[71] T. A. Arias, J. D. Joannopoulos, Phys. Rev. Lett. 73 (1994) 680.

[72] F. H. Stillinger, T. A. Weber, Phys. Rev. B 31 (1985) 5262.

[73] W. Cai, unpublished.

[74] L. Pizzagalli, P. Beauchamp, J. Rabier, Phil. Mag. A (2002) submitted.

[75] W. Cai, V. V. Bulatov, J. Chang, J. Li, S. Yip, Phil. Mag. A (2002) submitted.

[76] T. Suzuki, T. Yasutomi, T. Tokuoka, Phil. Mag. A 79 (11) (1999) 2637.

[77] E. Weber, H. Alexander, Inst. Phys. Conf. Ser 31 (1977) 266.

[78] L. C. Kimerling, J. R. Patel, Appl. Phys. Lett. 34 (1979) 73.

[79] C. Kisielowski-Kemmerich, Phys. Stat. Solidi B 161 (1990) 11.

[80] J. Weber, Solid State Phenomena 37-38 (1994) 13.

[81] J. F. Justo, M. de Koning, W. Cai, V. V. Bulatov, Phys. Rev. Lett. 84 (2000) 2172.

[82] G. Csányi, S. Ismail-Beigi, T. A. Arias, Phys. Rev. Lett. 80 (1998) 3984.

[83] Y. M. Huang, J. C. H. Spence, O. F. Sankey, Phys. Rev. Lett. 74 (1995) 3392.

[84] H. Gottschalk, H. Alexander, V. Dietz, Inst. Phys. Conf. Ser 87 (1987) 339.

[85] G. Vanderschaeve, C. Levade, D. Caillard, J. Phys. Condens. Matter 12 (2000) 10093.

[86] B. Y. Farber, Y. L. Iunin, V. I. Nikitenko, Phys. Stat. Solidi A 97 (1986) 469.

[87] V. V. Bulatov, J. F. Justo, W. Cai, S. Yip, Phys. Rev. Lett. 79 (1997) 5042.

[88] J. Tersoff, Phys. Rev. Lett. 56 (1986) 632.

[89] R. W. Nunes, J. Bennetto, D. Vanderbilt, Phys. Rev. Lett. 77 (1996) 1516.

[90] M. I. Heggie, R. Jones, A. Umerski, Phys. Stat. Solidi A 138 (1993) 383.

[91] S. Oberg, P. K. Sitch, R. Jones, M. I. Heggie, Phys. Rev. B 51 (1995) 13138.

[92] A. Valladares, J. A. White, A. P. Sutton, Phys. Rev. Lett. 81 (1998) 4903.

[93] P. B. Hirsch, A. Ourmazd, P. Pirouz, Inst. Phys. Conf. Ser 60 (1981) 29.

[94] M. Miyata, T. Fujiwara, Phys. Rev. B 63 (2001) 45206.

[95] A. George, G. Champier, Phys. Stat. Solidi A 53 (1979) 529.

[96] A. George, J. Rabier, Revue Phys. Appl. 22 (1987) 941.

[97] A. George, C. Escaravage, G. Champier, W. Schröter, Phys. Stat. Solidi B 53 (1972) 483.

[98] A. George, C. Escaravage, W. Schröter, G. Champier, Cryst. Latt. Def. 4 (1973) 29.

[99] P. Tu, H. Yizhen, Phys. Stat. Solidi A 59 (1980) 195.

[100] A. George, J. Phys. (Paris) 40 C-6 (1979) 133.

[101] F. Louchet, Phil. Mag. A 43 (1981) 1289.

[102] F. Louchet, A. George, J. Phys. (Paris) C4 (1983) 44.

[103] B. Y. Farber, V. I. Nikitenko, Phys. Stat. Solidi A 73 (1982) K141.

[104] M. Imai, K. Sumino, Phil. Mag. A 47 (1983) 599.

[105] V. I. Nikitenko, B. Y. Farber, E. B. Yakimov, Cryst. Res. & Technol. 19 (1984) 295.

[106] V. I. Nikitenko, B. Y. Farber, H. G. Minasyan, in: K. Sumino (Ed.), Defect Control in Semiconductors, Elsevier Science Publishers, B. V. North-Holland, 1990.

[107] V. I. Nikitenko, B. Y. Farber, Y. L. Iunin, V. I. Orlov, in: J. H. Werner, H. P. Strunk (Eds.), Springer Proceedings in Physics, Vol. 54, Springer-Verlag Berlin, Heidelberg, 1991.

[108] T. E. Mitchell, J. P. Hirth, A. Misra, Acta Mater. 50 (2002) 1087.

[109] V. N. Erofeev, V. I. Nikitenko, V. B. Osvenskii, Phys. Stat. Solidi 35 (1969) 79.

[110] S. Marklund, Solid State Communications 54 (1985) 555.

[111] H. J. Möller, Acta Metall. 26 (1978) 963.

[112] W. Cai, V. V. Bulatov, J. F. Justo, S. Yip, A. S. Argon, Phys. Rev. Lett. 84 (2000) 3346.

[113] A. Jacques, A. George, Script. Metall. 45 (2001) 1279.

[114] R. Jones, J. Phys. (Paris) 44 (1983) C4–61.

[115] K. Maeda, Y. Yamashita, IPCS 104 (1989) 269.

[116] S. A. Erofeeva, Phil. Mag. A 70 (1994) 943.

[117] V. Celli, M. Kabler, T. Ninomiya, R. Thomson, Phys. Rev. 131 (1963) 58.

[118] H.-J. Möller, J. Buchholz, Phys. Stat. Solidi A 20 (1973) 545.

[119] P. B. Hirsch, J. Phys. (Paris) 40 (1979) C6–117.

[120] N. V. Abrosimov, V. Alex, D. V. Dyachenko-Dekov, Y. L. Iunin, V. I. Nikitenko, V. I. Orlov, S. N. Rossolenko, W. Schroeder, Mater. Sci. Eng. A 234 (1997) 735.

[121] H.-J. Kaufmann, A. Luft, D. Schulze, Cryst. Res. Technol. 19 (1984) 357.

[122] T. Imura, K. Noda, H. Matsui, H. Saka, H. Kimura, in: Dislocations in Solids, University of Tokyo Press, 1985, p. 287.

[123] A. Lawley, H. L. Gaigher, Phil. Mag. 10.

[124] H. L. Prekel, A. Lawley, H. Conrad, Acta Metall. 16 (1968) 337.

[125] E. B. Leiko, E. M. Nadgornyi, Kristallografiya 19 (1974) 584.

[126] E. Nadgornyi, Prog. Mater. Sci. 31 (1988) 1.

[127] C. S. Barrett, G. Ansel, R. F. Mehl, Trans. ASM 25 (1937) 702.

[128] G. I. Taylor, C. F. Elam, Proc. R. Soc. London A 112 (1926) 337.

[129] J. F. L. Vogel, R. M. Brick, Trans. AIME 197 (1953) 700.

[130] B. Sestak, S. Libovicky, Acta Metall. 11 (1963) 1190.

[131] M. S. Duesbery, V. Vitek, Acta Mater. 46 (1998) 1481.

[132] A. H. Cottrell, B. A. Bilby, Phil. Mag. 42 (1951) 573.

[133] J. B. Cohen, R. Hinton, K. Lay, S. Sass, Acta Metall. 10 (1962) 894.

[134] F. C. Frank, J. F. Nicholas, Phil. Mag. 44 (1953) 1213.

[135] P. B. Hirsch, in: 5th International Conference on Crystallography, Cambridge University, 1960, p. 139.

[136] V. Vitek, Cryst. Latt. Def. 5 (1974) 1.

[137] V. Vitek, F. Kroupa, Phil. Mag. 19 (1969) 265.

[138] M. S. Duesbery, G. Y. Richardson, Critical Reviews in Solid State and Materials Sciences 17(1) (1991) 1.

[139] C. Woodward, S. I. Rao, Phys. Rev. Lett. 88 (2002) 216402.

[140] V. Vitek, R. C. Perrin, D. K. Bowen, Phil. Mag. 21 (1970) 1049.

[141] M. S. Duesbery, Acta Metall. 31 (1983) 1747.

[142] W. Xu, J. Moriarty, Phys. Rev. B 54 (1996) 6941.

[143] W. Xu, J. Moriarty, Comput. Mater. Sci. 9 (1998) 348.

[144] S. Ismail-Beigi, T. A. Arias, Phys. Rev. Lett. 84 (2000) 1499.

[145] L. H. Yang, P. Soderlind, J. A. Moriarty, Phil. Mag. A 81 (2001) 1355.

[146] L. H. Yang, P. Soderlin, J. A. Moriarty, Mater. Sci. Eng. A 309 (2001) 102.

[147] C. Woodward, S. I. Rao, Phil. Mag. A 81 (2001) 1305.

[148] W. Sigle, Phil. Mag. A 79 (1999) 1009.

[149] A. Seeger, C. Wuthrich, Nuovo Cimento 33B (1976) 38.

[150] G. Wang, unpublished.

[151] M. S. Duesbery, V. V. Vitek, D. K. Bowen, Proc. R. Soc. Lond. A 332 (1973) 85.

[152] V. Vitek, Proc. R. Soc. Lond. A 352 (1976) 109.

[153] E. Schmid, W. Boas, Plasticity of Crystals, with Special Reference to Metals, F. A. Hughes, London, 1950.

[154] E. Schmid, PICAM (1924) 342.

[155] M. S. Duesbery, Proc. R. Soc. Lond. A 392 (1984) 145.

[156] M. S. Duesbery, Proc. R. Soc. Lond. A 392 (1984) 175.

[157] M. Tang, L. P. Kubin, G. R. Canova, Acta Mater. 46 (1998) 3221.

[158] S. Takeuchi, K. Maeda, Acta Metall. 25 (1977) 1485.

[159] A. H. A. Ngan, M. Wen, Phys. Rev. Lett. 8707 (2001) 075505.

[160] M. S. Duesbery, W. Xu, Script. Metall. 39 (1998) 283.

[161] V. Vitek, M. Yamaguchi, J. Phys. F Metal Phys. 3 (1973) 537.

[162] M. Yamaguchi, V. Vitek, J. Phys. F Metal Phys. 3 (1973) 523.

[163] A. P. Sutton, R. W. Baluffi, Interfaces in Crystalline Materials, Oxford University Press, New York, 1996.

[164] W. Cai, V. V. Bulatov, J. Chang, J. Li, S. Yip, Phys. Rev. Lett. 86 (2001) 5727.

[165] C. Wuthrich, Phil. Mag. 35 (1977) 325.

[166] C. Wuthrich, Phil. Mag. 35 (1977) 337.

[167] J. E. Dorn, S. Rajnak, Trans. Met. Soc. AIME 45 (1967) 983.

[168] M. S. Duesbery, in: F. R. N. Nabarro (Ed.), Dislocations in Solids, Vol. 8, Elsevier, Amsterdam, 1989.

[169] A. H. W. Ngan, Phil. Mag. A 79 (1999) 1697.

[170] A. H. W. Ngan, Key Eng. Mat. 177 (2000) 135.

[171] K. Edagawa, T. Suzuki, S. Takeuchi, Phys. Rev. B 55 (1997) 6180.

[172] G. Henkelman, B. P. Uberuaga, H. Jónsson, J. Chem. Phys. 113 (2000) 9901.

[173] G. Henkelman, H. Jónsson, J. Chem. Phys. 113 (2000) 9978.

[174] M. Wen, A. H. W. Ngan, Acta Mater. 48 (2000) 4255.

[175] H. Matsui, H. Kimura, Script. Metall. 9 (9) (1975) 971.

[176] W. Wasserbäch, Phil. Mag. 51 (1985) 619.

[177] H. Saka, K. Noda, T. Imura, H. Matsui, H. Kimura, Phil. Mag. 34 (1) (1976) 33.

[178] A. J. Garratt-Reed, G. Taylor, Phil. Mag. A 39 (1979) 597.

[179] V. V. Bulatov, W. Cai, Phys. Rev. Lett. 89 (2002) 115501.

[180] E. B. Leiko, D. V. Lotsko, E. M. Nadgornyi, V. I. Trefilov, Sov. Phys. Solid State 17 (1975) 1814.

[181] E. B. Leiko, A. Luft, E. M. Nadgornyi, Phys. Stat. Solidi A 44 (1977) 285.

[182] E. B. Leiko, A. Luft, Phys. Stat. Solidi A 67 (1981) 435.

[183] M. Kiritani, K. Yasunaga, Y. Matsukawa, M. Komatsu, Rad. Eff. Defect. Solids 157 (2002) 3.

[184] A. Luft, Phys. Stat. Solidi 42 (1970) 429.

[185] G. J. Ackland, R. Thetford, Phil. Mag. A 56 (1987) 15.

[186] W. Cai, Atomistic and mesoscale modeling of dislocation mobility, Ph.D. thesis, Massachusetts Institute of Technology (June 2001).

[187] A. Portevin, F. Lechatelier, C. R. Acad. Sci. 176 (1923) 507.

[188] G. J. Ackland, D. J. Bacon, A. F. Calder, T. Harry, Phil. Mag. A 75 (1997) 713.

[189] W. Cai, V. V. Bulatov, S. Yip, A. S. Argon, Mater. Sci. Eng. A 309 (2001) 270.

[190] C. L. Kelchner, S. J. Plimpton, J. C. Hamilton, Phys. Rev. B 58 (1998) 11085.

[191] F. Louchet, B. Viguier, Phil. Mag. A 80 (2000) 765.

[192] S. Sriram, D. M. Dimiduk, P. M. Hazzeldine, V. K. Vasudevan, Phil. Mag. A 76 (1997) 965.

[193] M. Parrinello, A. Rahman, J. Appl. Phys. 52 (1981) 7182.

[194] P. Gumbsch, H. Gao, Science 283 (1999) 968.

[195] J. J. Gilman, Metall. Mater. Trans. A 31 (2000) 811.

[196] G. Chang, A. Stracha, T. Cagin, W. A. Goddard, J. Computer-Aided Materials Design 8 (2002) 117.

[197] J. A. Moriarty, J. F. Belak, R. E. Rudd, P. Soderlind, F. H. Streitz, L. H. Yang, J. Phys. Condens. Matter 14 (2002) 2825.